J. Fluid Mech. (2014), *vol.* 757, *pp.* 701–746.
doi:10.1017/jfm.2014.431

Pressure, density, temperature and entropy fluctuations in compressible turbulent plane channel flow

G. A. Gerolymos[1] and I. Vallet[1,†]

[1]Faculty of Engineering, Université Pierre-et-Marie-Curie (UPMC), 4 place Jussieu, 75005 Paris, France

(Received 18 November 2013; revised 25 May 2014; accepted 23 July 2014;
first published online 26 September 2014)

We investigate the fluctuations of thermodynamic state variables in compressible aerodynamic wall turbulence, using results of direct numerical simulation (DNS) of compressible turbulent plane channel flow. The basic transport equations governing the behaviour of thermodynamic variables (density, pressure, temperature and entropy) are reviewed and used to derive the exact transport equations for the variances and fluxes (transport by the fluctuating velocity field) of the thermodynamic fluctuations. The scaling with Reynolds and Mach number of compressible turbulent plane channel flow is discussed. Statistics and correlation coefficients of the thermodynamic fluctuations are examined. Finally, detailed budgets of the transport equations for the variances and fluxes of the thermodynamic variables are analysed. The implications of these results, leading both to the understanding of the thermodynamic interactions in compressible wall turbulence and to possible improvements in statistical modelling, are assessed. Finally, the required extension of existing DNS data to fully characterise this canonical flow is discussed.

Key words: compressible turbulence, turbulence simulation, turbulent boundary layers

1. Introduction

Analysis of compressible turbulence is invariably related to the dynamics of thermodynamic fluctuations, namely ρ', p', T' and s' (where ρ is the density, p is the pressure, T is the temperature and s is the entropy). This is exemplified by the early work of Kovásznay (1953) on the modal decomposition of compressible turbulence. From this analysis (Kovásznay 1953) it follows that vortical, acoustic and entropic fluctuation modes are only coupled one with another by nonlinear (high-fluctuation-amplitude) effects (Chu & Kovásznay 1958). Building upon this modal description, Morkovin (1962) formulated his hypothesis that in supersonic boundary layers (external flow Mach number $\bar{M}_e \lessapprox 5$) the vorticity–entropy coupling, which is expected to be the dominant 'compressible feedback mechanism' is not sufficiently strong to 'affect the essential dynamics of the boundary-layer but rather modulates them through (stratified) mean values of $\bar{\rho}(y)$ and $\bar{T}(y)$' (where y is the wall-normal coordinate). The main corollary of Morkovin's hypothesis is Bradshaw (1977) that turbulent structure (correlation coefficients and spectra)

† Email address for correspondence: isabelle.vallet@upmc.fr

does not change substantially compared with constant-density flow. The correlation coefficient between streamwise-velocity and temperature fluctuations $c_{u'T'}$ is central in the analysis of Morkovin (1962). Bradshaw (1977) uses the relative value of density-r.m.s. $[\rho']_{rms} := [\overline{\rho'^2}]^{1/2}$ (where r.m.s. denotes root-mean-square, $\overline{(\cdot)}$ denotes Reynolds averaging and $(\cdot)'$ are Reynolds fluctuations) with respect to mean density $\bar{\rho}$ as the main criterion of validity of Morkovin's hypothesis (Morkovin 1962), setting the limit at $[\rho']_{rms} \lessapprox \bar{\rho}/10$.

Although measurement techniques for turbulent fluctuations of pressure p' (Tsuji *et al.* 2007), density ρ' (Panda & Seasholtz 2002) and temperature T' (Teitel & Antonia 1993) are available, there are complex cross-correlations, especially in the near-wall region, that are still beyond experimental reach. Therefore, in line with incompressible flow practice (Kim 2012), direct numerical simulation (DNS) 'its limitation to low-*Re* notwithstanding, ... has played an essential role by providing accurate and detailed information, which are not readily available from experimental results' (where *Re* denotes an appropriate Reynolds number).

Recently, Donzis & Jagannathan (2013) studied the statistics of $\{p',\rho',T'\}$ obtained from DNS of sustained (solenoidal forcing at the large scales) compressible homogeneous isotropic turbulence (HIT), for Taylor-microscale Reynolds numbers $Re_\lambda := [(2/3)k]^{1/2}\lambda_f \breve{\nu}^{-1} \in [30, 430]$ and turbulent Mach numbers $\breve{M}_T := \breve{a}^{-1}[2k]^{1/2} \in [0.1, 0.6]$ (where k is the turbulent kinetic energy, λ_f is the longitudinal Taylor microscale and $\breve{\nu}$ and $\breve{a}$ are the kinematic viscosity and the sound speed at mean conditions, respectively), corresponding to relative density fluctuation r.m.s. levels (coefficients of variation of ρ) $[\bar{\rho}^{-1}\rho']_{rms} \in [3/10\,\%, 16\,\%]$. We prefer using the coefficient of variation of density as a measure of compressibility when transposing the HIT results to wall-bounded flows, because the turbulent Mach number $\breve{M}_T$ is not an appropriate scaling for shear flows (Sarkar 1995; Pantano & Sarkar 2002). In sustained compressible HIT the coefficients of variation $\{[\bar{\rho}^{-1}\rho']_{rms}, [\bar{T}^{-1}T']_{rms}, [\bar{p}^{-1}p']_{rms}\}$ scale reasonably well with $\breve{M}_T^2$ (Donzis & Jagannathan 2013, figure 2, p. 227), and the fluctuations follow on the average a polytropic exponent $n_p \approxeq 1.2$, slightly increasing with increasing $[\bar{\rho}^{-1}\rho']_{rms}$ (Donzis & Jagannathan 2013, figure 7, p. 227). However, wall turbulence includes several phenomena that are absent in HIT, such as mean shear inducing rapid pressure fluctuations (Chou 1945), mean density and temperature gradients producing fluctuations ρ' and T' (Taulbee & VanOsdol 1991; Tamano & Morinishi 2006), and the presence of solid walls introducing wall-echo effects on p' (Gerolymos, Sénéchal & Vallet 2013), and requires therefore specific study.

The detailed study of canonical incompressible wall-bounded flows, namely flat-plate zero-pressure-gradient (ZPG) boundary layer and internal fully developed (streamwise invariant in the mean) flows (plane channel and pipe), has substantially advanced our understanding of wall turbulence (Smits, McKeon & Marusic 2011), although there is still debate on the differences in behaviour with increasing Reynolds number between boundary layers and internal flows (Monty *et al.* 2009), especially concerning the scaling of the streamwise-velocity fluctuation $\overline{u'^2}$ near-wall peak (Hultmark, Bailey & Smits 2010) and of wall-pressure variance $\overline{p_w'^2}$ (Tsuji *et al.* 2012). Regarding incompressible DNS studies, Schlatter & Örlü (2010) show that boundary-layer results are sensitive to inflow and boundary conditions used by different authors, contrary to fully developed internal flows which apply unambiguous streamwise-periodicity conditions. This also applies to the compressible turbulent boundary layer (Spina, Smits & Robinson 1994), with the added difficulty of

prescribing inflow conditions for the thermodynamic quantities as well (Xu & Martín 2004). For this reason, always keeping in mind possible differences in behaviour at the high-*Re* limit (Monty *et al.* 2009), the study of compressible turbulent plane channel flow can provide insight to the physics of 'near-wall boundary-layer flow as it appears in high-speed flight' (Friedrich 2007).

Coleman, Kim & Moser (1995) established the canonical case of compressible turbulent plane channel flow between two isothermal walls, made streamwise invariant in the mean by the introduction of a body-acceleration term, adjusted to enforce the target massflow. Their results included distributions of $\{[p']_{rms}, [\rho']_{rms}, [T']_{rms}\}$ (Coleman *et al.* 1995, figures 10 and 14, pp. 170 and 172), of two-point correlations in the homogeneous streamwise ($\{R^{(x)}_{p'p'}, R^{(x)}_{T'T'}\}$) and spanwise ($\{R^{(z)}_{p'p'}, R^{(z)}_{T'T'}\}$) directions (Coleman *et al.* 1995, figures 3–4, pp. 165–166), and joint p.d.f.s (probability density functions) of $\{(T', \rho'), (T', u')\}$ (Coleman *et al.* 1995, figure 11, p. 171). The data obtained by Coleman *et al.* (1995) were further analysed by Huang, Coleman & Bradshaw (1995), who found that for the cases studied (centreline Mach number $\bar{M}_{CL} \in \{1.5, 2.2\}$) the influence of density fluctuations ρ' on the Reynolds shear stress $\overline{\rho u'' v''}$ and on the wall-normal turbulent temperature transport $\overline{\rho v'' T''}$ were quite small (where $(\cdot)''$ are Favre fluctuations, u is the streamwise velocity component, and v is the wall-normal velocity component), that the strong Reynolds analogy (SRA) which assumes negligible total temperature fluctuations (Morkovin 1962) is unsatisfactory for these flows, and that the Reynolds averages of Favre fluctuations $\{\overline{u''}, \overline{v''}, \overline{T''}\}$ could be reasonably well modelled by assuming an isobaric polytropic process for the thermodynamic fluctuations. Lechner, Sesterhenn & Friedrich (2001) studied scatter plots of $\{(T', \rho'), (T', u'), (T', v'), (\rho', p'), (s', \rho'), (s', p'), (s', T')\}$ (Lechner *et al.* 2001, figures 8–11, pp. 12–14), briefly discussed, without plotting detailed budgets, the transport equations for the variances of density $\overline{\rho'^2}$ (Lechner *et al.* 2001, (32), p. 10) and pressure $\overline{p'^2}$ (Lechner *et al.* 2001, (42), p. 13), and studied the budgets of the transport equations for the Reynolds stresses $\overline{\rho u_i'' u_j''}$ and the turbulent kinetic energy $\overline{\rho u_i'' u_i''}/2$, this last equation having also been scrutinised by Huang *et al.* (1995). From the study of the scatter plots for the thermodynamic variables, Lechner *et al.* (2001, figures 8–11, pp. 12–14) concluded that near the wall ($y^+ \approxeq 9$, where y^+ is the distance from the wall in wall units) considering isobaric fluctuations (neglecting p') was a reasonable approximation. However, examination of the scatter plots (Lechner *et al.* 2001, figures 8–11, pp. 12–14) at the centreline invalidates the isobaric assumption in the outer part of the flow. Morinishi, Tamano & Nakabayashi (2004) investigated both the standard symmetric configuration with two isothermal walls at equal temperatures and the asymmetric case of a cold wall and a hot wall, either adiabatic or isothermal at the adiabatic-wall temperature (Tamano & Morinishi 2006), and studied the budgets of the transport equation for the temperature variance $\overline{\rho T''^2}$ (Tamano & Morinishi 2006). Sénéchal (2009) used data from coarse-grid DNS computations to calculate the budgets of the transport equations for the variances of thermodynamic fluctuations ($\overline{\rho'^2}$, $\overline{\rho T''^2}$, $\overline{p'^2}$), and observed that the coefficient of variation of density $[\bar{\rho}^{-1}\rho']_{rms}$ at constant friction Reynolds number (3.1*b*) $Re_{\tau_w} \approxeq 230$ and $\bar{M}_{CL} \in \{1.5, 0.34\}$, plotted against the outer-scaled wall distance $\delta^{-1}(y - y_w)$ (δ is the channel half-height) varied as $\bar{M}^2_{CL}$. Finally, Wei & Pollard (2011*a*) examined the influence of Mach number ($\bar{M}_{CL} \in \{0.2, 0.7, 1.5\}$) at constant bulk Reynolds number Re_{B_w} (3.1*a*) on the variance, skewness and flatness of $\{u', v', w', p', \rho', T'\}$ (where w is the spanwise velocity component). They further analysed these DNS results (Wei & Pollard 2011*b*) to study the influence of Mach number on the correlation coefficient $c_{\rho' p'}$ (Wei & Pollard

2011*b*, figure 1, p. 6) and on correlations between the fluctuating pressure gradient and the fluctuating vorticity gradients (and also vorticity fluxes). They also presented budgets of the transport equation for $\overline{\rho'\omega'_z}$ (where $\boldsymbol{\omega} := \mathrm{rot}\,\boldsymbol{V}$ is the vorticity and z is the spanwise direction), and found a surprisingly strong influence of the term $\overline{\rho\omega_z\Theta}$ (where $\Theta := \mathrm{div}\,\boldsymbol{V}$ is the dilatation rate) in this equation (Wei & Pollard 2011*b*, (3.7), p. 12) with decreasing Mach number (Wei & Pollard 2011*b*, figure 8, p. 13).

Foysi, Sarkar & Friedrich (2004) focused on the behaviour of pressure fluctuations p' in compressible turbulent plane channel flow, using the compressible analogue (Gerolymos *et al.* 2013, (A 1e), p. 46) of the incompressible flow Poisson equation for $\nabla^2 p'$ (Chou 1945), and found that the observed reduction with increasing Mach number of the absolute magnitude of pressure–strain correlations could be satisfactorily accounted for by mean-density stratification $\bar{\rho}(y)$, in line with Morkovin's hypothesis (Morkovin 1962), the terms associated with ρ' in Foysi *et al.* (2004, (4.1), p. 213) having marginal influence. This contrasts with the free shear-layer case, where acoustic propagation of ρ' effects (Pantano & Sarkar 2002, (4.7), p. 347) were found to be important (Mahle *et al.* 2007). Ghosh, Foysi & Friedrich (2010) also studied the case of compressible turbulent pipe flow and found again that Morkovin's hypothesis (Morkovin 1962) was applicable. The only potential issue in the analysis of compressible turbulent plane channel flow is that, as the Mach number increases, strong viscous heating (§ 3.1) substantially increases mean temperature in the centreline (outer) region, and radiative heat transfer may need to be taken into account. Nonetheless, computations by Ghosh *et al.* (2011) indicate that, although radiative heat transfer slightly reduces the effects of compressibility, its influence is not expected to be important for airflow at the Reynolds numbers investigated in the present work.

Several related studies concern the compressible turbulent ZPG boundary layer developing on a flat plate (Guarini *et al.* 2000; Maeder, Adams & Kleiser 2001; Pirozzoli, Grasso & Gatski 2004; Martín 2007; Duan, Beekman & Martín 2010, 2011; Bernardini & Pirozzoli 2011; Duan & Martín 2011; Lagha *et al.* 2011*a*,*b*; Shahab *et al.* 2011), covering, although in no systematic way, the range $\bar{M}_e \in [2.2, 8]$ and $\bar{T}_w \in [\bar{T}_e, 12\bar{T}_e]$ (where $(\cdot)_e$ indicates the boundary-layer edge). A few computations at higher Mach numbers (Duan *et al.* 2010; Lagha *et al.* 2011*b*) correspond to very high wall temperatures, for which more complex thermodynamics (Duan & Martín 2011) and/or radiative heat transfer (Ghosh *et al.* 2011) should be taken into account. In the boundary-layer case the external and wall temperatures can be chosen arbitrarily, independent of one another or of $\bar{M}_e$, contrary to the compressible plane channel case, where the difference $\bar{T}_{CL} - \bar{T}_w$ is the result of intense viscous heating (Coleman *et al.* 1995), and is therefore a unique function of the Mach and Reynolds numbers. More importantly, in the compressible plane channel case generated heat can only be evacuated across the walls, implying that $\bar{T}_w < \bar{T}_{CL}$, contrary to the boundary-layer studies where $\bar{T}_w \geqslant \bar{T}_e$ was invariably chosen, with the exception of the high-enthalpy cases studied by Duan *et al.* (2011, Table 2, p. 21). Guarini *et al.* (2000) studied a $\bar{M}_e \approxeq 2.5$ turbulent boundary layer along an adiabatic wall and explained the success (Guarini *et al.* 2000, figure 16, p. 18) of the HCB-modified (Huang *et al.* 1995, (4.10), p. 208) SRA by showing that this form implied the approximate equality of the correlation coefficients for wall-normal turbulent transport of velocity and temperature, namely $c_{u'v'} \approxeq -c_{T'v'}$ (Guarini *et al.* 2000, (4.20), p. 20), which was approximately satisfied over a large part of the boundary layer (Guarini *et al.* 2000, figure 19, p. 21). This conclusion on the validity of the HCB-modified (Huang *et al.* 1995, (4.10), p. 208) SRA has been confirmed in the other boundary-layer studies

(Maeder *et al.* 2001, figure 20, p. 208; Pirozzoli *et al.* 2004, figure 16, p. 540; Duan *et al.* 2010, figure 10, p. 431; Duan *et al.* 2011, figure 10, p. 255; Shahab *et al.* 2011, figure 20, p. 393) as well. Shahab *et al.* (2011, figures 18–19, pp. 390–391) presented budgets of the transport equations for the fluxes $\overline{\rho u_i'' T''}$, and Lagha *et al.* (2011*a*, figures 18–21, pp. 11–12) for the transport equation for the spanwise vorticity variance $\overline{\omega_z'^2}$, which was used to analyse the near-wall dynamics.

With the exception of the transport equations for the temperature-fluctuations variance (Tamano & Morinishi 2006) and fluxes (Shahab *et al.* 2011), the transport equations associated with the fluctuations of thermodynamic quantities have not been analysed in DNS studies of wall-turbulence. Nonetheless, these transport equations are necessary to understand the associated phenomena, and are used in theoretical and modelling studies of compressible turbulence. Taulbee & VanOsdol (1991) studied the transport equations for the density variance $\overline{\rho'^2}$ (Taulbee & VanOsdol 1991, (17), p. 4) and for the turbulent mass-flux $\overline{\rho' u_i'} = -\bar{\rho}^{-1}\overline{u_i''}$ (Taulbee & VanOsdol 1991, (23), p. 4), proposed closures for the unknown terms in these equations, and applied their model to supersonic ZPG turbulent boundary-layers ($\bar{M}_e \in \{1.7, 3, 4.7\}$). Although the absence of DNS data of compressible wall-bounded turbulence at that time (Taulbee & VanOsdol 1991) made impossible the term-by-term analysis of the equations and of the proposed closures, comparison with experimental data of $\overline{\rho'^2}$ and $\overline{u_i''}$ was encouraging (Taulbee & VanOsdol 1991, figures 1–3, p. 8). Yoshizawa (1992) developed a model for the density variance equation based on TSDIA (two-scale direct-interaction approximation), and remarked that closures obtained for various compressible terms (Yoshizawa 1992, (B7–B13), p. 3303) were proportional to $[\bar{\rho}^{-1}\rho']_{rms}$, suggesting that this is presumably the most generally applicable scaling of compressibility effects. Hamba & Blaisdell (1997) further developed this type of TSDIA-based closure, which they calibrated using DNS data of compressible homogeneous turbulence. Hamba (1999) used approximate transport equations for $\overline{p'^2}$ (Hamba 1999, (11), p. 1625) and $\overline{s'^2}$ (Hamba 1999, (12), p. 1625), in which all viscous terms, except for heat-conduction (Hamba 1999, (13), p. 1625), were dropped. Yoshizawa, Matsuo & Mizobuchi (2013) studied theoretically the transport equations for $\overline{\rho'^2}$, $\overline{\rho' u_i'}$ and $\overline{\rho' p'}$, but viscous terms were neglected from the outset. Finally, note that the equation for the dilatation variance $\overline{\Theta'^2}$ used by Erlebacher & Sarkar (1993, (16), p. 3244) can also be interpreted, because of the continuity equation (Gerolymos *et al.* 2013, (A 1b), p. 45), as a transport equation for $\overline{(\rho^{-1} D_t \rho)'^2}$ (where D_t is the substantial derivative).

In the present work we study the behaviour of the fluctuations of thermodynamic variables in low-Reynolds-number compressible turbulent plane channel flow. In § 2 we summarise the flow model (§ 2.1) and the DNS computations (§ 2.2), and recall the transport equations for the thermodynamic variables (§ 2.3) which are implied by the system of the Navier–Stokes equations (§ 2.1). In § 3 we discuss the basic scalings of compressible turbulent plane channel flow and study the effect of Mach and Reynolds numbers on turbulence structure (correlation coefficients). In § 4 we work out the transport equations for the variances and fluxes of $\{p', \rho', T'', s''\}$ and study their budgets obtained from DNS. Finally, in § 5 we summarise the basic results of the present analysis and discuss directions for further research.

2. Basic equations and DNS computations

The compressible Navier–Stokes equations (§ 2.1) used in the present DNS computations (§ 2.2) imply transport equations for the thermodynamic variables

(§ 2.3), from which transport equations for their variances and fluxes can be obtained. Favre averaging does not commute with differentiation, and care should be taken to avoid notational misuse of the operator $\widetilde{(\cdot)}$ (§ 2.4.2).

2.1. *Flow model*

The DNS computations were performed using the solver developed by Gerolymos, Sénéchal & Vallet (2010). The flow is modelled by the compressible Navier–Stokes equations (Gerolymos *et al.* 2010, (34–37), pp. 785–786)

$$\frac{\partial \rho}{\partial t}+\frac{\partial}{\partial x_\ell}(\rho u_\ell)=0 \tag{2.1a}$$

$$\frac{\partial \rho u_i}{\partial t}+\frac{\partial}{\partial x_\ell}(\rho u_i u_\ell)=-\frac{\partial p}{\partial x_i}+\frac{\partial \tau_{i\ell}}{\partial x_\ell}+\rho f_{V_i} \tag{2.1b}$$

$$\frac{\partial \rho e_t}{\partial t}+\frac{\partial}{\partial x_\ell}(\rho h_t u_\ell)=\frac{\partial}{\partial x_\ell}(u_m\tau_{m\ell}-q_\ell)+\rho f_{V_m}u_m \tag{2.1c}$$

with perfect-gas constant-c_p thermodynamics

$$p=\rho R_g T;\quad R_g=\text{const.};\quad c_p=\frac{\gamma}{\gamma-1}R_g=\text{const.};\quad c_v=\frac{R_g}{\gamma-1}=\text{const.};\quad a=\sqrt{\gamma\frac{p}{\rho}} \tag{2.1d}$$

and linear constitutive relations

$$\tau_{ij}=2\mu\left(\mathcal{S}_{ij}-\frac{1}{3}\Theta\delta_{ij}\right)+\mu_b\Theta\delta_{ij};\quad \mathcal{S}_{ij}:=\frac{1}{2}\left(\frac{\partial u_i}{\partial x_j}+\frac{\partial u_j}{\partial x_i}\right);\quad \Theta:=\frac{\partial u_\ell}{\partial x_\ell}=\mathcal{S}_{\ell\ell} \tag{2.1e}$$

$$q_i=-\lambda\frac{\partial T}{\partial x_i} \tag{2.1f}$$

with

$$\mu_b=0;\quad \mu(T)=\mu_0\left[\frac{T}{T_{\mu_0}}\right]^{3/2}\frac{\mathcal{S}_\mu+T_{\mu_0}}{\mathcal{S}_\mu+T};\quad \lambda(T)=\lambda_0\frac{\mu(T)}{\mu_0}[1+A_\lambda(T-T_{\mu_0})]. \tag{2.1g}$$

In (2.1), t is the time, $x_i\in\{x,y,z\}$ are the Cartesian space coordinates, $u_i\in\{u,v,w\}$ are the velocity components, h is the enthalpy, $h_t:=h+u_iu_i/2$ is the total enthalpy, $e_t:=e+u_iu_i/2=h_t-\rho^{-1}p$ is the total energy, e is the internal energy, $\boldsymbol{\tau}_{ij}$ is the viscous-stress tensor, q_i is the molecular heat flux, f_{V_i} are body-acceleration terms, R_g is the gas constant, γ is the isentropic exponent, c_p is the heat capacity at constant pressure, c_v is the heat capacity at constant volume (density), a is the sound speed, $\mathcal{S}_{ij}$ is the strain-rate tensor, Θ is the dilatation rate, μ is the dynamic viscosity, μ_b is the bulk viscosity and λ is the heat conductivity. The present computations model airflow, for which the various coefficients and constants are (Gerolymos 1990; Gerolymos *et al.* 2010) $R_g=287.04$ m^2 s^{-2} K^{-1}, $\gamma=1.4$, $\mu_0:=\mu(T_{\mu_0})=17.11\times10^{-6}$ Pa s, $T_{\mu_0}=273.15$ K, $\mathcal{S}_\mu=110.4$ K, $\lambda_0:=\lambda(T_{\mu_0})=0.0242$ W m^{-1} K^{-1}, $A_\lambda=0.00023$ K^{-1}.

$Re_{\tau\star}$	$\bar{M}_{CL}$	$N_x \times N_y \times N_z$	L_x	L_y	L_z	Δx^+	Δy_w^+	$N_{y^+\leqslant 10}$	Δy_{CL}^+	Δz^+	Δt^+	t_{OBS}^+	Δt_s^+
64	1.62	$137 \times 113 \times 201$	$8\pi\delta$	2δ	$4\pi\delta$	18.4	0.17	22	3.1	6.2	0.0115	988	0.0115
112	2.48	$801 \times 241 \times 1201$	$8\pi\delta$	2δ	$4\pi\delta$	15.5	0.18	21	5.4	5.1	0.0072	243	0.0072
113	1.51	$257 \times 129 \times 385$	$8\pi\delta$	2δ	$4\pi\delta$	16.6	0.21	21	4.7	5.5	0.0150	1373	0.0150
152	1.50	$345 \times 137 \times 529$	$8\pi\delta$	2δ	$4\pi\delta$	16.6	0.23	19	5.6	5.4	0.0166	1001	0.0166
150	1.50	$361 \times 149 \times 433$	$4\pi\delta$	2δ	$\frac{4}{3}\pi\delta$	7.9	0.22	19	4.7	2.1	0.0164	868	0.0164
176	0.34	$257 \times 129 \times 385$	$8\pi\delta$	2δ	$4\pi\delta$	17.6	0.23	20	5.0	5.8	0.0066	841	0.0066
176	0.34	$193 \times 129 \times 169$	$4\pi\delta$	2δ	$\frac{4}{3}\pi\delta$	11.7	0.22	20	4.9	4.4	0.0064	2329	0.0064
341	1.52	$801 \times 241 \times 1201$	$8\pi\delta$	2δ	$4\pi\delta$	16.3	0.19	21	5.7	5.4	0.0143	352	0.0143

TABLE 1. Parameters of the DNS computations (L_x, L_y, L_z (N_x, N_y, N_z) are the dimensions (number of grid points) of the computational domain (x is the homogeneous streamwise, y is the wall-normal and z is the homogeneous spanwise direction); δ is the channel half-height; Δx^+, Δy_w^+, Δy_{CL}^+, Δz^+ are the mesh sizes in wall units (3.2*a*); $(\cdot)_w$ denotes wall and $(\cdot)_{CL}$ centreline values; $N_{y^+\leqslant 10}$ is the number of grid points between the wall and $y^+ = 10$; $Re_{\tau\star} := \sqrt{\bar{\rho}_{CL}\,\bar{\tau}_w}\delta[\bar{\mu}_{CL}]^{-1}$ is the friction Reynolds number in HCB scaling (3.1*c*); $\bar{M}_{CL}$ is the centreline Mach number; Δt^+ is the computational time step in wall units (3.2*a*); t_{OBS}^+ is the observation period in wall units (3.2*a*) over which single-point statistics were computed; Δt_s^+ is the sampling time step for the single-point statistics in wall units (3.2*a*)).

2.2. *DNS computations*

DNS computations (table 1) were run using an $O(\Delta x^{17})$ upwind-biased scheme (Gerolymos, Sénéchal & Vallet 2009*b*) for the convective terms and an $O(\Delta x^2)$ conservative centred scheme (Gerolymos *et al.* 2010) for the viscous terms, using explicit dual-time-stepping time integration (Gerolymos, Sénéchal & Vallet 2009*a*). Statistics were acquired using an onboard moving-averages technique (Gerolymos *et al.* 2010, § 4.4, p. 791). The numerical methodology has been validated (Gerolymos *et al.* 2010, 2013) by comparison with standard DNS data for incompressible (Kim, Moin & Moser 1987; Moser, Kim & Mansour 1999; del Álamo *et al.* 2004) and compressible (Coleman *et al.* 1995; Lechner *et al.* 2001) fully developed turbulent channel flow, and carefully assessed (§ 4) for grid resolution and statistical convergence of results.

Following standard practice (Coleman *et al.* 1995), a spatially constant body acceleration f_{V_x} is applied in the streamwise direction to counteract viscous friction and to apply a target bulk massflow $\dot{m}_B$ (Gerolymos *et al.* 2010, (46b, 48), p. 791), bulk density ρ_B is maintained constant at every subiteration (Gerolymos *et al.* 2010, (46a, 47), p. 791), isothermal no-slip wall conditions are applied at $y \in \{0, 2\delta\}$ (Gerolymos *et al.* 2010, (45), p. 790), and periodic conditions are applied in the homogeneous streamwise (x) and spanwise (z) directions (Gerolymos *et al.* 2010, p. 790).

Note that the algebraic correction of density (Gerolymos *et al.* 2010, (46a, 47), p. 791) applied at every numerical subiteration to enforce constant ρ_B is tantamount to including a source term Q_ρ in the continuity equation. Detailed examination of the time evolution of the computations (table 1) reveals that this term is quite small (in wall units) and its influence (Q'_ρ should appear in most turbulence transport equations) was neglected, in line with standard practice (Coleman *et al.* 1995; Huang *et al.* 1995; Lechner *et al.* 2001; Morinishi, Tamano & Nakabayashi 2003; Foysi *et al.* 2004; Morinishi *et al.* 2004; Kreuzinger, Friedrich & Gatski 2006; Tamano &

$Re_{\tau^\star}$	$\bar{M}_{CL}$	M_{B_w}	M_{τ_w}	Re_{τ_w}	Re_{B_w}	Re_{θ_w}	$Re_{\theta_{CL}}$	$Re_{\theta_{CLw}}$	$\bar{T}_w$ (K)	$\bar{T}_{CL}/\bar{T}_w$	B_{q_w}	$\max_y[\rho'_{rms}/\bar{\rho}]$
64	1.62	1.50	0.0848	99	1300	238	129	168	298	1.417	−0.0508	0.04256
112	2.48	3.83	0.1299	494	4438	1638	196	459	298	3.540	−0.2000	0.14187
113	1.51	1.48	0.0825	169	2259	326	185	235	298	1.379	−0.0484	0.04390
152	1.50	1.50	0.0815	227	3100	439	249	316	298	1.383	−0.0485	0.04600
176	0.34	0.30	0.0191	180	2785	291	283	286	298	1.015	−0.0022	0.00237
341	1.52	1.56	0.0748	520	7813	1144	633	813	298	1.403	−0.0461	0.04900

TABLE 2. Global non-dimensional parameters of the large box ($L_x \times L_y \times L_z = 8\pi\delta \times 2\delta \times 4\pi\delta$) computations (table 1) ($Re_{\tau^\star}$ is the friction Reynolds number in HCB scaling (3.1*c*); $\bar{M}_{CL}$ (3.1*d*) is the centreline Mach number; M_{B_w} (3.1*a*) is the bulk Mach number; $M_{\tau_w} := \bar{a}_w^{-1} u_\tau$ is the friction Mach number based on u_τ (3.2*b*) and sound velocity at wall conditions; $Re_{\tau_w} := \bar{\rho}_w u_\tau \delta\, \bar{\mu}_w^{-1}$ (3.1*b*) is the friction Reynolds number; Re_{B_w} (3.1*a*) is the bulk Reynolds number; $Re_{\theta_w} := \bar{\rho}_w \bar{u}_{CL} \theta\, \bar{\mu}_w^{-1}$ is the momentum-thickness (θ) Reynolds number at wall conditions; $Re_{\theta_{CL}} := \bar{\rho}_{CL} \bar{u}_{CL} \theta\, \bar{\mu}_{CL}^{-1}$ is the momentum-thickness Reynolds number at centreline conditions; $Re_{\theta_{CLw}} := \bar{\rho}_{CL} \bar{u}_{CL} \theta\, \bar{\mu}_w^{-1}$ is the momentum-thickness Reynolds number with mixed scaling ($\bar{\rho}_{CL}$ and $\bar{\mu}_w$); $\bar{T}_{CL}$ is the centreline temperature; $\bar{T}_w$ is the wall temperature; $B_{q_w} := (\bar{\rho}_w u_\tau \bar{h}_w)^{-1} \bar{q}_w$ is the non-dimensional wall heat flux (Coleman *et al.* 1995); $\max_y[\bar{\rho}^{-1}\, \rho'_{rms}]$ is the maximum r.m.s. level of relative density fluctuations).

Morinishi 2006; Friedrich 2007; Gerolymos *et al.* 2010, 2013; Ghosh *et al.* 2010, 2011; Wei & Pollard 2011*a*,*b*).

In the present work we analyse DNS computations (table 1) covering, although without a systematic variation of both parameters, the range $Re_{\tau^\star} \in [64, 341]$ and $\bar{M}_{CL} \in [0.34, 2.48]$, corresponding to $Re_{\tau_w} \in [99, 525]$ and $M_{B_w} \in [0.3, 3.83]$ (table 2). Available DNS data (Coleman *et al.* 1995; Friedrich, Foysi & Sesterhenn 2006; Tamano & Morinishi 2006; Gerolymos *et al.* 2010; Wei & Pollard 2011*b*) cover the range $Re_{\tau^\star} \in [150,300]$ and $\bar{M}_{CL} \in [0.35, 2.25]$, again without systematic variation of both parameters. Previous grid-convergence studies with the present DNS solver (Gerolymos *et al.* 2010, figures 5–6, pp. 794–795) indicate that the computational grid resolution (table 1), in wall units, is adequate for the accurate computation of the various two-moment statistics analysed in the present work. For $(Re_{\tau^\star}, \bar{M}_{CL}) \in \{(150, 1.50), (176, 0.34)\}$, computations in a smaller box but with higher resolution (in wall units) were run (table 1), to verify the large-box computations, and, in the case $(Re_{\tau^\star}, \bar{M}_{CL}) = (150, 1.50)$, to obtain well-resolved statistics for the budgets of the transport equations (§ 4).

2.3. *Transport of thermodynamic variables*

Assuming bivariate thermodynamics (Liepmann & Roshko 1957; Kestin 1979), the knowledge of the transport equations for two thermodynamic variables suffices to obtain the transport equations for all of the others, using thermodynamic derivatives (Bridgman 1961; Kestin 1979). The fundamental conservation equations (2.1) already contain the transport equation for the density ρ, which follows from the continuity equation (2.1*a*). Furthermore they can be combined, by subtracting the momentum equation (2.1*b*) multiplied by u_i (kinetic energy equation) from the total energy equation (2.1*c*), to obtain the transport equation for the entropy s (White 1974; Sesterhenn 2001). Using thermodynamic derivatives (Bridgman 1961; Kestin 1979),

transport equations for p, T and h are readily obtained from the transport equations for ρ and s

$$\frac{\mathrm{D}p}{\mathrm{D}t} = \left(\frac{\partial p}{\partial \rho}\right)_s \frac{\mathrm{D}\rho}{\mathrm{D}t} + \left(\frac{\partial p}{\partial s}\right)_\rho \frac{\mathrm{D}s}{\mathrm{D}t} \tag{2.2a}$$

$$\frac{\mathrm{D}T}{\mathrm{D}t} = \left(\frac{\partial T}{\partial \rho}\right)_s \frac{\mathrm{D}\rho}{\mathrm{D}t} + \left(\frac{\partial T}{\partial s}\right)_\rho \quad \frac{\mathrm{D}s}{\mathrm{D}t} = \left(\frac{\partial T}{\partial p}\right)_s \frac{\mathrm{D}p}{\mathrm{D}t} + \left(\frac{\partial T}{\partial s}\right)_p \frac{\mathrm{D}s}{\mathrm{D}t} \tag{2.2b}$$

$$\frac{\mathrm{D}h}{\mathrm{D}t} = \left(\frac{\partial h}{\partial \rho}\right)_s \frac{\mathrm{D}\rho}{\mathrm{D}t} + \left(\frac{\partial h}{\partial s}\right)_\rho \quad \frac{\mathrm{D}s}{\mathrm{D}t} = \left(\frac{\partial h}{\partial p}\right)_s \frac{\mathrm{D}p}{\mathrm{D}t} + \left(\frac{\partial h}{\partial s}\right)_p \frac{\mathrm{D}s}{\mathrm{D}t} \tag{2.2c}$$

where $D_t(\cdot) := \partial_t(\cdot) + u_\ell \partial_{x_\ell}(\cdot)$ is the substantial derivative (Pope 2000, p. 13). For the perfect-gas thermodynamics (2.1*d*) used in the present DNS calculations, the thermodynamic derivatives in (2.2) can be expressed in terms of R_g and γ as (Liepmann & Roshko 1957; Bridgman 1961; Kestin 1979)

$$(2.1d) \Longrightarrow \begin{cases} \left(\dfrac{\partial p}{\partial \rho}\right)_s = a^2 = \gamma \dfrac{p}{\rho} & \left(\dfrac{\partial p}{\partial s}\right)_\rho = (\gamma - 1)\rho T \\ \left(\dfrac{\partial T}{\partial \rho}\right)_s = (\gamma - 1)\dfrac{T}{\rho} & \left(\dfrac{\partial T}{\partial s}\right)_\rho = \dfrac{T}{c_v} \\ \left(\dfrac{\partial T}{\partial p}\right)_s = \dfrac{1}{\rho c_p} & \left(\dfrac{\partial T}{\partial s}\right)_p = \dfrac{T}{c_p} \\ \left(\dfrac{\partial h}{\partial \rho}\right)_s = \dfrac{a^2}{\rho} = \gamma \dfrac{p}{\rho^2} & \left(\dfrac{\partial h}{\partial s}\right)_\rho = \gamma T \\ \left(\dfrac{\partial h}{\partial p}\right)_s = \dfrac{1}{\rho} & \left(\dfrac{\partial h}{\partial s}\right)_p = T \end{cases} \tag{2.3}$$

where $a := \sqrt{(\partial_\rho p)_s} \overset{(2.3)}{=} \sqrt{\gamma p \rho^{-1}} \overset{(2.1d)}{=} \sqrt{\gamma R_g T}$ is the sound speed. Combining the equations for $D_t\rho$ (2.1*a*) and $D_t s$, obtained by (2.1*b*), (2.1*c*), with (2.3), (2.2) yields

$$\frac{\mathrm{D}\rho}{\mathrm{D}t} = -\rho \frac{\partial u_\ell}{\partial x_\ell} \tag{2.4a}$$

$$\rho \frac{\mathrm{D}s}{\mathrm{D}t} = \frac{1}{T}\left(\tau_{m\ell} S_{m\ell} - \frac{\partial q_\ell}{\partial x_\ell}\right) \tag{2.4b}$$

$$\frac{\mathrm{D}p}{\mathrm{D}t} = -\gamma p \frac{\partial u_\ell}{\partial x_\ell} + (\gamma - 1)\left(\tau_{m\ell} S_{m\ell} - \frac{\partial q_\ell}{\partial x_\ell}\right) \tag{2.4c}$$

$$\rho \frac{\mathrm{D}T}{\mathrm{D}t} = -\frac{1}{c_v} p \frac{\partial u_\ell}{\partial x_\ell} + \frac{1}{c_v}\left(\tau_{m\ell} S_{m\ell} - \frac{\partial q_\ell}{\partial x_\ell}\right) \tag{2.4d}$$

$$= \frac{1}{c_p}\frac{\mathrm{D}p}{\mathrm{D}t} + \frac{1}{c_p}\left(\tau_{m\ell} S_{m\ell} - \frac{\partial q_\ell}{\partial x_\ell}\right) \tag{2.4e}$$

$$\rho \frac{\mathrm{D}h}{\mathrm{D}t} = -\gamma p \frac{\partial u_\ell}{\partial x_\ell} + \gamma\left(\tau_{m\ell} S_{m\ell} - \frac{\partial q_\ell}{\partial x_\ell}\right) \tag{2.4f}$$

$$= \frac{\mathrm{D}p}{\mathrm{D}t} + \left(\tau_{m\ell} S_{m\ell} - \frac{\partial q_\ell}{\partial x_\ell}\right). \tag{2.4g}$$

These transport equations (2.4) are the starting point for the analysis of the dynamics of the turbulent fluctuations of thermodynamic quantities. The material derivatives of pressure p (2.4*c*), temperature T (2.4*d*) and enthalpy h (2.4*f*), are expressed as the nonlinearly weighted sum of two terms, the first containing the dilatation rate $\Theta := \partial_{x_\ell} u_\ell$ (2.1*e*) which represents the opposite of the material derivative of relative density variations of a fluid particle $-\rho^{-1} D_t \rho$ (2.4*a*), and the second containing the viscous dissipation/conduction term $(\tau_{m\ell} S_{m\ell} - \partial_{x_\ell} q_\ell)$ which is responsible for the entropy variation of a fluid particle $\rho T D_t s$ (2.4*b*). In this respect, density and entropy are used as the independent thermodynamic variables. Therefore, the transport equations (2.4) clearly illustrate the coupling of entropy production $\rho T D_t s$ (2.4*b*) with the substantial derivatives of the other thermodynamic quantities $\{p,\ \rho,\ T\}$. This coupling may be non-negligible in regions of the flow where viscous effects (2.4*b*) are important, presumably in the near-wall region, and is related to the second-order theory of mode interaction (Chu & Kovásznay 1958).

Of course, under the assumption of perfect-gas thermodynamics (2.1*d*) the transport equations for temperature equation (2.4*d*) and enthalpy (2.4*f*) are identical (Liepmann & Roshko 1957; Bridgman 1961; Kestin 1979), under the constant proportionality coefficient c_p (2.1*d*), i.e. $D_t h = c_p D_t T$ (2.1*d*). Some authors (Canuto 1997; Le Ribault & Friedrich 1997), when studying the temperature variance and turbulent heat fluxes, prefer using the alternative equations (2.4*e*) for temperature or (2.4*g*) for enthalpy, which contain the material derivative of pressure $D_t p$ in lieu of the dilatation Θ (2.4*d*), (2.4*f*).

Recall also that for the thermodynamics (2.1*d*) assumed in the present work, integration of (2.2*b*), using the expressions (2.3) for $(\partial_p T)_s$ and $(\partial_s T)_p$, yields the expression of entropy as a function of (p, T) or (ρ, T)

$$(2.1d) \Longrightarrow \frac{s - s_{ISA}}{R_g} = \frac{\gamma}{\gamma - 1} \ln \frac{T}{T_{ISA}} - \ln \frac{p}{p_{ISA}} = \frac{1}{\gamma - 1} \ln \frac{T}{T_{ISA}} - \ln \frac{\rho}{\rho_{ISA}} \tag{2.5}$$

with respect to an arbitrary reference condition $(\cdot)_{ISA}$ (which was chosen here as the sea-level conditions of the international standard atmosphere, $T_{ISA} = 288.15$ K and $p_{ISA} = 101\,325$ Pa), implying by (2.1*d*) $\rho_{ISA} \approxeq 1.225055$ kg m^{-3}.

2.4. *Statistics and averaging*

Using (Huang *et al.* 1995, (2.1), p. 188) Reynolds decomposition for p and ρ and Favre decomposition for u_i, s, T and h, in (2.1*b*) and (2.4), we can work out transport equations for the variances ($\overline{\rho'^2}$, $\overline{p'^2}$, $\overline{\rho s''^2}$ and $\overline{\rho h''^2} \overset{(2.1d)}{=} c_p\, \overline{\rho T''^2}$) and the fluxes ($\overline{\rho' u_i'}$, $\overline{p' u_i'}$, $\overline{\rho s'' u_i''}$ and $\overline{\rho h'' u_i''} \overset{(2.1d)}{=} c_p\, \overline{\rho T'' u_i''}$) of the turbulent fluctuations of the thermodynamic state variables. The algebra for the development of the equations albeit straightforward is quite lengthy, but can be formulated in a systematic way.

2.4.1. *Reynolds and Favre decomposition*

The usual decompositions of the fluctuating quantities (Huang *et al.* 1995, (2.1), p. 188)

$$(\cdot) = \overline{(\cdot)} + (\cdot)' = \widetilde{(\cdot)} + (\cdot)'' \tag{2.6a}$$

are used consistently throughout the paper. In (2.6*a*), $(\cdot)$ denotes any flow quantity, $\overline{(\cdot)}$ denotes Reynolds (ensemble) averaging with fluctuations $(\cdot)'$ satisfying

$$\overline{(\cdot)'} = 0 \tag{2.6b}$$

and $\widetilde{(\cdot)}$ denotes Favre averaging with fluctuations $(\cdot)''$ defined by

$$\left.\begin{aligned}\widetilde{(\cdot)} &:= \frac{1}{\bar\rho}\overline{\rho\,(\cdot)}\\ (\cdot)'' &:= (\cdot) - \widetilde{(\cdot)}\end{aligned}\right\} \overset{(2.6a),(2.6b)}{\Longrightarrow} \begin{cases}\overline{\rho\,(\cdot)''} = 0\\ \overline{(\cdot)''} = -\dfrac{1}{\bar\rho}\overline{\rho'\,(\cdot)'} = \overline{(\cdot)} - \widetilde{(\cdot)}\\ (\cdot)'' = (\cdot)' + \overline{(\cdot)''}.\end{cases} \tag{2.6c}$$

Recall also that any two flow quantities $[\cdot]$ and $(\cdot)$ satisfy the important identity (Sarkar *et al.* 1991; Canuto 1997)

$$\overline{[\cdot]'\,(\cdot)''} = \overline{[\cdot]''\,(\cdot)'} = \overline{[\cdot]'\,(\cdot)'} \tag{2.6d}$$

which is readily obtained by replacing $(\cdot)'' \overset{(2.6c)}{=} (\cdot)' + \overline{(\cdot)''}$ and $[\cdot]'' \overset{(2.6c)}{=} [\cdot]' + \overline{[\cdot]''}$ in (2.6*d*).

2.4.2. *Need for additional notation*

Favre averaging defined by (2.6*c*) does not commute with differentiation, contrary to Reynolds averaging, because

$$\widetilde{\left(\frac{\partial(\cdot)}{\partial x_j}\right)} \overset{(2.6c)}{:=} \frac{1}{\bar\rho}\overline{\left(\rho\frac{\partial(\cdot)}{\partial x_j}\right)} \overset{(2.6a)}{:=} \frac{1}{\bar\rho}\overline{\left(\rho\frac{\partial\widetilde{(\cdot)}}{\partial x_j} + \rho\frac{\partial(\cdot)''}{\partial x_j}\right)} = \frac{\partial\widetilde{(\cdot)}}{\partial x_j} + \frac{1}{\bar\rho}\overline{\left(\rho\frac{\partial(\cdot)''}{\partial x_j}\right)} \tag{2.7a}$$

$$= \frac{\partial\widetilde{(\cdot)}}{\partial x_j} + \frac{1}{\bar\rho}\left(\frac{\partial\overline{\rho\,(\cdot)''}}{\partial x_j} - \overline{(\cdot)''\frac{\partial\rho}{\partial x_j}}\right) \overset{(2.6c)}{:=} \frac{\partial\widetilde{(\cdot)}}{\partial x_j} - \frac{\overline{(\cdot)''}}{\bar\rho}\frac{\partial\rho}{\partial x_j}. \tag{2.7b}$$

In the same way, the Favre-fluctuation operator $(\cdot)''$ (2.6*c*) does not commute with differentiation, and we have by straightforward computation

$$\frac{\partial(\cdot)''}{\partial x_j} \overset{(2.6a)}{=} \frac{\partial(\cdot)}{\partial x_j} - \frac{\partial\widetilde{(\cdot)}}{\partial x_j} \neq \left(\frac{\partial(\cdot)}{\partial x_j}\right)'' \overset{(2.6c)}{:=} \frac{\partial(\cdot)}{\partial x_j} - \widetilde{\left(\frac{\partial(\cdot)}{\partial x_j}\right)}$$

$$\overset{(2.6a),(2.7a)}{=} \frac{\partial(\cdot)''}{\partial x_j} - \frac{1}{\bar\rho}\overline{\left(\rho\frac{\partial(\cdot)''}{\partial x_j}\right)} \tag{2.7c}$$

$$\overset{(2.6a),(2.7b)}{=} \frac{\partial(\cdot)''}{\partial x_j} + \frac{\overline{(\cdot)''}}{\bar\rho}\frac{\partial\rho}{\partial x_j}. \tag{2.7d}$$

Often in the development of transport equations appear terms of the form $\partial_{x_j}\widetilde{(\cdot)}$ or $\partial_{x_j}(\cdot)''$, especially for the strain-rate tensor $\mathcal{S}_{ij}$ (2.1*e*) or for the dilatation rate $\Theta := \partial_{x_\ell}u_\ell = S_{\ell\ell}$ (2.1*e*). To avoid the inconsistent, yet widespread, notation $\tilde{\mathcal{S}}_{ij}$ or $\mathcal{S}''_{ij}$ ($\tilde\Theta$ or Θ'') for such terms it is useful to introduce a new decomposition

$$\mathcal{S}_{ij} = \breve{\mathcal{S}}_{ij} + \mathcal{S}^{\shortparallel}_{ij}; \quad \breve{\mathcal{S}}_{ij} := \frac{1}{2}\left(\frac{\partial\tilde u_i}{\partial x_j} + \frac{\partial\tilde u_j}{\partial x_i}\right); \quad \mathcal{S}^{\shortparallel}_{ij} := \frac{1}{2}\left(\frac{\partial u_i''}{\partial x_j} + \frac{\partial u_j''}{\partial x_i}\right) \tag{2.8a}$$

$$\Theta = \breve\Theta + \Theta^{\shortparallel}; \quad \breve\Theta := \frac{\partial\tilde u_\ell}{\partial x_\ell}; \quad \Theta^{\shortparallel} := \frac{\partial u_\ell''}{\partial x_\ell}. \tag{2.8b}$$

Quantities $\breve{(\cdot)}$ are not averages, but functions of averaged quantities (Gerolymos & Vallet 1996), and are different from Favre averages, because by (2.7*b*)

$$\tilde{\mathcal{S}}_{ij} \overset{(2.1e),(2.7b),(2.8a)}{=} \breve{\mathcal{S}}_{ij} - \frac{1}{2}\left(\frac{\overline{u_i''}}{\bar\rho}\frac{\partial\rho}{\partial x_j} + \frac{\overline{u_j''}}{\bar\rho}\frac{\partial\rho}{\partial x_i}\right) \tag{2.8c}$$

$$\tilde{\Theta} \overset{(2.7b),(2.8a)}{=} \breve{\Theta} - \overline{\frac{u''_\ell}{\bar{\rho}} \frac{\partial \rho}{\partial x_\ell}}. \tag{2.8d}$$

Finally, note that identity (2.6*d*) also holds for S''_{ij} and Θ'', i.e.

$$\overline{(\cdot)'[\cdot]''} = \overline{(\cdot)''[\cdot]'} = \overline{(\cdot)'[\cdot]'}; \quad \overline{(\cdot)'S''_{ij}} = \overline{(\cdot)'S'_{ij}}; \quad \overline{(\cdot)'\Theta''} = \overline{(\cdot)'\Theta'} \tag{2.8e}$$

as can be verified by replacing $S''_{ij} \overset{(2.6a),(2.8a)}{=} \breve{S}_{ij} - \breve{S}_{ij} + S'_{ij}$ and $\Theta'' \overset{(2.6a),(2.8b)}{=} \breve{\Theta} - \breve{\Theta} + \Theta'$ in (2.8*e*).

3. Scalings

In addition to Re scaling which uniquely defines incompressible plane channel flow (Moser *et al.* 1999), M-scaling with respect to a representative Mach number is necessary in the compressible flow case (Coleman *et al.* 1995; Huang *et al.* 1995).

3.1. *Compressible channel flow*

In Coleman *et al.* (1995), the DNS operating point was defined by a bulk Reynolds number Re_{B_w} and a bulk Mach number M_{B_w}, defined as

$$Re_{B_w} := \frac{\bar{\rho}_B \breve{u}_B \delta}{\bar{\mu}_w}; \quad M_{B_w} := \frac{\breve{u}_B}{\bar{a}_w} \tag{3.1a}$$

where $\bar{\mu}_w$ is the dynamic viscosity at the wall, $\bar{a}_w$ is the sound-speed at the wall (in the isothermal wall case studied here, $T_w = \bar{T}_w = \breve{T}_w = \text{const.}$, so that $\bar{\mu}_w \overset{(2.1g)}{=} \mu(T_w)$ and $\bar{a}_w \overset{(2.1d)}{=} a(T_w)$), and the subscript $(\cdot)_B$ denotes volume averaging over the entire computational domain (Gerolymos *et al.* 2010, (46), p. 791). Huang *et al.* (1995) found that the standard wall coordinates and friction Reynolds number

$$y^+ := \frac{\bar{\rho}_w \sqrt{\dfrac{\bar{\tau}_w}{\bar{\rho}_w}} (y - y_w)}{\bar{\mu}_w}; \quad Re_{\tau_w} := \delta^+ \tag{3.1b}$$

did not correctly represent the effect of rapid wall-normal variation $\bar{\rho}(y)$ and $\bar{\mu}(y)$ near the wall, and did a poor job in collapsing profiles of different variables. They suggested instead an empirical mixed scaling

$$y^\star := \frac{\bar{\rho}(y) \sqrt{\dfrac{\bar{\tau}_w}{\bar{\rho}(y)}} (y - y_w)}{\bar{\mu}(y)} \overset{(3.1b)}{=} \frac{\sqrt{\dfrac{\bar{\rho}(y)}{\bar{\rho}_w}}}{\dfrac{\bar{\mu}(y)}{\bar{\mu}_w}} y^+; \quad Re_{\tau^\star} := \delta^\star = \frac{\sqrt{\dfrac{\bar{\rho}_{CL}}{\bar{\rho}_w}}}{\dfrac{\bar{\mu}_{CL}}{\bar{\mu}_w}} \delta^+ \tag{3.1c}$$

that we will call hereafter HCB scaling (Huang *et al.* 1995), and which has proven useful in approximately collapsing the profiles of the Reynolds stresses (Foysi *et al.* 2004; Morinishi *et al.* 2004) for different values of (Re_{B_w}, M_{B_w}).

Since the wall is colder than the centreline region ($\bar{T}_{CL} > \bar{T}_w$) in the compressible plane channel case (Coleman *et al.* 1995, table 3, p. 169), the centreline Mach number

$$\bar{M}_{CL} := \overline{\left(\frac{u_{CL}}{a_{CL}}\right)}; \quad \breve{M}_{CL} := \frac{\breve{u}_{CL}}{\breve{a}_{CL}} \tag{3.1d}$$

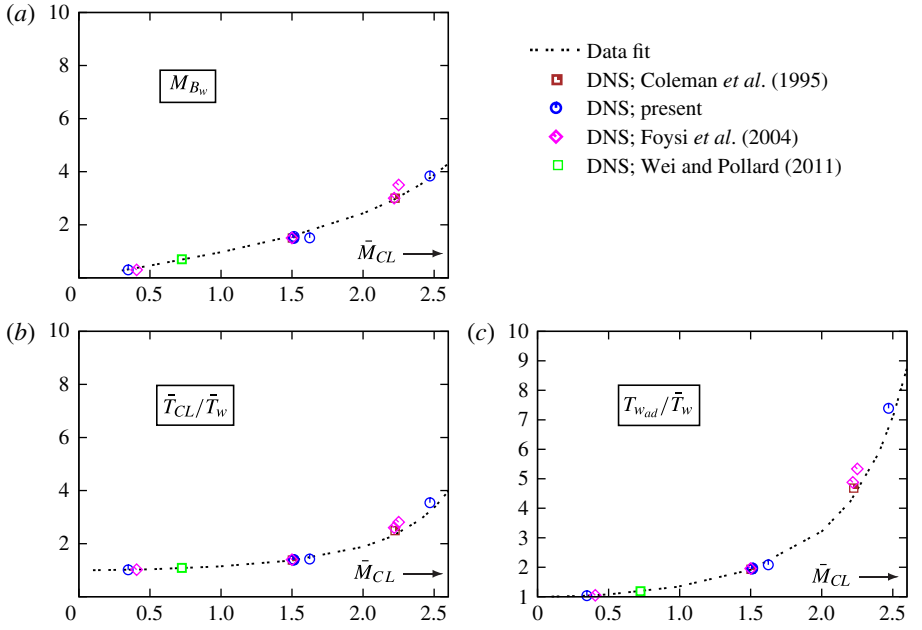

FIGURE 1. (Colour online) Evolution of bulk Mach number M_{B_w} (3.1*a*), ratio of centreline-to-wall static temperatures, and wall-to-theoretical-adiabatic-wall temperatures (3.1*e*), as a function of centreline Mach number $\bar{M}_{CL}$ (3.1*d*), for various Reynolds numbers, using the present large-box DNS results (table 2) and other available DNS data (Coleman *et al.* 1995; Foysi *et al.* 2004; Friedrich *et al.* 2006; Wei & Pollard 2011*a*,*b*).

where $\breve{a}_{CL} \overset{(2.1d)}{:=} \sqrt{\gamma R_g \tilde{T}_{CL}}$, is systematically smaller than the bulk Mach number M_{B_w} (3.1*a*), mainly (table 2) because of the difference in the sound speeds appearing in (3.1*a*), (3.1*d*). Both definitions in (3.1*d*) can be used and are numerically very close.

The non-dimensional form (Coleman *et al.* 1995, (3), p. 161) of the static temperature equation (2.4*e*) suggests that viscous heating $\overline{\tau_{m\ell} S_{m\ell}}$ increases with Mach number, thus increasing the centreline temperature $\bar{T}_{CL}$ compared with wall temperature $\bar{T}_w$ (figure 1). This increase is nonlinear with $\bar{M}_{CL}$ and the ratio $[\bar{T}_w^{-1}\,\bar{T}_{CL}]$ rises sharply when $\bar{M}_{CL} \gtrapprox 2$ (figure 1). Since the sound speed varies as $\sqrt{T}$ (2.1*d*), the ratio of $\breve{a}_{CL}$ to $\bar{a}_w$ increases, and so does the ratio of M_{B_w} (3.1*a*) to $\bar{M}_{CL}$ (3.1*d*), nonlinearly with $\bar{M}_{CL}$ (figure 1). Thus, for the present computations, $\bar{M}_{CL} \approxeq 2.48$ corresponds to $M_{B_w} \approxeq 3.83$ (figure 1). A more careful examination of the data (table 2) indicates also a slight dependence on Reynolds number. Therefore, M scalings with M_{B_w} (3.1*a*) or $\bar{M}_{CL}$ (3.1*d*) are not equivalent, and, for instance, the coefficients of variation of thermodynamic fluctuations ($[\bar{\rho}^{-1}\rho']_{rms}$, $[\bar{p}^{-1}p']_{rms}$ and $[\bar{T}^{-1}T']_{rms}$) may scale with some power of either $\bar{M}_{B_w}$ or $\bar{M}_{CL}$, but not both. It will be shown in the following (§ 3.4) that, contrary to usual practice (Huang *et al.* 1995; Friedrich 2007), the centreline Mach number $\bar{M}_{CL}$ scales better the data.

Obviously, the wall is colder than the centreline region (figure 1), as was the case of the boundary-layer computations of Duan & Martín (2011, table 2, p. 31). However, in the plane channel case, the viscous heating that is responsible for the high temperatures in the centreline region is part of the solution, and temperature ratio $\bar{T}_w^{-1}\,\bar{T}_{CL}$ increases (table 2), the wall getting colder relative to the centreline

region, with increasing $\bar{M}_{CL}$. This can be better quantified by comparing $\bar{T}_w$ with the theoretical adiabatic wall temperature (Schlichting 1979, (23.35)–(23.36), pp. 713–714)

$$T_{w_{ad}} := \bar{T}_{CL}\left(1 + r_f \frac{\gamma-1}{2}\bar{M}_{CL}^2\right); \quad r_f := 0.89 \tag{3.1e}$$

where the value of the recovery factor r_f (3.1*e*) is appropriate for airflow. The ratio $\bar{T}_w^{-1}T_{w_{ad}}$ increases rapidly with $\bar{M}_{CL}$, from $\bar{T}_w^{-1}T_{w_{ad}} \approxeq 2$ at $\bar{M}_{CL}=1.5$ to $\bar{T}_w^{-1}T_{w_{ad}} \approxeq 7.5$ at $\bar{M}_{CL}=2.5$, which corresponds to the boundary-layer temperature ratios studied in Duan & Martín (2011, table 2, p. 31). Note that all of the DNS computations, reported in the present work, apply the same constant wall temperature $T_w = \bar{T}_w = \tilde{T}_w = 298$ K (table 2), so that the highest local temperature $\bar{T}_{CL}(Re_{\tau^\star}=112, \bar{M}_{CL}=2.48) \approxeq 1055$ K is far from dissociation limits (Hansen 1958, figure 1, p. 57) which would invalidate the perfect-gas equation of state (2.1*d*) approximation. On the other hand, the variation of $c_p(T)$ in this temperature range $\bar{T} \in [298, 1055]$ is $\sim$10 % (Eckert & Drake 1972, pp. 64–66, 780) and should be taken into account in future studies.

3.2. *Wall units*

In line with standard incompressible (Kim *et al.* 1987) and compressible (Coleman *et al.* 1995) wall-bounded flow analysis, the independent variables, in wall units, are defined as

$$t^+ := \frac{t}{\left(\frac{\breve{\nu}_w}{u_\tau^2}\right)}; \quad x_i^+ := \frac{x_i - \delta_{iy}y_w}{\left(\frac{\breve{\nu}_w}{u_\tau}\right)} \tag{3.2a}$$

where the term $\delta_{iy}y_w$ serves to position the lower wall at $y^+=0$, and

$$u_\tau := \sqrt{\frac{\bar{\tau}_w}{\bar{\rho}_w}}; \quad \breve{\nu}_w := \frac{\bar{\mu}_w}{\bar{\rho}_w}. \tag{3.2b}$$

A consistent scaling is chosen for the non-dimensionalisation of the thermodynamic variables, i.e. one for which the flow (2.1), (2.4) retains exactly the same form when written in wall units, without the appearance of non-dimensional numbers (Mach, Reynolds, ...). Therefore, by (2.1*a–c*),

$$u_i^+ := \frac{u_i}{u_\tau}; \quad \rho^+ := \frac{\rho}{\bar{\rho}_w}; \quad p^+ := \frac{p}{\bar{\tau}_w}; \quad \tau_{ij}^+ := \frac{\tau_{ij}}{\bar{\tau}_w}; \quad h^+ := \frac{h}{u_\tau^2}; \quad q_i^+ := \frac{q_i}{\bar{\rho}_w u_\tau^3}. \tag{3.2c}$$

Obviously, the choices (3.2*c*) for the thermal quantities, h and q_i, are dictated by the scaling of the dynamic field. Choosing $\tilde{T}_w$ as the wall unit for T (Gatski & Bonnet 2009, p. 193), and requiring that (2.1), (2.4) hold in wall units without the appearance of non-dimensional numbers, yields

$$T^+ := \frac{T}{\tilde{T}_w}; \quad R_g^+ := \frac{R_g}{\left(\frac{\bar{\tau}_w}{\bar{\rho}_w\tilde{T}_w}\right)} \overset{(2.1d)}{=} \bar{p}_w^+; \quad c_p^+ := \frac{\gamma}{\gamma-1}R_g^+; \quad \gamma^+ := \gamma \tag{3.2d}$$

$$s^+ := \frac{s}{\left(\frac{\bar{\tau}_w}{\bar{\rho}_w\tilde{T}_w}\right)} \overset{(3.2d)}{\Longrightarrow} \frac{s^+}{R_g^+} = \frac{s}{R_g}; \quad \mu^+ := \frac{\mu}{\bar{\mu}_w}; \quad \lambda^+ := \frac{\lambda}{\left(\frac{\bar{\mu}_w u_\tau^2}{\tilde{T}_w}\right)} \tag{3.2e}$$

where the relation for R_g^+ is obtained from the state equation (2.1*d*), the relation for c_p^+ to satisfy the definition $c_p := (\partial_T h)_p$ (Kestin 1979, (2.43b), p. 552), the relation for s^+ to satisfy the definition $T\mathrm{d}s = \mathrm{d}h - \rho^{-1}\,\mathrm{d}p$ of entropy (Kestin 1979, table 12.1, p. 536), the definition of μ^+ to satisfy the stress–strain relation (2.1*e*), and the definition of λ^+ to satisfy Fourier's law (2.1*f*).

3.3. *Near-wall flow structure*

The near-wall instantaneous streamwise-velocity field exhibits the well-known organisation in streaks (Coleman *et al.* 1995; Jeong *et al.* 1997; Chernyshenko & Baig 2005), as can be seen for instance at $y^+ \approxeq 9.80$ for the $(Re_{\tau^\star}, \bar{M}_{CL}) = (341, 1.52)$ case (figure 2; the actual variation is $-7.17 \lessapprox u'^+ \lessapprox 12.23$).

The organisation in streaks is also clearly visible in the temperature (the actual variation is $-0.158 \lessapprox T'^+ \lessapprox 0.195$), density (the actual variation is $-0.161 \lessapprox \rho'^+ \lessapprox 0.152$) and entropy (the actual variation is $-0.466 \lessapprox s' R_g^{-1} \lessapprox 0.4657$) fields (figure 2). In contrast the pressure field (the actual variation is $-26.47 \lessapprox p'^+ \lessapprox 17.28$; figure 2) which is dominated by long-range interactions (Kim 1989; Chang, Piomelli & Blake 1999) has a different xz-organisation. For the snapshot (figure 2) of the $(Re_{\tau^\star}, \bar{M}_{CL}) = (341, 1.52)$ case at $y^+ \approxeq 9.80$, the instantaneous Mach number $M \in [0.079, 1.265]$, with subsonic fluctuation $M'' \in [-0.4700, 0.7154]$, where

$$M'' := M - \breve{M}; \quad \breve{M} := \frac{\tilde{u}}{\sqrt{\gamma R_g \tilde{T}}}. \tag{3.3}$$

3.4. *HCB scaling and $\bar{M}_{CL}$ scaling*

Examination of the profiles, plotted against y^+ (3.1*b*), of various flow statistics (figure 3), obtained from the DNS computations (table 1), illustrates the influence of $(Re_{\tau^\star}, \bar{M}_{CL})$, or equivalently (table 2) of (Re_{τ_w}, M_{B_w}). The deficit from unity of the maximum shear Reynolds stress in wall units, $\max_y[-\overline{\rho u'' v''}]^+$, quantifies the importance of viscous effects for each configuration, since the averaged streamwise-momentum equation (2.1*b*) reads $\bar{\tau}_{xy}^+ - [\overline{\rho u'' v''}]^+ = 1 - Re_{\tau_w}^{-1} y^+ = 1 - Re_{\tau^\star}^{-1} y^\star$. Obviously (figure 3), $Re_{\tau^\star}$ correlates well with the relative importance of viscous effects, contrary to Re_{τ_w} (table 2), in agreement with the arguments in justification of the HCB scaling (Huang *et al.* 1995). The $(Re_{\tau^\star}, \bar{M}_{CL}) = (64, 1.62)$ channel is a very-low-Re configuration, where the viscous shear stress dominates the flow, since $\max_y[-\overline{\rho u'' v''}]^+ \approxeq 0.35$ (figure 3), comparable with incompressible very-low-Re computations (Hu, Morfey & Sandham 2006). Furthermore, the $(Re_{\tau^\star}, \bar{M}_{CL}) \in \{(113, 1.51), (112, 2.48)\}$ channels which have different Re_{τ_w} (169 and 494, respectively; table 2), but approximately equal $Re_{\tau^\star}$ reach similar levels of $\max_y[-\overline{\rho u'' v''}]^+$ (figure 3).

Consideration (figure 3) of the van Driest-transformed velocity (Coleman *et al.* 1995, (6), p. 174)

$$\breve{u}_{VD}^+ := \int_0^{y^+} \sqrt{\frac{\bar{\rho}}{\bar{\rho}_w}}\,\frac{\mathrm{d}\bar{u}^+}{\mathrm{d}Y^+}\,\mathrm{d}Y^+ \tag{3.4}$$

confirms that $Re_{\tau^\star}$ is a representative Reynolds number in comparing flows with different $\bar{M}_{CL}$. As $Re_{\tau^\star}$ increases (figure 3), $\breve{u}_{VD}^+$ approaches a logarithmic zone, the $(Re_{\tau^\star}, \bar{M}_{CL}) = (341, 1.52)$ data following reasonably well $(\ln y^+)/0.4 + 5.5$ for $y^+ \gtrapprox 20$ and so do the $(Re_{\tau^\star}, \bar{M}_{CL}) = (176, 0.34)$ data (figure 3). Note the similar Re_{τ_w}-behaviour of the incompressible DNS data of Hu *et al.* (2006, figure (1.a), p. 1543). The low-Re effects in the $(Re_{\tau^\star}, \bar{M}_{CL}) \in \{(64, 1.62), (112, 2.48)\}$ channels

$Re_{\tau^\star}$	$\bar{M}_{CL}$	$N_x \times N_y \times N_z$	L_x	L_y	L_z	Δx^+	Δy^+_w	$N_{y^+\leqslant 10}$	Δy^+_{CL}	Δz^+	Δt^+	t^+_{OBS}	Δt^+_s
341	1.52	$801 \times 241 \times 1201$	$8\pi\delta$	2δ	$4\pi\delta$	16.3	0.19	21	5.7	5.4	0.0143	352	0.0143

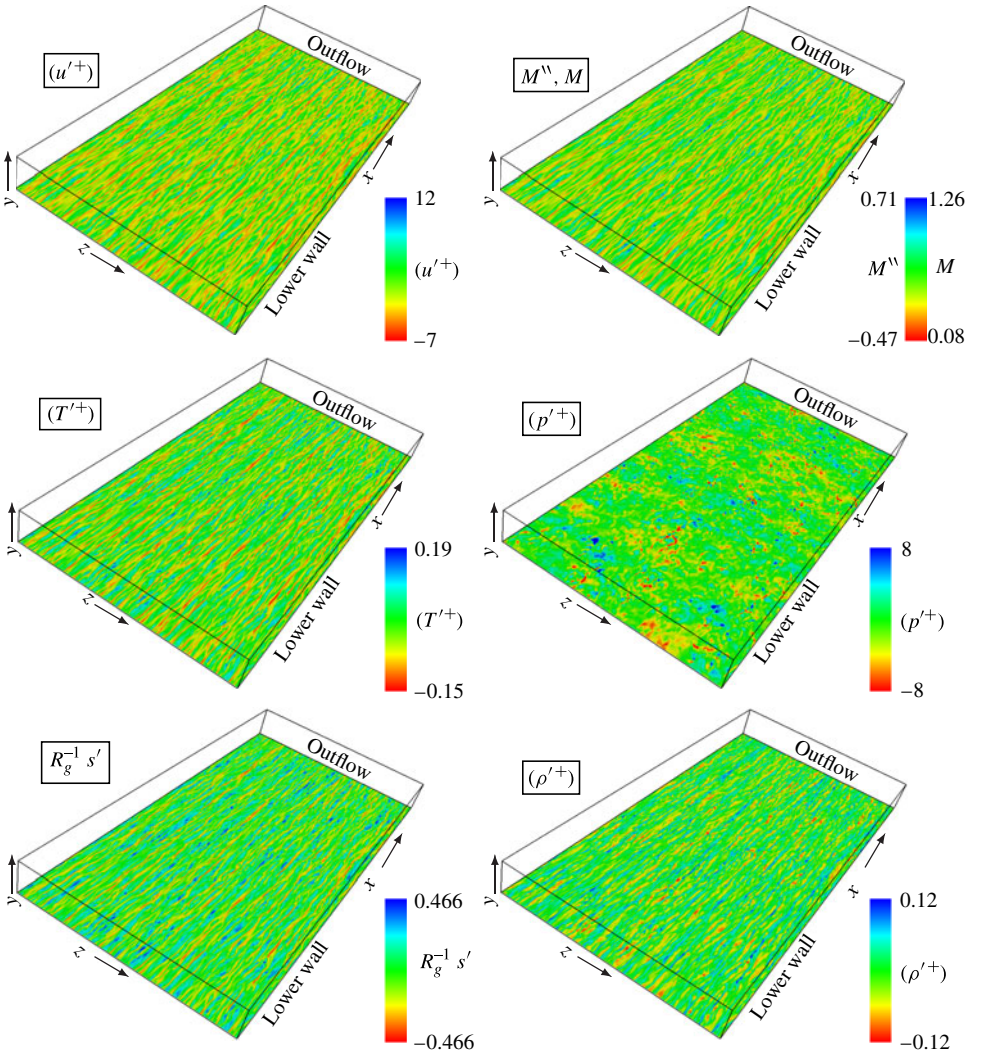

FIGURE 2. Near-wall ($y^+ \approxeq 9.80 \overset{(3.1)}{\Longleftrightarrow} y^* \approxeq 8.96$) instantaneous level plots of streamwise velocity (u'^+), Mach number (M'', M), temperature (T'^+), pressure (p'^+), non-dimensional entropy ($R_g^{-1}\, s'$) and density (ρ'^+), in wall units (3.2), obtained from DNS computations ($Re_{\tau^*} \approxeq 341$, $\bar{M}_{CL} \approxeq 1.52$; table 1).

are clearly seen, in the $\breve{u}^+_{VD}$ plots (figure 3). Mean density $\bar{\rho}^+$ decreases and mean temperature $\tilde{T}^+$ increases with y^+ (figure 3), with a clear $\bar{M}_{CL}$-dependence in these distributions. The strong $\bar{M}_{CL}$-dependence of the distributions of $\bar{\rho}^+ \leqslant 1$ and $\tilde{T}^+ \geqslant 1$ (figure 3) masks the influence of $Re_{\tau^\star}$. On the other hand, their product $(\bar{p}^+_w)^{-1}\bar{p}^+ \overset{(3.2d)}{=} (R^+_g)^{-1}\bar{p}^+ \overset{(2.1d),(2.6),(3.2)}{=} \bar{\rho}^+\tilde{T}^+ \leqslant 1$ is close to unity $\forall(Re_{\tau^\star}, \bar{M}_{CL})$,

	$Re_{\tau^\star}$	$\bar{M}_{CL}$	$N_x \times N_y \times N_z$	L_x	L_y	L_z	Δx^+	Δy_w^+	$N_{y^+\leqslant 10}$	Δy_{CL}^+	Δz^+	Δt^+	t_{OBS}^+	Δt_s^+
------	64	1.62	$137 \times 113 \times 201$	$8\pi\delta$	2δ	$4\pi\delta$	18.4	0.17	22	3.1	6.2	0.0115	989	0.0115
– · – ·	112	2.48	$801 \times 241 \times 1201$	$8\pi\delta$	2δ	$4\pi\delta$	15.5	0.18	21	5.4	5.1	0.0072	243	0.0072
– · · – · ·	113	1.51	$257 \times 129 \times 385$	$8\pi\delta$	2δ	$4\pi\delta$	16.6	0.21	21	4.7	5.5	0.0150	1373	0.0150
———	152	1.50	$345 \times 137 \times 529$	$8\pi\delta$	2δ	$4\pi\delta$	16.6	0.23	19	5.6	5.4	0.0166	1001	0.0166
·····	176	0.34	$257 \times 129 \times 385$	$8\pi\delta$	2δ	$4\pi\delta$	17.6	0.23	20	5.0	5.8	0.0066	841	0.0066
·····	341	1.52	$801 \times 241 \times 1201$	$8\pi\delta$	2δ	$4\pi\delta$	16.3	0.19	21	5.7	5.4	0.0143	352	0.0143

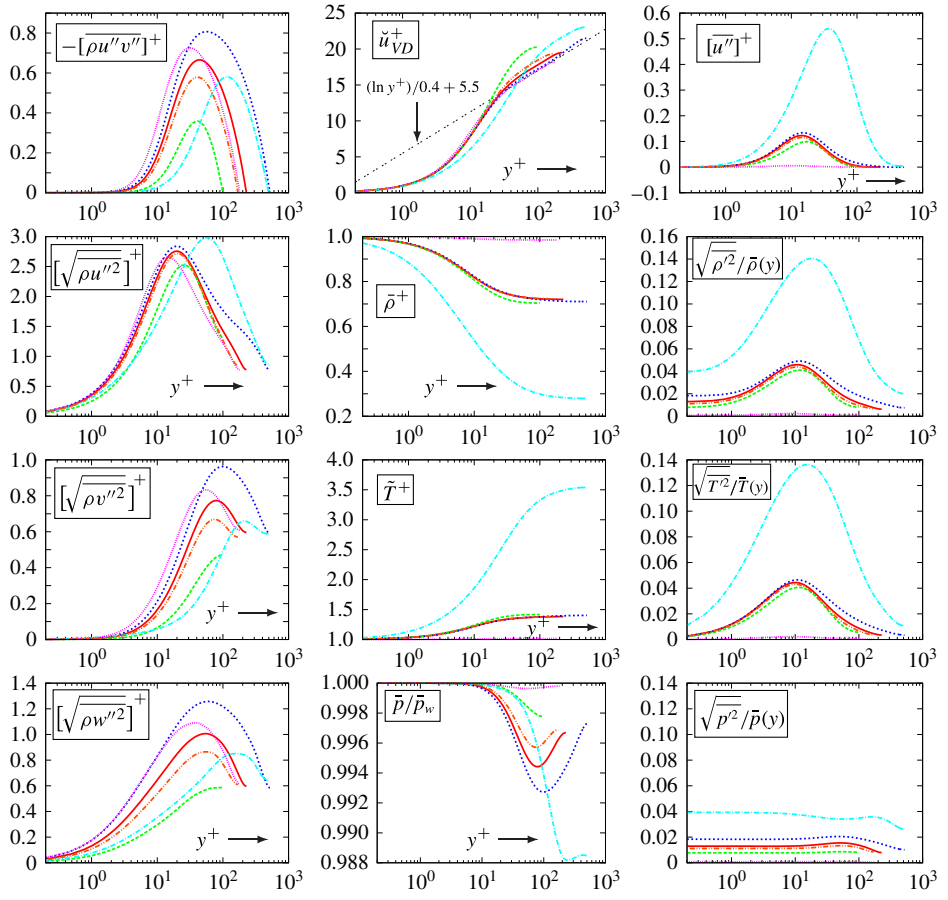

FIGURE 3. (Colour online) DNS (table 1) results for the profiles of Reynolds stresses in wall units $[\overline{\rho u_i'' u_j''}]^+$, of the van Driest-transformed (3.5) mean velocity $\breve{u}_{VD}^+$, of the evolution of mean thermodynamic variables relative to their wall values ($\bar{\rho}_w^{-1}\bar{\rho} \overset{(3.2c)}{=} \bar{\rho}^+$, $\tilde{T}_w^{-1}\tilde{T} \overset{(3.2d)}{=} \tilde{T}^+$ and $\bar{p}_w^{-1}\bar{p}$), of the Reynolds average of the Favre fluctuations of the streamwise velocity in wall units $[\overline{u''}]^+$, and of the relative r.m.s. levels of thermodynamic variables ($\bar{\rho}^{-1}\,\rho'_{rms}$, $\bar{T}^{-1}\,T'_{rms}$ and $\bar{p}^{-1}\,p'_{rms}$), plotted against y^+ (3.1*b*).

exhibiting dependence on both of these parameters. Concerning the streamwise mass flux $[\overline{u''}]^+ \overset{(2.6c)}{=} -[\bar{\rho}^{-1}\overline{\rho' u'}]^+$, there is, expectedly, a clear $\bar{M}_{CL}$-dependence which is also observed (figure 3) in the coefficients of variation of density and temperature ($[\bar{\rho}^{-1}\rho']_{rms}$ and $[\bar{T}^{-1}T']_{rms}$), while the coefficient of variation of pressure ($[\bar{p}^{-1}p']_{rms}$) shows strong dependence on both parameters, $Re_{\tau^\star}$ and $\bar{M}_{CL}$ (figure 3).

	$Re_{\tau^\star}$	$\bar{M}_{CL}$	$N_x \times N_y \times N_z$	L_x	L_y	L_z	Δx^+	Δy_w^+	$N_{y^+\leqslant 10}$	Δy_{CL}^+	Δz^+	Δt^+	t_{OBS}^+	Δt_s^+
------	64	1.62	$137 \times 113 \times 201$	$8\pi\delta$	2δ	$4\pi\delta$	18.4	0.17	22	3.1	6.2	0.0115	989	0.0115
-·-·-	112	2.48	$801 \times 241 \times 1201$	$8\pi\delta$	2δ	$4\pi\delta$	15.5	0.18	21	5.4	5.1	0.0072	243	0.0072
-·-·-	113	1.51	$257 \times 129 \times 385$	$8\pi\delta$	2δ	$4\pi\delta$	16.6	0.21	21	4.7	5.5	0.0150	1373	0.0150
———	152	1.50	$345 \times 137 \times 529$	$8\pi\delta$	2δ	$4\pi\delta$	16.6	0.23	19	5.6	5.4	0.0166	1001	0.0166
·····	176	0.34	$257 \times 129 \times 385$	$8\pi\delta$	2δ	$4\pi\delta$	17.6	0.23	20	5.0	5.8	0.0066	841	0.0066
·····	341	1.52	$801 \times 241 \times 1201$	$8\pi\delta$	2δ	$4\pi\delta$	16.3	0.19	21	5.7	5.4	0.0143	352	0.0143

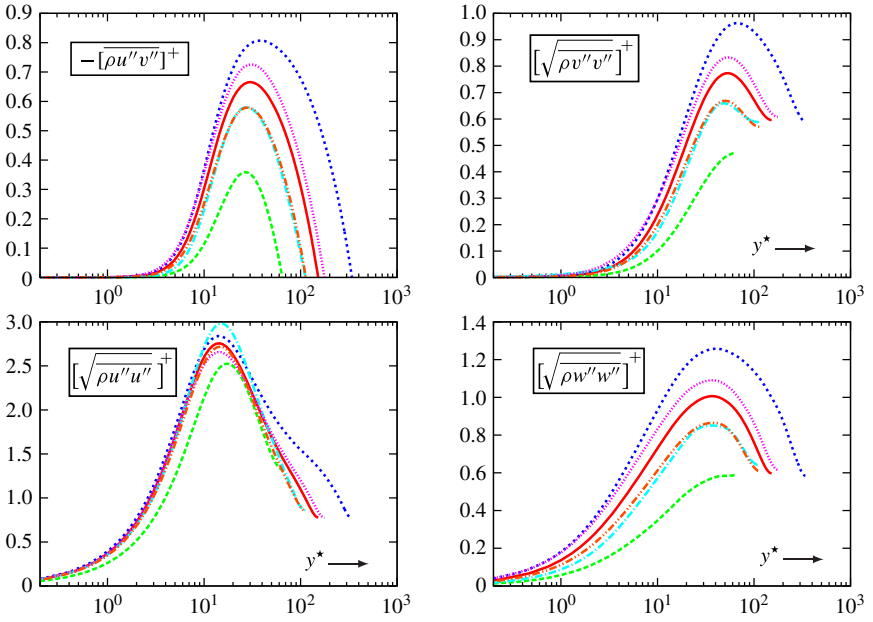

FIGURE 4. (Colour online) DNS (table 1) results for the profiles of Reynolds stresses in wall units $[\overline{\rho u_i'' u_j''}]^+$ (which corresponds to HCB scaling), plotted against $y^\star$ (3.1*c*).

The behaviour of the Reynolds stress (figure 3) is better understood (figure 4) by considering semilocal HCB scaling (Huang *et al.* 1995). The Reynolds stresses in wall units are defined as $[-\overline{\rho u_i'' u_j''}]^+ \overset{(3.2c)}{:=} -\bar{\tau}_w^{-1}\overline{\rho u_i'' u_j''}$, and are therefore already HCB scaled, or equivalently density scaled (Pirozzoli & Bernardini 2013). The shear Reynolds stress $[-\overline{\rho u'' v''}]^+$, plotted against $y^\star$ (3.1*c*), scales with $Re_{\tau^\star}$ and is independent of $\bar{M}_{CL}$, as evidenced by the data for $(Re_{\tau^\star}, \bar{M}_{CL}) \in \{(113, 1.51), (112, 2.48)\}$ which are practically indistinguishable (figure 4), thus confirming the validity of HCB scaling for $[-\overline{\rho u'' v''}]^+$. The same validity of HCB scaling (Huang *et al.* 1995) applies to the wall-normal $[\overline{\rho v'' v''}]^+$ and to the spanwise $[\overline{\rho w'' w''}]^+$ components (figure 4), despite a small difference between the $(Re_{\tau^\star}, \bar{M}_{CL}) \in \{(113, 1.51), (112, 2.48)\}$ distributions in the centreline region. Regarding the streamwise component $[\overline{\rho u'' u''}]^+$, all of the data, with the exception of the very-low-Re $(Re_{\tau^\star}, \bar{M}_{CL}) = (64, 1.62)$ case, collapse on a single curve (figure 4) between the wall and the maximum peak ($0 \lessapprox y^\star \lessapprox 15$), and then decrease to approximately the same centreline value. There is, nonetheless, a small difference in the peak value of $[\overline{\rho u'' u''}]^+$ between the $(Re_{\tau^\star}, \bar{M}_{CL}) \in \{(113, 1.51), (112, 2.48)\}$ distributions. As a conclusion, HCB scaling filters out reasonably well any influence of $\bar{M}_{CL}$ on the Reynolds stresses $[-\overline{\rho u_i'' u_j''}]^+$ (figure 4), except perhaps for the near-wall peak of the streamwise component which

seems to be weakly $\bar{M}_{CL}$-dependent, although more DNS data at $\bar{M}_{CL} \geqslant 2$ and at higher $Re_{\tau^\star}$ are required to fully substantiate and quantify this observation.

Expectedly, the coefficients of variation of the thermodynamic variables ($[\bar{\rho}^{-1}\rho']_{rms}$, $[\bar{T}^{-1}T']_{rms}$ and $[\bar{p}^{-1}p']_{rms}$) exhibit strong $\bar{M}_{CL}$-dependence (figure 3), and closer examination of the data suggests that they scale reasonably well as $\bar{M}_{CL}^2$ (figure 5). As discussed in § 3.1, this implies that they do not scale with some power of M_{B_w} (table 2), suggesting that $\bar{M}_{CL}$ and not M_{B_w} is the correct choice of representative Mach number. Actually, M_{B_w} is widely used (Huang *et al.* 1995; Friedrich 2007) simply because the constraints and boundary conditions applied in the DNS calculations (§ 2.2) fix the value of M_{B_w} (3.1*a*). Before discussing in detail the $y^\star$ distributions of the $\bar{M}_{CL}^2$-scaled coefficients of variation of the thermodynamic fluctuations, it is useful to summarise the implications of the strictly isothermal wall boundary condition ($T_w = \bar{T}_w = \tilde{T}_w = \text{const.} \Longrightarrow T'_w = 0$) used in the present DNS computations, which implies, because of the equation of state (2.1*d*)

$$T'_w = 0 \overset{(2.1d)}{\Longrightarrow} \begin{cases} a_w = \bar{a}_w = \breve{a}_w = \sqrt{\gamma R_g \bar{T}_w} \\ \gamma \bar{p}_w = \bar{a}_w^2 \bar{\rho}_w \\ \gamma p'_w = \bar{a}_w^2 \rho'_w. \end{cases} \tag{3.5}$$

Plotted against the inner-scaled wall distance $y^\star$ (3.1*c*), $[\bar{M}_{CL}^{-2}\bar{p}^{-1}p']_{rms}$ (figure 5) shows clearly a $Re_{\tau^\star}$ influence, in line with incompressible flow data for $[p']^+_{rms}$ (Hu *et al.* 2006, figure 6, p. 1546). Note, nonetheless, the specific behaviour of the $(Re_{\tau^\star}, \bar{M}_{CL}) = (112, 2.48)$ data, which are quasi-identical with the $(Re_{\tau^\star}, \bar{M}_{CL}) = (113, 1.51)$ data for $y^\star \gtrapprox 10$, but differ very near to the wall ($y^\star \lessapprox 10$), where the $\bar{M}_{CL} = 2.48$ data indicate that $[\bar{p}^{-1}p']_{rms,w}$ is higher than the peak of $[\bar{p}^{-1}p']_{rms}$ at $y^\star \approxeq 35$, contrary to the other cases (figure 5). When plotted against the outer-scaled wall distance $\delta^{-1}(y - y_w)$, $[\bar{M}_{CL}^{-2}\bar{p}^{-1}p']_{rms}$ (figure 5) depends on both parameters $(Re_{\tau^\star}, \bar{M}_{CL})$, the centreline value increasing with increasing $Re_{\tau^\star}$ (at constant $\bar{M}_{CL}$, e.g. $(Re_{\tau^\star}, \bar{M}_{CL}) \in \{(64, 1.62), (113, 1.51), (152, 1.50), (341, 1.52)\}$) or with increasing $\bar{M}_{CL}$ (at constant $Re_{\tau^\star}$, e.g. $(Re_{\tau^\star}, \bar{M}_{CL}) \in \{(113, 1.51), (112, 2.48)\}$). On the other hand, comparison of the $[\bar{M}_{CL}^{-2}\bar{p}^{-1}p']_{rms}$ plots, against inner-scaled (figure 5) and outer-scaled (figure 5) wall distance, highlights the behaviour of the near-wall peak, whose level is clearly a function of $Re_{\tau^\star}$ only (figure 5). In particular (figure 5), the difference of the near-wall peak value of $[\bar{M}_{CL}^{-2}\bar{p}^{-1}p']_{rms}$ from the centreline value increases with increasing $Re_{\tau^\star}$, the very-low-Re $(Re_{\tau^\star}, \bar{M}_{CL}) = (64, 1.62)$ case having a nearly constant $[\bar{M}_{CL}^{-2}\bar{p}^{-1}p']_{rms}$ for all y (figure 5).

The plots against the inner-scaled wall distance $y^\star$ (3.1*c*) of the $\bar{M}_{CL}^2$-scaled relative r.m.s. levels of the other thermodynamic fluctuations ($[\bar{M}_{CL}^{-2}\bar{\rho}^{-1}\rho']_{rms}$, $[\bar{M}_{CL}^{-2}\bar{T}^{-1}T']_{rms}$ and $[\bar{M}_{CL}^{-2}R_g^{-1}s']_{rms}$), indicate reasonable superposition for $y^\star \gtrapprox 10$ (figure 5), with a $Re_{\tau^\star}$ effect which is particularly visible for the very-low-Re $(Re_{\tau^\star}, \bar{M}_{CL}) = (64, 1.62)$ case (figure 5). Again, near the wall ($y^\star \lessapprox 10$), the $\bar{M}_{CL} = 2.48$ data indicate higher fluctuation levels. Note that the perfect correlation (3.5) between ρ'_w and p'_w imposed by the strictly isothermal wall condition introduces a $Re_{\tau^\star}$-dependence of $[\bar{M}_{CL}^{-2}\bar{\rho}^{-1}\rho']_{rms}$ in the viscous sublayer which does not extend beyond $y^\star \approxeq 3$ (figure 5). Finally, by (2.5), entropy fluctuations non-dimensionalised by the gas-constant R_g (2.1*d*) are related to the relative fluctuations of T and ρ by

$$\frac{s'}{R_g} \overset{(2.5)}{=} \frac{1}{\gamma - 1} \ln\left(1 + \frac{T'}{\bar{T}}\right) - \ln\left(1 + \frac{\rho'}{\bar{\rho}}\right) - \left[\frac{\bar{s} - s_{ISA}}{R_g} - \left(\frac{1}{\gamma - 1} \ln\frac{\bar{T}}{T_{ISA}} - \ln\frac{\bar{\rho}}{\rho_{ISA}}\right)\right] \tag{3.6}$$

	$Re_{\tau^\star}$	$\bar{M}_{CL}$	$N_x \times N_y \times N_z$	L_x	L_y	L_z	Δx^+	Δy_w^+	$N_{y^+\leqslant 10}$	Δy_{CL}^+	Δz^+	Δt^+	t_{OBS}^+	Δt_s^+
------	64	1.62	$137 \times 113 \times 201$	$8\pi\delta$	2δ	$4\pi\delta$	18.4	0.17	22	3.1	6.2	0.0115	989	0.0115
- - - -	112	2.48	$801 \times 241 \times 1201$	$8\pi\delta$	2δ	$4\pi\delta$	15.5	0.18	21	5.4	5.1	0.0072	243	0.0072
-·-·-	113	1.51	$257 \times 129 \times 385$	$8\pi\delta$	2δ	$4\pi\delta$	16.6	0.21	21	4.7	5.5	0.0150	1373	0.0150
———	152	1.50	$345 \times 137 \times 529$	$8\pi\delta$	2δ	$4\pi\delta$	16.6	0.23	19	5.6	5.4	0.0166	1001	0.0166
·····	176	0.34	$257 \times 129 \times 385$	$8\pi\delta$	2δ	$4\pi\delta$	17.6	0.23	20	5.0	5.8	0.0066	841	0.0066
·····	341	1.52	$801 \times 241 \times 1201$	$8\pi\delta$	2δ	$4\pi\delta$	16.3	0.19	21	5.7	5.4	0.0143	352	0.0143

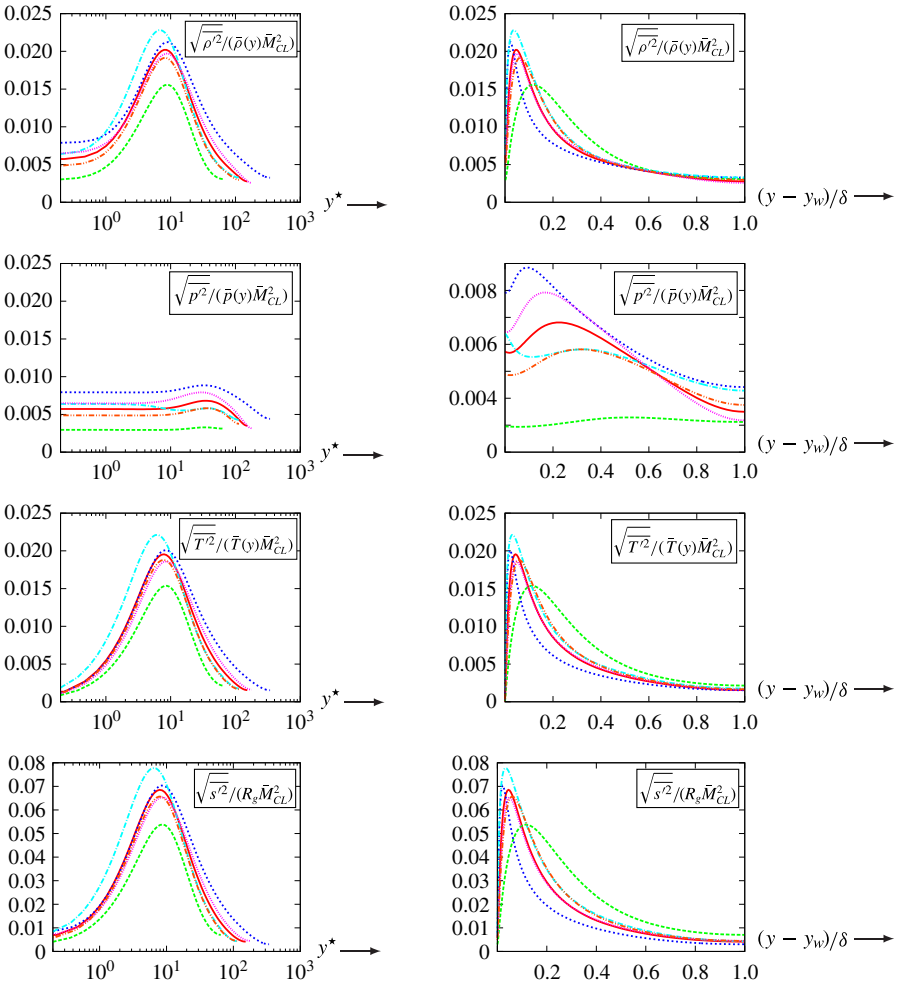

FIGURE 5. (Colour online) DNS (table 1) results for the profiles of the relative fluctuation levels of thermodynamic quantities ($[\bar{\rho}^{-1}\rho']_{rms}$, $[\bar{p}^{-1}p']_{rms}$, $[\bar{T}^{-1}T']_{rms}$ and $[R_g^{-1}s']_{rms}$), scaled by $\bar{M}_{CL}^2$, and of the skewness and flatness of the thermodynamic fluctuations, plotted (inner scaling) against $y^\star$ (3.1*c*) and (outer scaling) against $\delta^{-1}(y-y_w)$.

explaining the similarity between the $y^\star$-distributions of $[\bar{M}_{CL}^{-2}R_g^{-1}s']_{rms}$ and $[\bar{M}_{CL}^{-2}\bar{T}^{-1}T']_{rms}$, as well as the slight $Re_{\tau^\star}$-dependence for $y^\star \lessapprox 3$ related to $[\bar{M}_{CL}^{-2}\bar{\rho}^{-1}\rho']_{rms}$ (figure 5). This relation (3.6) shows that $R_g^{-1}s'$ is a function of the relative fluctuations $\bar{\rho}^{-1}\rho'$ and $\bar{T}^{-1}T'$, thereby explaining the choice of plotting $[\bar{M}_{CL}^{-2}R_g^{-1}s']_{rms}$, instead of

	$Re_{\tau^\star}$	$\bar{M}_{CL}$	$N_x \times N_y \times N_z$	L_x	L_y	L_z	Δx^+	Δy_w^+	$N_{y^+\leqslant 10}$	Δy_{CL}^+	Δz^+	Δt^+	t_{OBS}^+	Δt_s^+
------	64	1.62	$137 \times 113 \times 201$	$8\pi\delta$	2δ	$4\pi\delta$	18.4	0.17	22	3.1	6.2	0.0115	989	0.0115
-·-·-	112	2.48	$801 \times 241 \times 1201$	$8\pi\delta$	2δ	$4\pi\delta$	15.5	0.18	21	5.4	5.1	0.0072	243	0.0072
-·-·-	113	1.51	$257 \times 129 \times 385$	$8\pi\delta$	2δ	$4\pi\delta$	16.6	0.21	21	4.7	5.5	0.0150	1373	0.0150
———	152	1.50	$345 \times 137 \times 529$	$8\pi\delta$	2δ	$4\pi\delta$	16.6	0.23	19	5.6	5.4	0.0166	1001	0.0166
·····	176	0.34	$257 \times 129 \times 385$	$8\pi\delta$	2δ	$4\pi\delta$	17.6	0.23	20	5.0	5.8	0.0066	841	0.0066
·····	341	1.52	$801 \times 241 \times 1201$	$8\pi\delta$	2δ	$4\pi\delta$	16.3	0.19	21	5.7	5.4	0.0143	352	0.0143

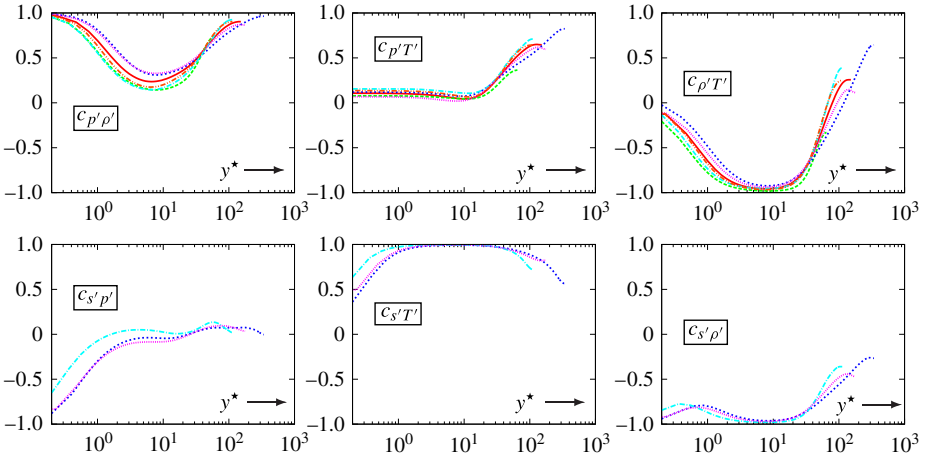

FIGURE 6. (Colour online) DNS (table 1) results for the profiles of the correlation coefficients (3.8) between thermodynamic fluctuations ($c_{p'\rho'}$, $c_{p'T'}$, $c_{\rho'T'}$, $c_{s'p'}$, $c_{s'T'}$, $c_{s'\rho'}$; coefficients containing s' were not acquired for all of the DNS computations), plotted (inner scaling) against $y^\star$ (3.1*c*).

the coefficient of variation of entropy, because by (2.5) only entropy variations have physical meaning. Note the non-fluctuating term $[\cdot]$ in (3.6) which represents the difference between the Reynolds-averaged entropy and the expression (2.5) evaluated at mean temperature and density. When plotted against the outer-scaled wall distance $\delta^{-1}(y - y_w)$, $\{[\bar{M}_{CL}^{-2}\bar{\rho}^{-1}\rho']_{rms}$, $[\bar{M}_{CL}^{-2}\bar{T}^{-1}T']_{rms}$, $[\bar{M}_{CL}^{-2}R_g^{-1}s']_{rms}\}$ collapse (figure 5) reasonably well on a single curve, except perhaps for $[\bar{M}_{CL}^{-2}R_g^{-1}s']_{rms}$ in the very-low-Re $(Re_{\tau^\star}, \bar{M}_{CL}) = (64, 1.62)$ case.

An interesting observation from the above results (figures 3, 5 and 6) is that, invariably,

$$O\left(\frac{\sqrt{\overline{T'^2}}}{\bar{T}}\right) = O\left(\frac{\sqrt{\overline{\rho'^2}}}{\bar{\rho}}\right) = O\left(\frac{\sqrt{\overline{p'^2}}}{\bar{p}}\right) \quad \forall y^\star \quad \forall (Re_{\tau^\star}, \bar{M}_{CL}) \tag{3.7}$$

are of the same order of magnitude everywhere in the channel, and for all $(Re_{\tau^\star}, \bar{M}_{CL})$ that were investigated (figures 3 and 5), even at the low-Mach-number limit, and that the correlation coefficients (figure 6) show little dependence on $\bar{M}_{CL}$, except perhaps very near the wall. The order-of-magnitude relation (3.7) is also valid in sustained compressible HIT (Donzis & Jagannathan 2013, table 1, p. 225). The reason for this is that the basic thermodynamic variables (p, ρ, T) are related by the equation of state (2.1*d*), independently of the specific flow under study. In the present DNS

computations (table 1), $[\bar\rho^{-1}\rho']_{rms}\lessapprox 0.14$ and $[\bar T^{-1}T']_{rms}\lessapprox 0.14$ (figure 3). These values prevail for $\bar M_{CL}=2.48$ (figure 3), and are attained at the near-wall peaks located at $y^\star\approxeq 10$. For $\bar M_{CL}\approxeq 1.50$ these maximum values drop to $\sim$0.04 (figure 3), since they scale with $\bar M_{CL}^2$ (figure 5).

3.5. *Correlation coefficients*

The correlation coefficient between any two flow quantities $[\cdot]$ and $(\cdot)$ is defined by

$$c_{(\cdot)'[\cdot]'}:=\frac{\overline{(\cdot)'[\cdot]'}}{\sqrt{\overline{(\cdot)'^2}}\sqrt{\overline{[\cdot]'^2}}}. \tag{3.8}$$

Correlations between fluctuations are of particular importance both to understand the complex interactions between different quantities and to model unclosed terms (Taulbee & VanOsdol 1991). For instance, the exact relations

$$\frac{\overline{T''}}{\bar T}\overset{(2.6c)}{=}-\frac{\overline{\rho'T'}}{\bar\rho\,\bar T}\overset{(3.8)}{=}-c_{\rho'T'}\frac{\sqrt{\overline{\rho'^2}}}{\bar\rho}\frac{\sqrt{\overline{T'^2}}}{\bar T} \tag{3.9a}$$

$$\frac{\overline{u''}}{\bar u}\overset{(2.6c)}{=}-\frac{\overline{\rho'u'}}{\bar\rho\,\bar u}\overset{(3.8)}{=}-c_{\rho'u'}\frac{\sqrt{\overline{\rho'^2}}}{\bar\rho}\frac{\sqrt{\overline{u'^2}}}{\bar u} \tag{3.9b}$$

$$\frac{\overline{v''}}{\bar u}\overset{(2.6c)}{=}-\frac{\overline{\rho'v'}}{\bar\rho\,\bar u}\overset{(3.8)}{=}-c_{\rho'v'}\frac{\sqrt{\overline{v'^2}}}{\sqrt{\overline{u'^2}}}\frac{\sqrt{\overline{\rho'^2}}}{\bar\rho}\frac{\sqrt{\overline{u'^2}}}{\bar u} \tag{3.9c}$$

expressing the Reynolds averages of Favre fluctuations contain correlation coefficients ($c_{\rho'T'}$, $c_{\rho'u'}$, $c_{\rho'v'}$), coefficients of variation ($[\bar\rho^{-1}\rho']_{rms}$, $[\bar T^{-1}T']_{rms}$, $[\bar u^{-1}u']_{rms}$) and structure parameters ($[u']_{rms}^{-1}[v']_{rms}$).

Consideration of the correlation coefficients between thermodynamic fluctuations ($c_{p'\rho'}$, $c_{p'T'}$, $c_{\rho'T'}$, $c_{s'p'}$, $c_{s'T'}$, $c_{s'\rho'}$), plotted (figure 6) against the inner-scaled wall distance $y^\star$ (3.1*c*), indicates weak influence of $Re_{\tau^\star}$ or $\bar M_{CL}$, except very close to the wall ($y^\star\lessapprox 3$), where the wall boundary condition (3.5) dominates the behaviour of the correlation coefficients (figure 6). By (3.5), pressure and density, are perfectly correlated at the strictly isothermal wall, implying $[c_{p'\rho'}]_w=1$ (figure 6). The correlation coefficient $c_{p'\rho'}$ decreases from this maximum value with distance from the wall (figure 6), to a value around $\sim$0.25, in the neighbourhood of $y^\star\approxeq 10$, which is the location of the $[\bar\rho^{-1}\rho']_{rms}$ peak (figure 5), and then increases again approaching one in the centreline region (figure 6). When plotted against the outer-scaled wall-distance $\delta^{-1}(y-y_w)$ (figure 7), $c_{p'\rho'}$ exhibits a $Re_{\tau^\star}$-dependence, with the centreline value being closer to one as $Re_{\tau^\star}$ increases (figure 7). Since, at the wall, ρ' is perfectly correlated with p' (3.5), it is weakly correlated with T', so that $c_{\rho'T'}$ has values close to zero as $y^\star\to 0$ (figure 6). Further away from the wall, $c_{\rho'T'}$ rapidly reaches values close to -1 (figure 6), in the region $y^\star\in[3,\,20]$, i.e. in the neighbourhood of $y^\star\approxeq 10$ where are located the peaks of $[\bar\rho^{-1}\rho']_{rms}$ and $[\bar T^{-1}T']_{rms}$ (figure 5), and then increases again, reaching slightly positive values at the centreline (figure 6), provided that $Re_{\tau^\star}$ is sufficiently high. When plotted against the outer-scaled wall distance $\delta^{-1}(y-y_w)$, $c_{\rho'T'}$ exhibits $Re_{\tau^\star}$-dependence (figure 7). Finally the coefficient $c_{p'T'}$ is low near the wall ($y^\star\lessapprox 10$) and then increases towards the centreline region. Note that both $c_{p'\rho'}>0$ for all $y^\star$ and $c_{p'T'}>0$ for all $y^\star$, while $c_{\rho'T'}<0$ for all $y^\star\lessapprox 60$,

	$Re_{\tau^\star}$	$\bar{M}_{CL}$	$N_x \times N_y \times N_z$	L_x	L_y	L_z	Δx^+	Δy_w^+	$N_{y^+\leqslant 10}$	Δy_{CL}^+	Δz^+	Δt^+	t_{OBS}^+	Δt_s^+
------	64	1.62	$137 \times 113 \times 201$	$8\pi\delta$	2δ	$4\pi\delta$	18.4	0.17	22	3.1	6.2	0.0115	989	0.0115
- - - -	112	2.48	$801 \times 241 \times 1201$	$8\pi\delta$	2δ	$4\pi\delta$	15.5	0.18	21	5.4	5.1	0.0072	243	0.0072
- · - ·	113	1.51	$257 \times 129 \times 385$	$8\pi\delta$	2δ	$4\pi\delta$	16.6	0.21	21	4.7	5.5	0.0150	1373	0.0150
———	152	1.50	$345 \times 137 \times 529$	$8\pi\delta$	2δ	$4\pi\delta$	16.6	0.23	19	5.6	5.4	0.0166	1001	0.0166
·····	176	0.34	$257 \times 129 \times 385$	$8\pi\delta$	2δ	$4\pi\delta$	17.6	0.23	20	5.0	5.8	0.0066	841	0.0066
·····	341	1.52	$801 \times 241 \times 1201$	$8\pi\delta$	2δ	$4\pi\delta$	16.3	0.19	21	5.7	5.4	0.0143	352	0.0143

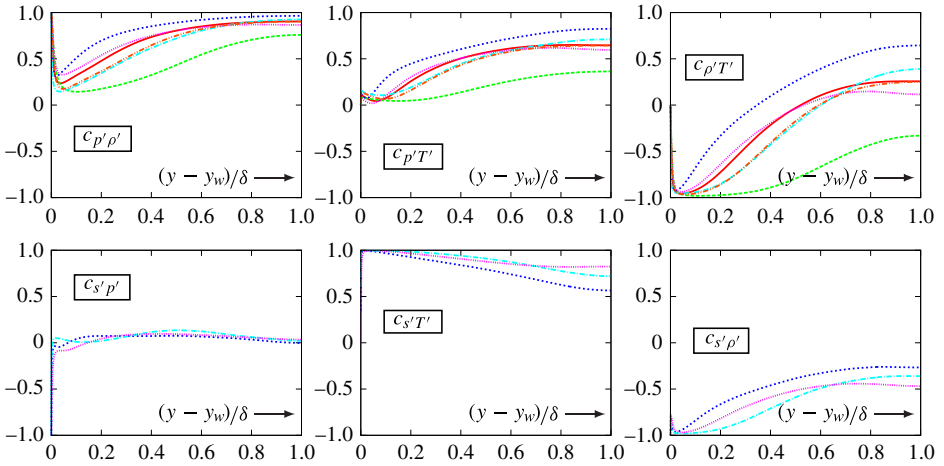

FIGURE 7. (Colour online) DNS (table 1) results for the profiles of the correlation coefficients (3.8) between thermodynamic fluctuations ($c_{p'\rho'}$, $c_{p'T'}$, $c_{\rho'T'}$, $c_{s'p'}$, $c_{s'T'}$, $c_{s'\rho'}$; coefficients containing s' were not acquired for all of the DNS computations), plotted (outer scaling) against $\delta^{-1}(y - y_w)$.

then rising towards $[c_{\rho'T'}]_{CL} > 0$, provided that $Re_{\tau^\star}$ is sufficiently high (figure 7). Hence, independently of $(Re_{\tau^\star}, \bar{M}_{CL})$, p' is always positively correlated with ρ' and T', although this correlation may be weak (close to 0; figure 6). On the other hand ρ' is negatively correlated with T' in the wall region and positively correlated near the centreline (figure 6), provided that $Re_{\tau^\star}$ is sufficiently high. Note that in sustained HIT $c_{\rho'T'} > 0$ also (Donzis & Jagannathan 2013, table 1, p. 225), highlighting the strong anisotropy that prevails when approaching the wall, and also that in the $Re_{\tau^\star} \approxeq 64$ case wall effects dominate the entire flow up to the centreline (figures 6, 7).

The fluctuating entropy s' is positively correlated with T' ($c_{s'T'} > 0$) and negatively correlated with ρ' ($c_{\rho'T'} > 0$), and in both cases the correlation or anticorrelation is generally strong (figures 6, 7). The correlation $c_{s'T'}$ (figure 6) decreases very near the wall ($y^\star \lessapprox 1$) but is nearly one for $y^\star \in [1, 50]$, and then decreases towards centreline (figure 7). The generally strong correlation of s' with T' was mentioned in the early works of Kovásznay (1953) and Morkovin (1962). On the other hand, the correlation $c_{s'\rho'} < 0$ (figures 6, 7), approaching -1 in the region $y^\star \in [3, 20]$ where $c_{\rho'T'} \approxeq -1$ and $c_{s'T'} \approxeq 1$ (figure 6). Again, in the major part of the flow, the influence of $(Re_{\tau^\star}, \bar{M}_{CL})$ on the correlation coefficients ($c_{s'\rho'}$, $c_{s'p'}$, $c_{s'T'}$) is weak, especially with inner scaling of the wall-distance ($y^\star$; figure 6). Comparison of the plots of the correlation coefficients ($c_{p'\rho'}$, $c_{p'T'}$, $c_{\rho'T'}$, $c_{s'p'}$, $c_{s'T'}$, $c_{s'\rho'}$), with inner ($y^\star$; figure 6) and outer ($\delta^{-1}(y - y_w)$; figure 7) scaling of the wall distance, suggests that, for the range of $(Re_{\tau^\star}, \bar{M}_{CL})$ that was investigated (table 1), inner scaling ($y^\star$) provides reasonable collapse of the data

(figure 6), except very near the wall ($y^\star \lessapprox 3$) and that outer scaling ($\delta^{-1}(y-y_w)$) does not. Note also that $c_{s'p'} \cong 0$ in the major part of the flow (figures 6 and 7), except very near the wall ($y^\star \cong 3$; figure 6). Furthermore, the fluctuating entropy s' is not only strongly correlated with the fluctuating temperature T', but is equally strongly anticorrelated with the fluctuating density ρ' (figures 6 and 7).

The transport of thermodynamic fluctuations by the velocity field is represented by the streamwise ($c_{\rho'u'}$, $c_{T'u'}$, $c_{p'u'}$, $c_{s'u'}$) and wall-normal ($c_{\rho'v'}$, $c_{T'v'}$, $c_{p'v'}$, $c_{s'v'}$) correlation coefficients (figures 8 and 9). The present flow being streamwise invariant in the mean ($\partial_x\overline{(\cdot)}=0$), only wall-normal transport appears in various transport equations (§ 4), and in this respect it is interesting to consider the ratio of the wall-normal correlation coefficients ($c_{\rho'v'}$, $c_{T'v'}$, $c_{p'v'}$, $c_{s'v'}$) to $c_{u'v'}$ which represents wall-normal transport of the streamwise velocity fluctuation (figures 8, 9). The correlation coefficient of pressure transport, both streamwise $c_{p'u'}$ and wall-normal $c_{p'v'}$, which in the present flow is responsible for pressure diffusion (Sauret & Vallet 2007; Vallet 2007), are very weak in the major part of the channel (figure 9), except for $c_{p'v'}$ near the wall ($y^\star \lessapprox 15$; figure 8). This is also observed regarding the ratio $c^{-1}_{u'v'}c_{p'v'}$, which is quite small ($\lessapprox 0.1$) in the major part of the channel (figure 9), except very near the wall ($y^\star \lessapprox 30$; figure 8). In the very-near-wall region ($y^\star \lessapprox 3$; figure 8) a very marked dependence on $\bar{M}_{CL}$ is observed, both for $c_{p'v'}$ and $c^{-1}_{u'v'}c_{p'v'}$. For the other thermodynamic variables, wall-normal transport correlation coefficients ($c_{\rho'v'}$, $c_{T'v'}$, $c_{s'v'}$) when plotted against the outer-scaled wall-distance $\delta^{-1}(y-y_w)$ (figure 9) appear to be quite independent of ($Re_{\tau^\star}$, $\bar{M}_{CL}$), and this is also true for the inner-scaled wall distance ($y^\star$), in the region $y^\star \in [10,\,100]$ (figure 8). The ratio of the wall-normal transport correlation coefficients ($c_{\rho'v'}$, $c_{T'v'}$, $c_{s'v'}$) on $c_{u'v'}$, is reasonably independent of ($Re_{\tau^\star}$, $\bar{M}_{CL}$) when plotted against the inner-scaled wall distance $y^\star$, for $y^\star \gtrapprox 10$ (figure 8), but shows a marked $Re_{\tau^\star}$ influence when plotted against the outer-scaled wall distance $\delta^{-1}(y-y_w)$ (figure 9; note that the ratio is indeterminate at the centreline because, by symmetry, $[c_{u'v'}]_{CL}=0$). In particular, the ratio $c^{-1}_{u'v'}c_{T'v'}$ remains (figure 8) nearly constant and close to 1 ± 0.1 from the wall up to $y^\star \cong 100\ \forall(Re_{\tau^\star}, \bar{M}_{CL})$. It is positive in the present flow because the wall is very cold, and we have $c_{u'T'}>0$ and $c_{v'T'}<0$, contrary to the case of not-too-cold walls (Huang *et al.* 1995, p. 208), like in the boundary-layer DNS study of Guarini *et al.* (2000) where $c_{u'T'}<0$ and $c_{v'T'}>0$. It is easy to show, starting from the basic HCB–SRA relation (Huang *et al.* 1995, (4.10), p. 208), that HCB–SRA, and indeed all SRA extensions reviewed in Huang *et al.* (1995, pp. 207–208) imply $|c_{u'T'}|\cong 1$ and $c_{v'T'}\cong c_{u'T'}c_{u'v'}$ which generalises the relation given in Guarini *et al.* (2000, (4.20), p. 20). Finally, the streamwise correlation coefficients $c_{[\cdot]u'}$ ($c_{\rho'u'}$, $c_{T'u'}$, $c_{s'u'}$), when plotted against the inner-scaled wall distance $y^\star$ (figure 8), show little dependence on ($Re_{\tau^\star}$, $\bar{M}_{CL}$), except for $c_{\rho'u'}$ and $c_{s'u'}$ very near the wall ($y^\star \lessapprox 4$; figure 8), and a marked $Re_{\tau^\star}$-dependence when plotted against the outer-scaled wall distance $\delta^{-1}(y-y_w)$ (figure 9).

4. Budgets

Further insight into the dynamics of thermodynamic fluctuations and their interaction with the velocity field, can be gained by studying the budgets of the transport equations for the variances ($\overline{\rho'^2}$, $\overline{p'^2}$, $\overline{\rho s''^2}$ and $\overline{\rho h''^2} \overset{(2.1d)}{=} c_p\,\overline{\rho T''^2}$) and the fluxes ($\overline{\rho' u_i'}$, $\overline{p' u_i'}$, $\overline{\rho s'' u_i''}$ and $\overline{\rho h'' u_i''} \overset{(2.1d)}{=} c_p\,\overline{\rho T'' u_i''}$) of the turbulent fluctuations of the thermodynamic state variables (figure 10). Note (figure 10) that, for $\{T'',\, s'',\, p'\}$, the streamwise fluxes are $\geqslant 0$, while the wall-normal fluxes are $\leqslant 0$, contrary to ρ',

	$Re_{\tau^\star}$	$\bar{M}_{CL}$	$N_x \times N_y \times N_z$	L_x	L_y	L_z	Δx^+	Δy_w^+	$N_{y^+\leqslant 10}$	Δy_{CL}^+	Δz^+	Δt^+	t_{OBS}^+	Δt_s^+
------	64	1.62	$137 \times 113 \times 201$	$8\pi\delta$	2δ	$4\pi\delta$	18.4	0.17	22	3.1	6.2	0.0115	989	0.0115
-.-.-.	112	2.48	$801 \times 241 \times 1201$	$8\pi\delta$	2δ	$4\pi\delta$	15.5	0.18	21	5.4	5.1	0.0072	243	0.0072
-..-..	113	1.51	$257 \times 129 \times 385$	$8\pi\delta$	2δ	$4\pi\delta$	16.6	0.21	21	4.7	5.5	0.0150	1373	0.0150
———	152	1.50	$345 \times 137 \times 529$	$8\pi\delta$	2δ	$4\pi\delta$	16.6	0.23	19	5.6	5.4	0.0166	1001	0.0166
.....	176	0.34	$257 \times 129 \times 385$	$8\pi\delta$	2δ	$4\pi\delta$	17.6	0.23	20	5.0	5.8	0.0066	841	0.0066
------	341	1.52	$801 \times 241 \times 1201$	$8\pi\delta$	2δ	$4\pi\delta$	16.3	0.19	21	5.7	5.4	0.0143	352	0.0143

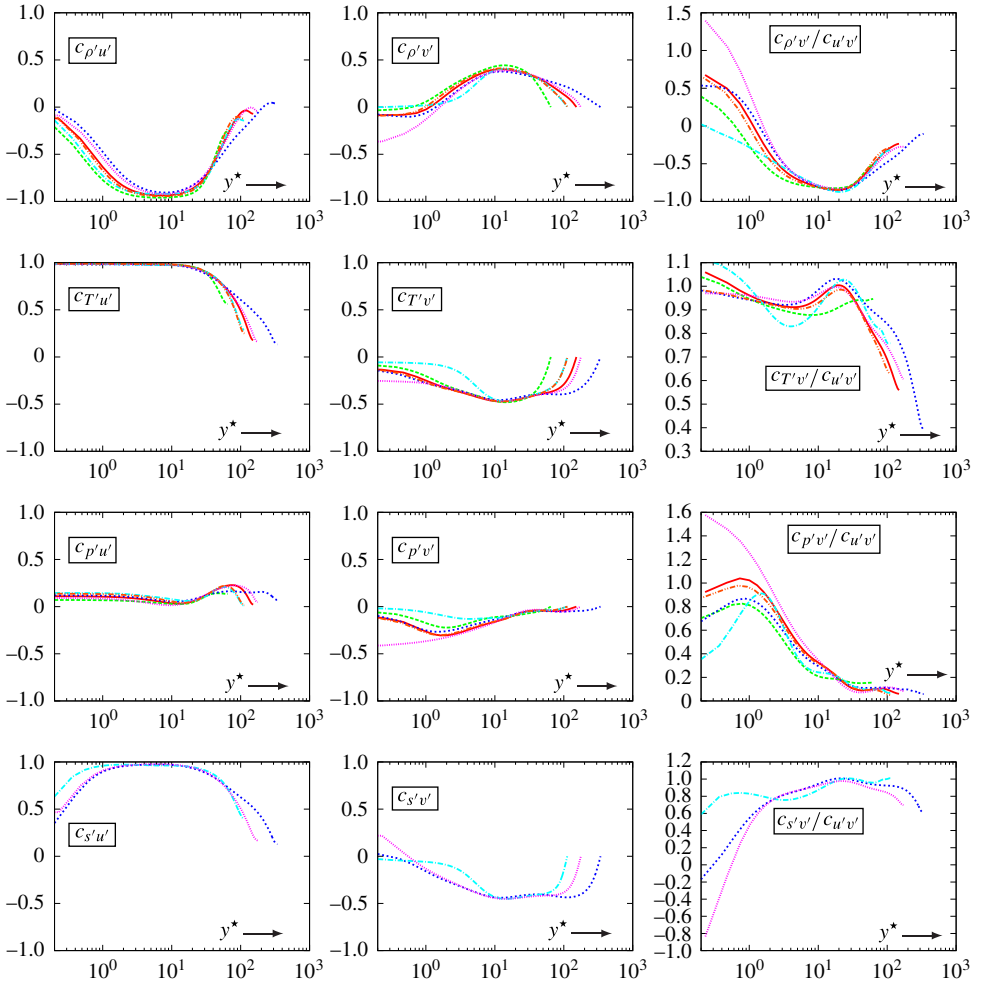

FIGURE 8. (Colour online) DNS (table 1) results for the profiles of the correlation coefficients (3.8) between thermodynamic fluctuations and the streamwise ($c_{\rho'u'}$, $c_{T'u'}$, $c_{p'u'}$, $c_{s'u'}$) and wall normal ($c_{\rho'v'}$, $c_{T'v'}$, $c_{p'v'}$, $c_{s'v'}$) velocity fluctuations, and of the ratio of the later (wall-normal transport of ρ', T', p' and s') to the shear momentum transport correlation coefficient $c_{u'v'}$, plotted (inner scaling) against $y^\star$ (3.1*c*).

for which $\overline{\rho' u'} \overset{(2.6c)}{=} -\bar{\rho}\widetilde{u''} \leqslant 0$ and $\overline{\rho' v'} \overset{(2.6c)}{=} -\bar{\rho}\widetilde{v''} \geqslant 0$ (figure 10). In § 4.1 we study the transport equations for $\widetilde{u_i''}$ ($\widetilde{u''} \geqslant 0$ and $\widetilde{v''} \leqslant 0$; figure 10). At the centreline all wall-normal fluxes are $= 0$ by symmetry (figure 10), and the DNS results suggest that the streamwise fluxes are also very small there (figure 10). The influence of

$Re_{\tau^\star}$	$\bar{M}_{CL}$	$N_x \times N_y \times N_z$	L_x	L_y	L_z	Δx^+	Δy_w^+	$N_{y^+\leqslant 10}$	Δy_{CL}^+	Δz^+	Δt^+	t_{OBS}^+	Δt_s^+
64	1.62	$137 \times 113 \times 201$	$8\pi\delta$	2δ	$4\pi\delta$	18.4	0.17	22	3.1	6.2	0.0115	989	0.0115
112	2.48	$801 \times 241 \times 1201$	$8\pi\delta$	2δ	$4\pi\delta$	15.5	0.18	21	5.4	5.1	0.0072	243	0.0072
113	1.51	$257 \times 129 \times 385$	$8\pi\delta$	2δ	$4\pi\delta$	16.6	0.21	21	4.7	5.5	0.0150	1373	0.0150
152	1.50	$345 \times 137 \times 529$	$8\pi\delta$	2δ	$4\pi\delta$	16.6	0.23	19	5.6	5.4	0.0166	1001	0.0166
176	0.34	$257 \times 129 \times 385$	$8\pi\delta$	2δ	$4\pi\delta$	17.6	0.23	20	5.0	5.8	0.0066	841	0.0066
341	1.52	$801 \times 241 \times 1201$	$8\pi\delta$	2δ	$4\pi\delta$	16.3	0.19	21	5.7	5.4	0.0143	352	0.0143

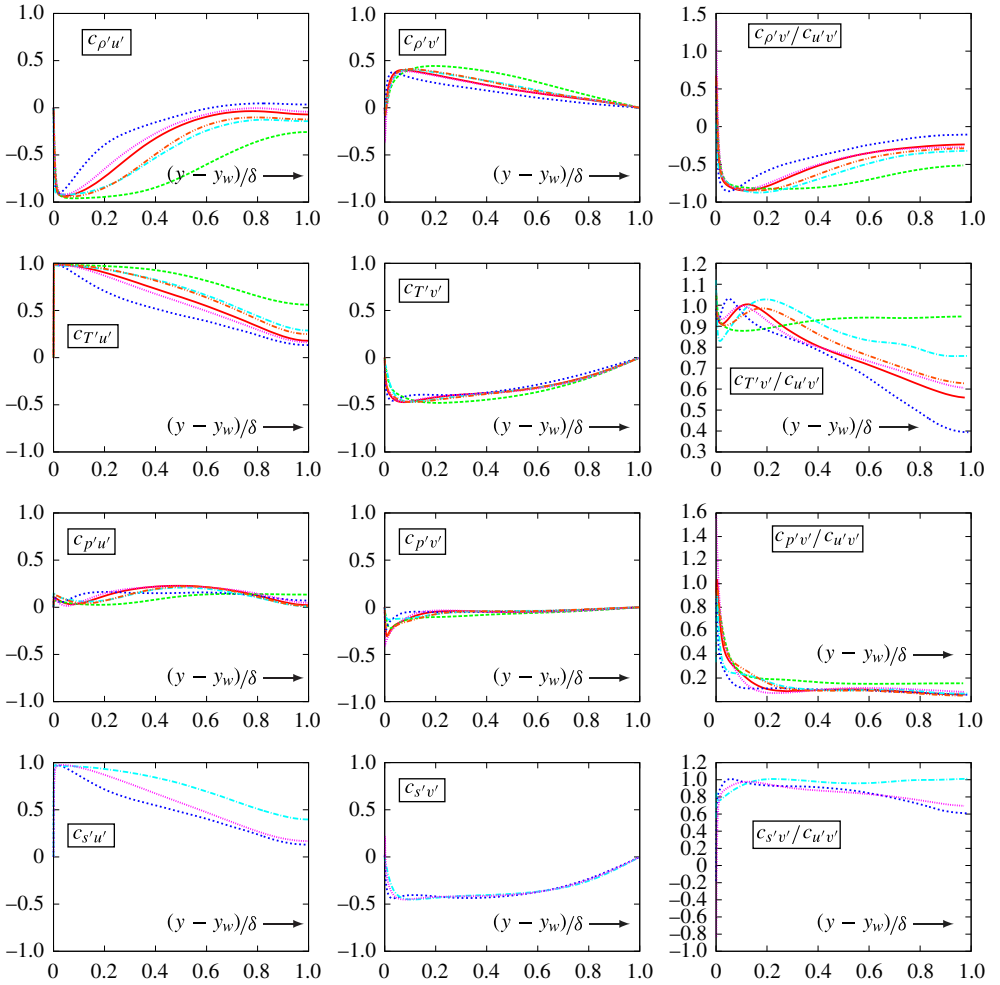

FIGURE 9. (Colour online) DNS (table 1) results for the profiles of the correlation coefficients (3.8) between thermodynamic fluctuations and the streamwise ($c_{\rho'u'}$, $c_{T'u'}$, $c_{p'u'}$, $c_{s'u'}$) and wall normal ($c_{\rho'v'}$, $c_{T'v'}$, $c_{p'v'}$, $c_{s'v'}$) velocity fluctuations, and of the ratio of the later (wall-normal transport of ρ', T', p' and s') to the shear momentum transport correlation coefficient $c_{u'v'}$, plotted (outer scaling) against $\delta^{-1}(y - y_w)$.

$(Re_{\tau^\star}, \bar{M}_{CL})$ on each term in the budgets of these transport equations is beyond the scope of the present study, and will be the subject of future work. We concentrate instead on the detailed analysis of the $(Re_{\tau^\star}, \bar{M}_{CL}) \approxeq (150, 1.5)$ case.

$Re_{\tau^\star}$	$\bar{M}_{CL}$	$N_x \times N_y \times N_z$	L_x	L_y	L_z	Δx^+	Δy_w^+	$N_{y^+\leqslant 10}$	Δy_{CL}^+	Δz^+	Δt^+	t_{OBS}^+	Δt_s^+
150	1.50	$361 \times 149 \times 433$	$4\pi\delta$	2δ	$\frac{4}{3}\pi\delta$	7.9	0.22	19	4.7	2.1	0.0164	868	0.0164

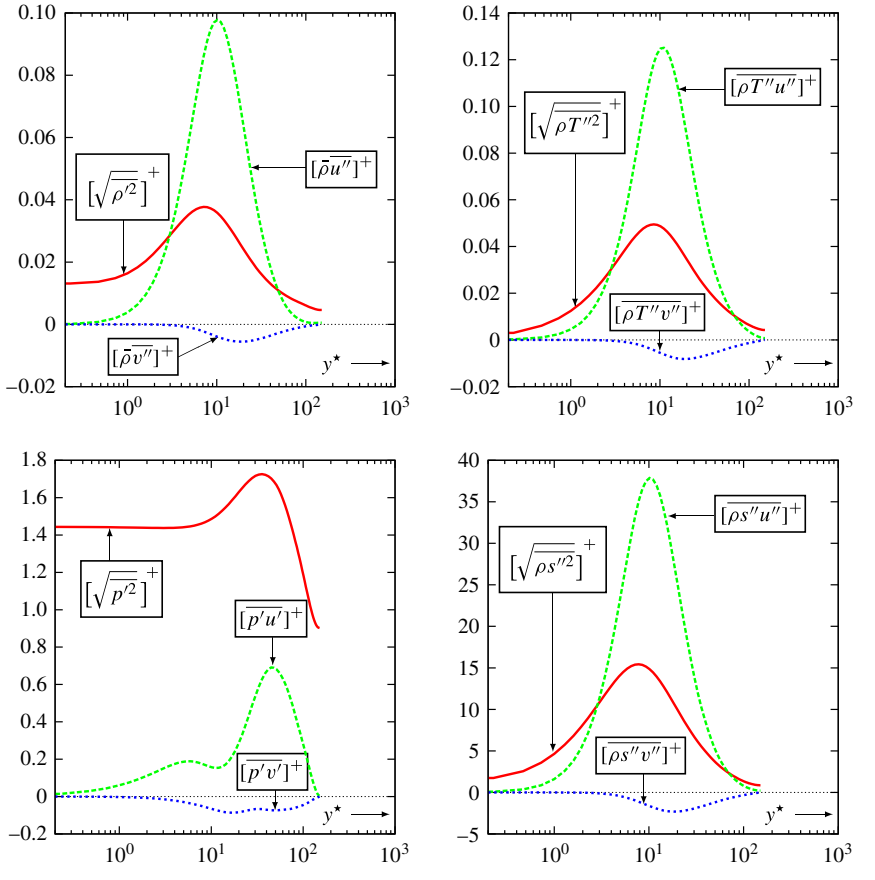

FIGURE 10. (Colour online) DNS results (small box; table 1) at $(Re_{\tau^\star}, \bar{M}_{CL}) = (150, 1.50)$ for the variances ($\overline{\rho'^2}$, $\overline{p'^2}$, $\overline{\rho T''^2}$ and $\overline{\rho s''^2}$) and the fluxes ($\overline{\rho}\,\overline{u''} \overset{(2.6b)}{=} -\overline{\rho' u_i'}$, $\overline{p' u_i'}$, $\overline{\rho T'' u_i''}$ and $\overline{\rho s'' u_i''}$) of the thermodynamic fluctuations (in wall units; § 3.2), plotted against $y^\star$ (3.1*c*).

The large-box computational grid for the $(Re_{\tau^\star}, \bar{M}_{CL}) = (152, 1.5)$ case has quite satisfactory resolution in wall units (table 1), with respect to usual compressible channel DNS standards (Coleman *et al.* 1995; Friedrich *et al.* 2006; Tamano & Morinishi 2006; Gerolymos *et al.* 2010; Wei & Pollard 2011*b*). Nonetheless, the transport equations for the variances and fluxes of thermodynamic variables contain complicated terms (§§ 4.1–4.4), including triple correlations of gradients of the fluctuating field and correlations containing the fluctuating dilatation Θ'', which require higher resolution to achieve grid convergence, compared with the basic second-order moments (Gerolymos *et al.* 2010). For this reason, the budgets of the transport equations were obtained on a finer grid with better resolution of the small scales ($\Delta x^+ \approxeq 7.9$ and $\Delta z^+ \approxeq 2.1$; table 1) but in the smaller computational box (table 1) used in the original computations of Coleman *et al.* (1995). Comparison of one-dimensional spectra, in the homogeneous streamwise (x) and spanwise (z) directions, for the fluctuations of the velocity components (u', v' and w') and of

$Re_{\tau^\star}$	$\bar{M}_{CL}$	$N_x \times N_y \times N_z$	L_x	L_y	L_z	Δx^+	Δy^+_w	$N_{y^+\leqslant 10}$	Δy^+_{CL}	Δz^+	Δt^+	$t^+_{OBS_{R_2}}$	$\Delta t^+_{s_{R_2}}$
152	1.50	$345 \times 137 \times 529$	$8\pi\delta$	2δ	$4\pi\delta$	16.6	0.23	19	5.6	5.4	0.0166	999	1.66
150	1.50	$361 \times 149 \times 433$	$4\pi\delta$	2δ	$\frac{4}{3}\pi\delta$	7.9	0.22	19	4.7	2.1	0.0164	1034	1.64

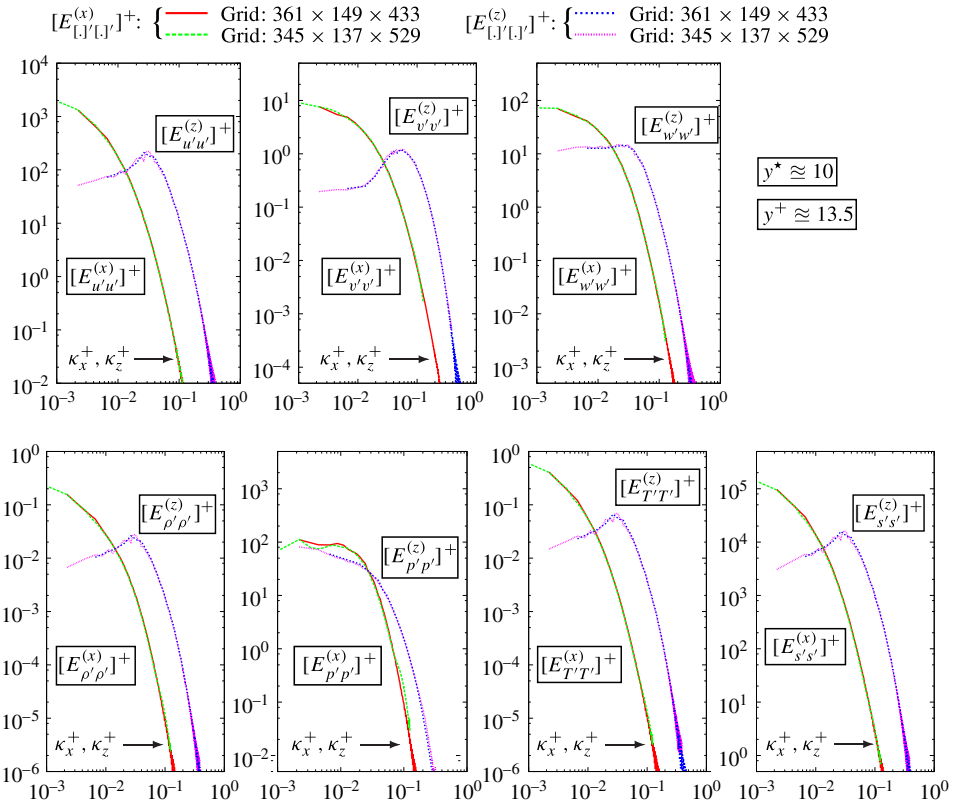

FIGURE 11. (Colour online) Comparison in the neighbourhood (figure 5) of the location of the maxima of thermodynamic fluctuations ($y^+ \approxeq 10 \iff y^\star \approxeq 13.5$), between the large-box and the small-box DNS results (table 1), of one-dimensional spectra (in wall units; § 3.2) in the homogeneous streamwise ($[E^{(x)}_{[\cdot]'[\cdot]'}]^+$) and spanwise ($[E^{(z)}_{[\cdot]'[\cdot]'}]^+$) directions, of the fluctuating fields of velocity components (u', v' and w') and of the thermodynamic state-variables (p', ρ', T' and s'), plotted against the corresponding non-dimensional wavenumbers (κ_x^+ or κ_z^+).

the thermodynamic state variables (p', ρ', T' and s'), between the small-box and the large-box computations (table 1), shows very good agreement in the region of small wavenumbers (figure 11) indicating that the small box is large enough. The finer grid small-box computations resolve scales with a separation of at least five orders of magnitude for the streamwise spectra ($[E^{(x)}_{[\cdot]'[\cdot]'}]^+$; figure 11) and of at least four orders of magnitude for the spanwise spectra ($[E^{(z)}_{[\cdot]'[\cdot]'}]^+$; figure 11). Notable improvements in resolution compared with the large-box computations are observed for $[E^{(x)}_{v'v'}]^+$ (almost two orders of magnitude; figure 11), for $[E^{(z)}_{v'v'}]^+$ (almost one order of magnitude; figure 11) and for $[E^{(x)}_{p'p'}]^+$ (almost two orders of magnitude; figure 11). Note that the one-dimensional spectra were computed (Gerolymos *et al.* 2010, p. 806) by taking

the scaled DFT (discrete Fourier transform) of two-point correlations obtained by sampling the computations every 100 iterations ($\Delta t^+_{sR_2} = 100\Delta t^+$) over approximately the same observation time as for the single-point statistics ($t^+_{OBSR_2} \approxeq t^+_{OBS}$) which were sampled at every iteration (table 1).

These single-point statistics were used to analyse (§§ 4.1–4.4) the budgets of the transport equations for the variances and fluxes of thermodynamic fluctuations. In the transport equations we use systematically the symbols $C_{(\cdot)}$ for convection, $d_{(\cdot)}$ for diffusion, $P_{(\cdot)}$ for production by mean-flow gradients, $\Pi_{(\cdot)}$ for terms containing the fluctuating pressure-gradient $\partial_{x_i} p'$, $\varepsilon_{(\cdot)}$ for destruction by molecular mechanisms (viscosity or heat conductivity), $K_{(\cdot)}$ for direct compressibility effects proportional to $\overline{(\cdot)''}$, $B_{(\cdot)}$ for terms containing the fluctuating dilatation Θ''' (2.8*e*) and $\Xi_{(\cdot)}$ for triple correlations. In the present work, contrary to a previous investigation (Sénéchal 2009) analysing DNS data (Gerolymos *et al.* 2010) obtained on coarser grids, the fluctuating viscous stresses τ'_{ij} and heat fluxes q'_i were not decomposed in the transport equations by expanding the fluctuating part of (2.1*e*), (2.1*f*), and statistics containing τ'_{ij} or q'_i were acquired directly using an onboard moving-averages technique (Gerolymos *et al.* 2010, § 4.4, p. 791).

When considering streamwise invariant in the mean compressible turbulent plane channel flow, the general forms of these transport equations can be simplified, because of the specific symmetries of the flow

$$\left.\begin{aligned} &\bar{w} = \tilde{w} = 0 \\ &\frac{\partial}{\partial t}\overline{(\cdot)} = \frac{\partial}{\partial t}\tilde{(\cdot)} = 0 \\ &\frac{\partial}{\partial x}\overline{(\cdot)} = \frac{\partial}{\partial x}\tilde{(\cdot)} = 0 \\ &\frac{\partial}{\partial z}\overline{(\cdot)} = \frac{\partial}{\partial z}\tilde{(\cdot)} = 0 \end{aligned}\right\} \overset{(2.1a),(2.6)}{\Longrightarrow} \begin{cases} \tilde{v} = 0 \\ \breve{\Theta} = \bar{\Theta} - \overline{\Theta'''} = 0 \end{cases} \tag{4.1}$$

which imply that convection by the Favre-averaged mean velocities $C_{(\cdot)} \overset{(4.1)}{=} 0$.

4.1. *Density variance and mass fluxes*

The transport equations for the density variance $\overline{\rho'^2}$ and for the mass fluxes $\bar{\rho}\overline{u''_i} \overset{(2.6c)}{=} -\overline{\rho' u'_i}$ were studied, in the context of compressible wall turbulence, by Taulbee & VanOsdol (1991). The transport equation for the density variance is also central in the work of Yoshizawa (1992) and other related studies (Hamba & Blaisdell 1997; Hamba 1999; Yoshizawa *et al.* 2013). The retained form of the equations which are obtained from the fluctuating parts of the continuity (2.1*a*) and momentum (2.1*b*) equations read

$$\underbrace{\frac{\partial \overline{\rho'^2}}{\partial t} + \tilde{u}_\ell \frac{\partial \overline{\rho'^2}}{\partial x_\ell}}_{C_{(\rho'^2)}} = \underbrace{-\frac{\partial \overline{\rho'^2 u''_\ell}}{\partial x_\ell}}_{d_{(\rho'^2)}} \underbrace{-2\overline{\rho' u'_\ell}\frac{\partial \bar{\rho}}{\partial x_\ell} - 2\overline{\rho'^2}\breve{\Theta}}_{P_{(\rho'^2)}} \underbrace{-2\bar{\rho}\overline{\rho'\Theta'''} - \overline{\rho'^2\Theta'''}}_{B_{(\rho'^2)}} \tag{4.2a}$$

$$\underbrace{\frac{\partial \bar{\rho}\overline{u''_i}}{\partial t} + \frac{\partial \bar{\rho}\overline{u''_i}\tilde{u}_\ell}{\partial x_\ell}}_{C_{(u''_i)}} = \underbrace{\frac{\partial}{\partial x_\ell}\left(\overline{\rho' u''_i u''_\ell} + \overline{\tau'_{i\ell}\left(\frac{\bar{\rho}}{\rho}\right)'}\right)}_{d_{(u''_i)}} \underbrace{-\bar{\rho}\overline{u''_\ell}\frac{\partial \tilde{u}_i}{\partial x_\ell} + \overline{u''_i u''_\ell}\frac{\partial \bar{\rho}}{\partial x_\ell}}_{P_{(u''_i)}}$$

$$+\underbrace{\bar\rho\overline{u_i''\Theta''}}_{B_{(u_i'')}}\underbrace{-\overline{\left(\frac{\bar\rho}{\rho}\right)'\frac{\partial p'}{\partial x_i}}}_{\Pi_{(u_i'')}}\underbrace{-\overline{\tau'_{i\ell}\frac{\partial}{\partial x_\ell}\left(\frac{\bar\rho}{\rho}\right)'}}_{\bar\rho\varepsilon_{(u_i'')}}$$
$$+\underbrace{\overline{\left(\frac{\bar\rho}{\rho}-1\right)\left(-\frac{\partial\bar p}{\partial x_i}+\frac{\partial\bar\tau_{i\ell}}{\partial x_\ell}\right)}}_{K_{(u_i'')}}+\bar\rho\overline{f''_{v_i}}. \tag{4.2b}$$

Note that, in line with Taulbee & VanOsdol (1991, (23), p. 4), the inverse of the relative density $\bar\rho\rho^{-1}$ was used in (4.2*b*).

As already stated, equation (4.1) implies that for streamwise invariant compressible turbulent plane channel flow $C_{(\rho'^2)}\overset{(4.2a),(4.1)}{=}0$ and $C_{(u_i'')}\overset{(4.2b),(4.1)}{=}0$. Furthermore, $(4.1)\Longrightarrow\breve\Theta=0$, so that, for the present flow $\overline{\rho'^2}$ is produced by density stratification only, i.e. $P_{(\rho'^2)}\overset{(4.2a),(4.1)}{=}-2\overline{\rho'v'}d_y\bar\rho\overset{(2.6c)}{=}2\bar\rho\overline{v''}d_y\bar\rho\geqslant0$ because $\overline{v''}\leqslant0$ (figure 10) and $d_y\bar\rho\leqslant0$ (figure 3). There is no explicit molecular mechanism (related to viscosity or heat conductivity) in (4.2*a*). Examination of the $y^\star$ distributions of the terms in (4.2*a*) indicates (figure 12) that the principal mechanism governing $\overline{\rho'^2}$ is a balance between production $P_{(\rho'^2)}\overset{(4.2a),(4.1),(2.6c)}{=}2\bar\rho\overline{v''}d_y\bar\rho\geqslant0\,\forall y^\star$ (gain) and the dilatational term $B_{(\rho'^2)}\leqslant0\,\forall y^\star$ (loss). The peak of production is located (figure 12) at $y^\star\approxeq9$, very near the $\overline{\rho'^2}$ peak (figure 10), while the peak of $B_{(\rho'^2)}$ is located (figure 12) at $y^\star\approxeq6$. Note that several equivalent expressions

$$-B_{(\rho'^2)}\overset{(4.2a)}{=}\overline{\left(2\bar\rho\rho'+\rho'^2\right)\Theta''}\overset{(2.6)}{=}\overline{\left(\rho^2-\bar\rho^2\right)\Theta''}\overset{(2.6)}{=}\overline{\left(2\rho\rho'-\rho'^2\right)\Theta''} \tag{4.3}$$

can be used for the dilatational term in (4.2*a*). Expectedly, diffusion $d_{(\rho'^2)}\overset{(4.2a),(4.1)}{=}-d_y(\overline{\rho'^2v''})$ contributes positively (gain) to $\overline{\rho'^2}$ in the region $y^\star\lessapprox7$, where $|B_{(\rho'^2)}|>P_{(\rho'^2)}$, by transporting high-$\overline{\rho'^2}$ fluid towards the wall (figure 10).

The limiting values at the wall of all of the mechanisms ($d_{(\rho'^2)}$, $P_{(\rho'^2)}$, $B_{(\rho'^2)}$) in (4.2*a*) are zero (figure 10). This can be shown analytically, by combining the no-slip condition at the wall

$$u_w=v_w=w_w\quad\forall x,z,t \tag{4.4a}$$

with the flow symmetries (4.1) and with the continuity equations (2.1*a*), (2.4*a*). Note first that

$$\Theta''_w\overset{(2.8b),(4.1)}{=}\Theta_w\overset{(2.1e),(4.4a)}{=}\left.\frac{\partial v}{\partial y}\right|_w\overset{(4.1)}{=}\left.\frac{\partial v''}{\partial y}\right|_w \tag{4.4b}$$

since by (4.4*a*) $(\partial_x u)_w=(\partial_x u'')_w=(\partial_z w)_w=(\partial_z w'')_w=0$. By (4.4a), (4.4b) the limiting form of the continuity equation (2.1a), (2.4a) at the wall reads

$$(2.1a),(2.4a)\overset{(4.1),(4.4a),(4.4b)}{\Longrightarrow}\frac{\partial\rho_w}{\partial t}+\rho_w\Theta''_w=0\Longrightarrow\left.\frac{\partial\overline{v''}}{\partial y}\right|_w\overset{(4.4b)}{=}\overline{\Theta''_w}=\frac{\partial}{\partial t}\left(\overline{\ln\frac{\bar\rho_w}{\rho_w}}\right)\overset{(4.1)}{=}0 \tag{4.4c}$$

where we used the fact that Reynolds averaging (non-weighted ensemble averaging) commutes with differentiation and that the flow is steady in the mean (4.1). Hence, the continuity equation (2.1*a*), (2.4*a*) implies that, although by (4.4*b*) the instantaneous velocity near the wall $[v''(x,y,z,t)]^+\sim-[\partial_t(\ln(\bar\rho_w^{-1}\rho_w))]y^+ + O(y^{+2})$ contains a linear

$Re_{\tau^\star}$	$\bar{M}_{CL}$	$N_x \times N_y \times N_z$	L_x	L_y	L_z	Δx^+	Δy_w^+	$N_{y^+\leqslant 10}$	Δy_{CL}^+	Δz^+	Δt^+	t_{OBS}^+	Δt_s^+
150	1.50	$361 \times 149 \times 433$	$4\pi\delta$	2δ	$\frac{4}{3}\pi\delta$	7.9	0.22	19	4.7	2.1	0.0164	868	0.0164

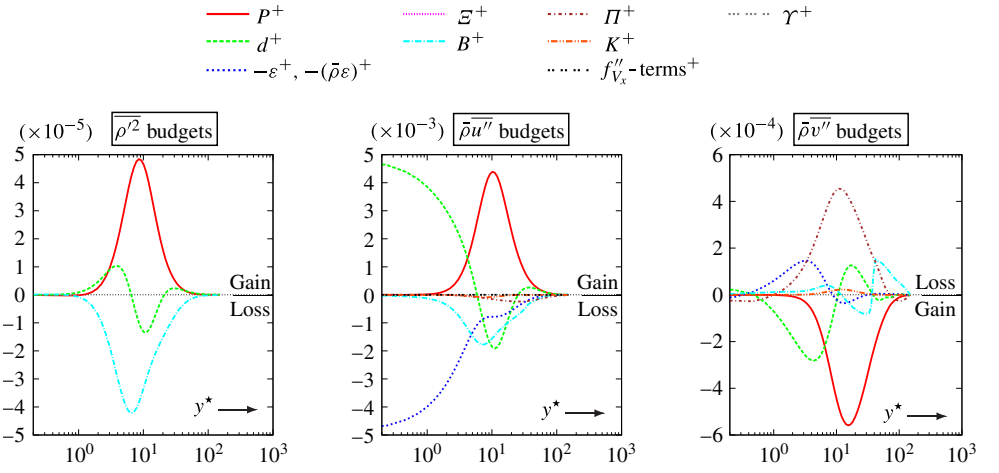

FIGURE 12. (Colour online) Budgets, in wall units (§ 3.2), of the transport equations (4.2*a*) for the density variance $\overline{\rho'^2}$ ($d_{(\rho'^2)}$, $P_{(\rho'^2)}$, $B_{(\rho'^2)}$) and (4.2*b*) for the mass fluxes $\overline{u_i''}$ ($d_{(u_i'')}$, $P_{(u_i'')}$, $B_{(u_i'')}$, $\Pi_{(u_i'')}$, $-\bar{\rho}\varepsilon_{(u_i'')}$, $K_{(u_i'')}$, $\bar{\rho}\overline{f''_{V_x}}$), obtained from DNS computations ($Re_{\tau^\star} \approxeq 150$, $\bar{M}_{CL} \approxeq 1.50$; table 1), plotted against $y^\star$ (3.1*c*).

with y^+ term, on the average $[\overline{v''}(y)]^+ \sim O(y^{+2})$, a behaviour verified by the DNS data (figure 10), implying also that $\overline{\Theta''_w} = 0$ (4.4*c*). Multiplying the limiting form (4.4*c*) of the continuity equation at the wall by ρ'_w and ρ_w, respectively, yields upon averaging

$$\bar{\rho}_w\overline{\rho'_w\Theta''_w} + \overline{\rho'^2_w\Theta''_w} \overset{(2.6a)}{=} \overline{\rho_w\rho'_w\Theta''_w} \overset{(4.4c)}{=} -\overline{\rho'_w\frac{\partial\rho_w}{\partial t}} \overset{(2.6a),(2.6b)}{=} -\frac{1}{2}\frac{\partial\overline{\rho'^2_w}}{\partial t} \overset{(4.1)}{=} 0 \quad (4.4d)$$

$$\bar{\rho}^2_w\overline{\Theta''_w} + 2\bar{\rho}_w\overline{\rho'_w\Theta''_w} + \overline{\rho'^2_w\Theta''_w} \overset{(2.6a)}{=} \overline{\rho^2_w\Theta''_w} \overset{(4.4c)}{=} -\frac{1}{2}\frac{\partial\overline{\rho^2_w}}{\partial t} \overset{(4.1)}{=} 0 \quad (4.4e)$$

which can be solved for $\overline{\rho'_w\Theta''_w}$ and $\overline{\rho'^2_w\Theta''_w}$, yielding using also (4.4*c*)

$$(4.4c\text{–}e) \Longrightarrow \bar{\rho}_w\overline{\rho'_w\Theta''_w} = \overline{\rho'^2_w\Theta''_w} = 0. \quad (4.4f)$$

Therefore,

$$[P_{(\rho'^2)}]_w \overset{(4.2a),(4.1)}{=} -\left[2\overline{\rho'v'}\frac{\mathrm{d}\bar{\rho}}{\mathrm{d}y}\right]_w \overset{(2.6a),(2.6b),(4.4a)}{=} 0 \quad (4.5a)$$

$$[d_{(\rho'^2)}]_w \overset{(4.2a),(4.1)}{=} -\left[\frac{\mathrm{d}}{\mathrm{d}y}\overline{\rho'^2v''}\right]_w \overset{(4.4a)}{=} -\left[\overline{\rho'^2\frac{\mathrm{d}v''}{\mathrm{d}y}}\right]_w \overset{(4.4b)}{=} -\overline{\rho'^2_w\Theta''_w} \overset{(4.4f)}{=} 0 \quad (4.5b)$$

$$[B_{(\rho'^2)}]_w \overset{(4.2a),(4.4f)}{=} 0. \quad (4.5c)$$

Regarding the streamwise mass flux $\bar{\rho}\overline{u''} \overset{(2.6c)}{=} -\overline{\rho' u'}$, production is related both with mean shear and with density stratification, $P_{(u'')} \overset{(4.2b),(4.1)}{=} -\bar{\rho}\overline{v''}d_y\tilde{u} + \overline{u''v''}d_y\bar{\rho} \geqslant 0$, because $\overline{v''} \leqslant 0$ (figure 10), $d_y\tilde{u} \geqslant 0$ (figure 3), $\overline{u''v''} \leqslant 0$ is of the same sign as $\overline{\rho u''v''}$ (figure 4) and $c_{u'v'}$ (figure 8), and $d_y\bar{\rho} \leqslant 0$ (figure 3). The production $P_{(u'')}$ peak is located (figure 12) at $y^\star \approxeq 10$ very near the $\overline{u''}$ peak (figure 10). The direct compressibility term in (4.2*b*) $K_{(u''^2)} \overset{(4.2b),(4.1)}{=} 0$ exactly, because of the streamwise invariance of the mean flow (4.1). The body-acceleration term $\bar{\rho}\overline{f''_{V_x}} \overset{(2.6c)}{=} -\overline{\rho' f'_{V_x}}$ in (4.2*b*) is negligibly small everywhere ($\forall y^\star$) in the $\overline{u''}$ budgets (figure 12). The term $\Pi_{(u'')}$ related with the fluctuating pressure gradient in (4.2*b*) is weak everywhere (figure 12), and negligibly small both near the wall ($y^\star \lessapprox 5$) and in the outer part of the flow (figure 12). Near the wall ($y^\star \lessapprox 4$) the budgets of the streamwise mass flux are dominated (figure 12) by the competition between destruction $-\bar{\rho}\varepsilon_{(u'')}$ (loss) and diffusion $d_{(u'')}$ (gain), both of which reach their maxima at the wall where $[P_{(u'')}]_w \overset{(4.2b),(4.4a)}{=} 0$. The dilatational term $B_{(u'')} \leqslant 0$ for all $y^\star$ (loss) is of the same magnitude as $-\bar{\rho}\varepsilon_{(u'')}$ for $y^\star \gtrapprox 5$ (figure 12).

The relative importance of various mechanisms in (4.2*b*) governing the wall-normal mass flux $\bar{\rho}\overline{v''} \overset{(2.6c)}{=} -\overline{\rho' v'} \leqslant 0$ (figure 10) differs (figure 12) from the streamwise mass-flux case. Production, because of the flow symmetries (4.1), is related to mean-density stratification only, $P_{(v'')} \overset{(4.2b),(4.1)}{=} \overline{v''^2}d_y\bar{\rho} \leqslant 0$, because $\overline{v''^2} \geqslant 0$ (figure 10) and $d_y\bar{\rho} \leqslant 0$ (figure 3), with a peak located at $y^\star \approxeq 16$ (figure 12), very near the $\overline{v''}$ peak (figure 10). Note that since $\overline{v''} \leqslant 0$ (figure 10), $P_{(v'')} \leqslant 0$ implies gain in the $\overline{v''}$ budgets. Contrary to the $\overline{u''}$ budgets, the principal mechanism opposing production $P_{(v'')}$ in the $\overline{v''}$ budgets (figure 12) is the fluctuating pressure-gradient term $\Pi_{(v'')} \geqslant 0$ for $y^\star \gtrsim 2$. Diffusion $d_{(v'')}$ and destruction $-\bar{\rho}\varepsilon_{(v'')}$ change sign two or three times across the channel generally opposing one another (figure 12). Near the wall $y^\star \in [1/2,\, 3]$ destruction $-\bar{\rho}\varepsilon_{(v'')} \geqslant \Pi_{(v'')}$ becomes the main loss mechanism in the $\overline{v''}$ budgets (figure 12), balanced by diffusion $d_{(v'')}$ (gain), while in the sublayer ($y^\star \lessapprox 0.5$) $\Pi_{(v'')} \leqslant 0$ (gain) opposing $d_{(v'')} \geqslant 0$ (loss) become the dominant mechanisms at the wall. Finally, the dilatational term $B_{(v'')}$ is active mainly in the outer part of the flow ($y^\star \gtrsim 40$; figure 12).

4.2. *Entropy variance and fluxes*

Entropy production (2.4*b*) and the continuity equation (2.4*a*) are the two generating relations in the development of transport equations for the thermodynamic variables (2.4*c–g*). In analogy with the continuity equation (2.4*a*) which expresses the substantial derivative of density $\bar{\rho}^{-1}D_t\rho$ in terms of the dilatation Θ (2.1*e*), (2.8*b*), the entropy transport equation expresses the substantial derivative of entropy $\rho TD_t s$ in terms of the viscous stresses and heat fluxes, representing the influence of viscosity and heat conductivity on the flow. Most of the studies involving thermodynamic fluctuations in compressible turbulence have focused on flows away from solid walls and have used simplified assumptions for the entropy fluctuations (Ristorcelli 1997; Rubinstein & Erlebacher 1997; Hamba 1999).

The evolution of the entropy variance and fluxes across the channel is very similar with those of density and temperature (figure 10), suggesting that the viscosity effects represented by $\rho TD_t s$ (2.4*b*), and hence entropy fluctuations, are important in wall-bounded flows. The exact equations for the mass-weighted entropy variance $\overline{\rho s''^2}$ and fluxes $\overline{\rho s'' u_i''}$ can be obtained from the fluctuating parts of the entropy (2.4*b*) and

momentum (2.1*b*) equations and read

$$\underbrace{\frac{\partial\overline{\rho s''^2}}{\partial t}+\frac{\partial\overline{\rho s''^2}\tilde{u}_\ell}{\partial x_\ell}}_{C_{(\rho s''^2)}}=\underbrace{-\frac{\partial\overline{\rho s''^2u''_\ell}}{\partial x_\ell}-\frac{\partial}{\partial x_\ell}\overline{\left(2\frac{s'q'_\ell}{T}\right)}}_{d_{(\rho s''^2)}}$$
$$\underbrace{-2\overline{\rho u''_\ell s''}\frac{\partial\tilde{s}}{\partial x_\ell}+2\overline{\frac{s'}{T}\tau'_{m\ell}}\bar{S}_{m\ell}+2\overline{\frac{s'}{T}S'_{m\ell}}\bar{\tau}_{m\ell}+2\overline{\left(\frac{s'}{T}\right)}\bar{\tau}_{m\ell}\bar{S}_{m\ell}-2\overline{\left(\frac{s'}{T}\right)}\frac{\partial\bar{q}_\ell}{\partial x_\ell}+2\overline{s'q'_\ell}\frac{\partial}{\partial x_\ell}\overline{\left(\frac{1}{T}\right)}}_{P_{(\rho s''^2)}}$$
$$\underbrace{-\left(-2\overline{\frac{q'_\ell}{T}\frac{\partial s'}{\partial x_\ell}}\right)}_{\bar{\rho}\varepsilon_{(\rho s''^2)}}\underbrace{+2\overline{s''}\left(\overline{\frac{\tau_{m\ell}S_{m\ell}}{T}}-\overline{\frac{1}{T}\frac{\partial q_\ell}{\partial x_\ell}}\right)}_{K_{(\rho s''^2)}}\underbrace{+2\overline{s'q'_\ell\frac{\partial}{\partial x_\ell}\left(\frac{1}{T}\right)'}+2\overline{\frac{s'}{T}\tau'_{m\ell}S'_{m\ell}}}_{\Xi_{(\rho s''^2)}} \tag{4.6a}$$

$$\underbrace{\frac{\partial\overline{\rho s''u''_i}}{\partial t}+\frac{\partial\overline{\rho s''u''_i}\tilde{u}_\ell}{\partial x_\ell}}_{C_{(\rho s''u''_i)}}$$
$$=\underbrace{-\frac{\partial\overline{\rho s''u''_iu''_\ell}}{\partial x_\ell}+\frac{\partial\overline{s'\tau'_{i\ell}}}{\partial x_\ell}-\frac{\partial}{\partial x_\ell}\overline{\left(\frac{u'_iq'_\ell}{T}\right)}}_{d_{(\rho s''u''_i)}}$$
$$\underbrace{-\overline{\rho u''_\ell s''}\frac{\partial\tilde{u}_i}{\partial x_\ell}-\overline{\rho u''_iu''_\ell}\frac{\partial\tilde{s}}{\partial x_\ell}+\overline{u'_iq'_\ell}\frac{\partial}{\partial x_\ell}\overline{\left(\frac{1}{T}\right)}-\overline{\left(\frac{u'_i}{T}\right)}\frac{\partial\bar{q}_\ell}{\partial x_\ell}}_{P_{(\rho s''u''_i)}}$$
$$\underbrace{+\overline{\frac{u'_i}{T}\tau'_{m\ell}}\bar{S}_{m\ell}+\overline{\frac{u'_i}{T}S'_{m\ell}}\bar{\tau}_{m\ell}+\overline{\left(\frac{u'_i}{T}\right)}\bar{\tau}_{m\ell}\bar{S}_{m\ell}}$$
$$\underbrace{+\overline{u''_i}\left(\overline{\frac{\tau_{m\ell}S_{m\ell}}{T}}-\overline{\frac{1}{T}\frac{\partial q_\ell}{\partial x_\ell}}\right)+\overline{s''}\left(-\frac{\partial\bar{p}}{\partial x_i}+\frac{\partial\bar{\tau}_{i\ell}}{\partial x_\ell}\right)}_{K_{(\rho s''u''_i)}}$$
$$\underbrace{+\overline{u'_iq'_\ell\frac{\partial}{\partial x_\ell}\left(\frac{1}{T}\right)'}+\overline{\frac{u'_i}{T}\tau'_{m\ell}S'_{m\ell}}}_{\Xi_{(\rho s''u''_i)}}\underbrace{-\left(-\overline{\frac{q'_\ell}{T}\frac{\partial u'_i}{\partial x_\ell}}+\overline{\tau'_{i\ell}\frac{\partial s'}{\partial x_\ell}}\right)}_{\bar{\rho}\varepsilon_{(\rho s''u''_i)}}\underbrace{-\overline{s'\frac{\partial p'}{\partial x_i}}}_{\Pi_{(\rho s''u''_i)}}+\overline{\rho s''f''_{V_i}}. \tag{4.6b}$$

Because of (2.4*b*), the factor T^{-1} appears in most of the terms of the transport equations for $\overline{\rho s''^2}$ (4.6*a*) and for $\overline{\rho s''u''_i}$ (4.6*b*). In the retained form of the (4.6), T^{-1} was treated as a weight, like ρ is treated in Favre-averaging (2.6*c*), in line with the general presentation of weighted averaging by Favre (1965).

The production of entropy fluctuations $P_{(\rho s''^2)}$ involves several mechanisms. Taking into account the flow symmetries (4.1), these mechanisms include (4.6*a*), (4.1) production by mean entropy stratification $-2\overline{\rho v''s''}d_y\tilde{s}$, by mean temperature stratification $2\overline{s'q'_y}d_y\overline{T^{-1}}$, by the gradient of the mean heat flux $-2\overline{T^{-1}s'}d_y\bar{q}_y$ (which involves because of Fourier's law (2.1*f*) the 2-derivative of mean temperature $d^2_{yy}\bar{T}$),

$Re_{\tau^\star}$	$\bar{M}_{CL}$	$N_x \times N_y \times N_z$	L_x	L_y	L_z	Δx^+	Δy_w^+	$N_{y^+\leqslant 10}$	Δy_{CL}^+	Δz^+	Δt^+	t_{OBS}^+	Δt_s^+
150	1.50	$361 \times 149 \times 433$	$4\pi\delta$	2δ	$\frac{4}{3}\pi\delta$	7.9	0.22	19	4.7	2.1	0.0164	868	0.0164

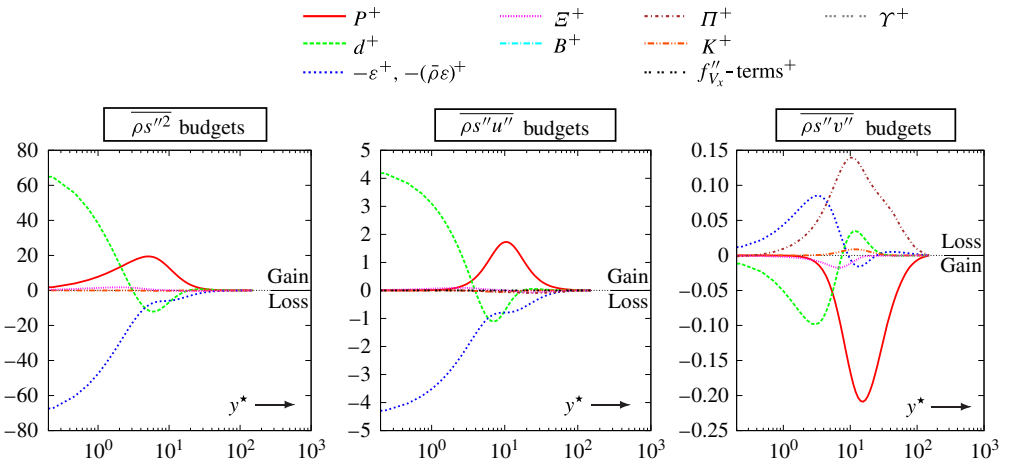

FIGURE 13. (Colour online) Budgets, in wall units (§ 3.2), of the transport equations (4.6*a*) for the entropy variance $\overline{\rho s''^2}$ ($d_{(\rho s''^2)}$, $P_{(\rho s''^2)}$, $-\bar{\rho}\varepsilon_{(\rho s''^2)}$, $K_{(\rho s''^2)}$, $\Xi_{(\rho s''^2)}$) and (4.6*b*) for the entropy fluxes $\overline{\rho s'' u_i''}$ ($d_{(\rho s'' u_i'')}$, $P_{(\rho s'' u_i'')}$, $K_{(\rho s'' u_i'')}$, $\Xi_{(\rho s'' u_i'')}$, $-\bar{\rho}\varepsilon_{(\rho s'' u_i'')}$, $\Pi_{(\rho s'' u_i'')}$, $\overline{\rho s'' f''_{V_x}}$), obtained from DNS computations ($Re_{\tau^\star} \approxeq 150$, $\bar{M}_{CL} \approxeq 1.50$; table 1), plotted against $y^\star$ (3.1*c*).

and three viscous work terms coming from the expansion of $\tau_{m\ell} S_{m\ell}$ in (2.4*b*). DNS data show that $P_{(\rho s''^2)} \geqslant 0$ (gain) everywhere (figure 13) with a peak located at $y^\star \approxeq 5$, and decays very slowly as $y^\star \to 0$. Destruction $-\bar{\rho}\varepsilon_{(\rho s''^2)} \leqslant 0$ (loss) everywhere (figure 13), while diffusion $d_{(\rho s''^2)} \leqslant 0$ (loss) for $y^\star \gtrapprox 3$ and $d_{(\rho s''^2)} \geqslant 0$ (gain) for $y^\star \lessapprox 3$ (figure 13). Very near the wall ($y^\star \lessapprox 2$) diffusion $d_{(\rho s''^2)} \geqslant 0$ (gain) mainly balances (figure 13) destruction $-\bar{\rho}\varepsilon_{(\rho s''^2)} \leqslant 0$ (loss). Finally, direct compressibility effects $K_{(\rho s''^2)}$ and the triple correlations term $\Xi_{(\rho s''^2)}$ are negligibly small everywhere (figure 13).

Regarding the streamwise entropy flux $\overline{\rho s'' u''} \geqslant 0$ (figure 10), production $P_{(\rho s'' u'')}$ (4.6*b*) involves all of the mechanisms present in $P_{(\rho s''^2)}$ (4.6*a*), and an extra mechanism, which for the present flow (4.1) is associated with mean shear, $-\overline{\rho s'' v''} d_y \tilde{u}$ (4.6*b*), (4.1). The DNS data indicate that $P_{(\rho s'' u'')} \geqslant 0$ (gain) everywhere (figure 13), with a peak located at $y^\star \approxeq 10$, and diminishes as $y^+ \to 0$, at a much faster rate compared with $P_{(\rho s''^2)}$. Note that all of the terms in $P_{(\rho s'' u_i'')}$ are proportional to correlations of the fluctuating velocities (4.6*b*), implying by (4.4*a*) that $[P_{(\rho s'' u'')}]_w = [P_{(\rho s'' v'')}]_w = 0$, whereas $[P_{(\rho s''^2)}]_w \neq 0$ (4.6*a*). The direct compressibility effects $K_{(\rho s'' u'')}$, the triple correlations term $\Xi_{(\rho s'' u'')}$, the term related with the fluctuating pressure gradient $\Pi_{(\rho s'' u'')}$ and the body-acceleration term $\overline{\rho s'' f''_{V_x}}$ are negligible everywhere (figure 13) in the $\overline{\rho s'' u''}$ budgets (4.6*b*). Diffusion $d_{(\rho s'' u'')}$ and destruction $-\bar{\rho}\varepsilon_{(\rho s'' u'')} \leqslant 0$ (loss) behave (figure 13) in a way similar with their counterparts in the $\overline{\rho s''^2}$ budgets, and approximately balance one another at the wall (figure 13).

Finally, the budgets of the wall-normal flux $\overline{\rho s'' v''} \leqslant 0$ (figure 10) differ (figure 13) from those of the streamwise flux $\overline{\rho s'' u''}$ because of the relative importance of the term $\Pi_{(\rho s'' v'')} \geqslant 0$ (loss) related with the fluctuating pressure gradient in (4.6*b*),

which (figure 13) is the main mechanism opposing production $P_{(\rho s''v'')} \leqslant 0$ (gain). The peak of production $P_{(\rho s''v'')}$ is located at $y^\star \approxeq 15$, near the peak of $\overline{\rho s''v''}$ (figure 10), while the peak of $\Pi_{(\rho s''v'')}$ is located at $y^\star \approxeq 10$ (figure 13). Both the triple correlations $\Xi_{(\rho s''v'')} \leqslant 0$ (gain) and the direct compressibility effects $K_{(\rho s''v'')} \geqslant 0$ (loss) have weak contribution to the $\overline{\rho s''v''}$ budgets (figure 13). Finally, destruction $-\bar{\rho}\varepsilon_{(\rho s''v'')} \geqslant 0$ for all $y^\star \lessapprox 9$ (loss) and diffusion $d_{(\rho s''v'')} \leqslant 0$ for all $y^\star \lessapprox 8$ (gain) oppose each other everywhere, and are the dominant mechanisms in the near-wall region ($y^\star \lessapprox 2$) where all of the other terms ($P_{(\rho s''v'')}$, $\Pi_{(\rho s''v'')}$, $\Xi_{(\rho s''v'')}$ and $K_{(\rho s''v'')}$) are negligibly small (figure 13).

4.3. *Temperature variance and heat fluxes*

Turbulent heat fluxes $\overline{\rho h''u_i''} \overset{(2.1d)}{=} -c_p\overline{\rho T''u_i''}$ (Bowersox 2009) are important in compressible flows because they appear in the mean energy equation (Huang *et al.* 1995, (3.6), p. 196) and affect the mean-flow via the mean static temperature field. Tamano & Morinishi (2006) studied the DNS budgets of the transport equation for the temperature variance $\overline{\rho T''^2}$ in compressible turbulent plane channel flow, and Shahab *et al.* (2011) those of the equation for temperature transport $\overline{\rho T''u_i''}$ in ZPG compressible turbulent boundary-layer flow ($\bar{M}_e \approxeq 2.25$) over both isothermal ($\bar{T}_e^{-1}\bar{T}_w = 1.35$) and adiabatic walls. Both these studies were based on the c_v form (2.4*d*) of the temperature equation, and contain dilatational ($[\cdot]\breve{\Theta}$ or $\overline{[\cdot]\Theta''}$) terms. Alternatively (Le Ribault & Friedrich 1997) it is possible to work with the c_p form, containing instead terms stemming from the correlation $c_p^{-1}\overline{T''(D_tp)'}$ in the equations for the temperature variance $\overline{\rho T''^2}$ or $c_p^{-1}\overline{u_i''(D_tp)'}$ in the equations for the temperature transport $\overline{\rho T''u_i''}$.

The c_v form of the transport equations for the mass-weighted temperature variance $\overline{\rho T''^2}$ and fluxes $\overline{\rho T''u_i''}$ is obtained from the fluctuating parts of the temperature (2.4*d*) and momentum (2.1*b*) equations, and reads

$$\underbrace{\frac{\partial\overline{\rho T''^2}}{\partial t}+\frac{\partial\overline{\rho T''^2}\tilde{u}_\ell}{\partial x_\ell}}_{C_{(\rho T''^2)}} = \underbrace{-\frac{\partial\overline{\rho T''^2u_\ell''}}{\partial x_\ell}-\frac{\partial}{\partial x_\ell}\left(\frac{2}{c_v}\overline{T'q_\ell'}\right)}_{d_{(\rho T''^2;c_v)}} \underbrace{-2\overline{\rho u_\ell''T''}\frac{\partial\tilde{T}}{\partial x_\ell}+\frac{2}{c_v}\overline{T'\tau_{m\ell}'}\bar{S}_{m\ell}+\frac{2}{c_v}\overline{T'S_{m\ell}'}\bar{\tau}_{m\ell}-\frac{2}{c_v}\overline{T'p'}\breve{\Theta}}_{P_{(\rho T''^2;c_v)}} \underbrace{-\left(-\frac{2}{c_v}\overline{q_\ell'\frac{\partial T'}{\partial x_\ell}}\right)}_{\bar{\rho}\varepsilon_{(\rho T''^2;c_v)}} \underbrace{+\frac{2}{c_v}\overline{T''}\left(-\overline{p\Theta}+\overline{\tau_{m\ell}S_{m\ell}}-\frac{\partial\bar{q}_\ell}{\partial x_\ell}\right)}_{K_{(\rho T''^2;c_v)}} \underbrace{+\frac{2}{c_v}\overline{T'\tau_{m\ell}'S_{m\ell}'}}_{\Xi_{(\rho T''^2;c_v)}} \underbrace{-\frac{2}{c_v}\overline{pT'\Theta''}}_{B_{(\rho T''^2;c_v)}} \tag{4.7a}$$

$$\underbrace{\frac{\partial\overline{\rho T''u_i''}}{\partial t}+\frac{\partial\overline{\rho T''u_i''}\tilde{u}_\ell}{\partial x_\ell}}_{C_{(\rho T''u_i'')}}=\underbrace{-\frac{\partial\overline{\rho T''u_i''u_\ell''}}{\partial x_\ell}+\frac{\partial\overline{T'\tau'_{i\ell}}}{\partial x_\ell}-\frac{\partial}{\partial x_\ell}\left(\frac{1}{c_v}\overline{u_i'q'_\ell}\right)}_{d_{(\rho T''u_i'';c_v)}}$$
$$\underbrace{-\overline{\rho u_\ell''T''}\frac{\partial\tilde{u}_i}{\partial x_\ell}-\overline{\rho u_i''u_\ell''}\frac{\partial\tilde{T}}{\partial x_\ell}+\frac{1}{c_v}\left(\overline{u_i'\tau'_{m\ell}}\bar{S}_{m\ell}+\overline{u_i'S'_{m\ell}}\bar{\tau}_{m\ell}\right)-\frac{1}{c_v}\overline{p'u_i'}\breve{\Theta}}_{P_{(\rho T''u_i'';c_v)}}$$
$$\underbrace{+\frac{1}{c_v}\overline{u_i''}\left(\overline{\tau_{m\ell}S_{m\ell}}-\frac{\partial\bar{q}_\ell}{\partial x_\ell}-\overline{p\Theta}\right)+\overline{T''}\left(-\frac{\partial\bar{p}}{\partial x_i}+\frac{\partial\bar{\tau}_{i\ell}}{\partial x_\ell}\right)}_{K_{(\rho T''u_i'';c_v)}}\underbrace{+\frac{1}{c_v}\overline{u_i'\tau'_{m\ell}S'_{m\ell}}}_{\Xi_{(\rho T''u_i'';c_v)}}$$
$$\underbrace{-\frac{1}{c_v}\overline{u_i'p\Theta''}}_{B_{(\rho T''u_i'';c_v)}}\underbrace{-\left(-\frac{1}{c_v}\overline{q'_\ell\frac{\partial u_i'}{\partial x_\ell}}+\overline{\tau'_{i\ell}\frac{\partial T'}{\partial x_\ell}}\right)}_{\tilde{\rho}\varepsilon_{(\rho T''u_i'';c_v)}}\underbrace{-\overline{T'\frac{\partial p'}{\partial x_i}}}_{\Pi_{(\rho T''u_i'')}}+\overline{\rho T''f''_{V_i}}. \tag{4.7b}$$

The terms in (4.7) which correspond to production by mean dilatation $\breve{\Theta}$, in $P_{(\rho T''^2;c_v)}$ (4.7*a*) and $P_{(\rho T''u_i'';c_v)}$ (4.7*b*), and those containing the fluctuating dilatation Θ'', i.e. $B_{(\rho T''^2;c_v)}$ (4.7*a*) and $B_{(\rho T''u_i'';c_v)}$ (4.7*b*), are generated by the term $-c_v^{-1}(p\Theta)'$ in the fluctuating part of (2.4*d*), and can be grouped together as

$$-\frac{2}{c_v}\overline{T'p'}\tilde{\Theta}+B_{(\rho T''^2;c_v)}\overset{(4.7a),(2.6)}{=}-\frac{2}{c_v}\overline{T''(p\Theta)'}\overset{(2.6d)}{=}-\frac{2}{c_v}\overline{T'(p\Theta)'} \tag{4.8a}$$
$$-\frac{2}{c_v}\overline{p'u_i'}\tilde{\Theta}+B_{(\rho T''u_i'';c_v)}\overset{(4.7b),(2.6)}{=}-\frac{2}{c_v}\overline{u_i''(p\Theta)'}\overset{(2.6d)}{=}-\frac{2}{c_v}\overline{u_i'(p\Theta)'}. \tag{4.8b}$$

Examination of the budgets of (4.7) reveals a striking similarity between the $y^\star$ distributions across the channel of the budgets of the mass-weighted variance and fluxes of entropy ($\overline{\rho s''^2}$, $\overline{\rho s''u_i''}$; figure 13) with those of temperature ($\overline{\rho T''^2}$, $\overline{\rho T''u_i''}$; figure 14), as could be expected because of the strong correlation coefficient $c_{s'T'}\approxeq 1$ for all $y^\star\in[1,50]$ (figure 6), and generally $c_{s'T'}\geqslant 6/10$ for all y (figure 7), in line with the statement on 'temperature (entropy) spots' of Kovásznay (1953, p. 661) when referring to the entropy mode of compressible turbulent fluctuations.

Alternatively, the fluctuating part of (2.4*e*) can be used in lieu of (2.4*d*), and yields the c_p form of the transport equations for the temperature variance $\overline{\rho T''^2}$ and fluxes $\overline{\rho T''u_i''}$

$$\underbrace{\frac{\partial\overline{\rho T''^2}}{\partial t}+\frac{\partial\overline{\rho T''^2}\tilde{u}_\ell}{\partial x_\ell}}_{C_{(\rho T''^2)}}=\underbrace{-\frac{\partial}{\partial x_\ell}\left(\overline{\rho T''^2u_\ell''}+\frac{2}{c_p}\overline{T'q'_\ell}\right)}_{d_{(\rho T''^2;c_p)}}$$
$$\underbrace{-2\overline{\rho u_\ell''T''}\frac{\partial\tilde{T}}{\partial x_\ell}+\frac{2}{c_p}\left(\overline{T'\tau'_{m\ell}}\bar{S}_{m\ell}+\overline{T'S'_{m\ell}}\bar{\tau}_{m\ell}\right)}_{P_{(\rho T''^2;c_p)}}$$

$Re_{\tau^\star}$	$\bar{M}_{CL}$	$N_x \times N_y \times N_z$	L_x	L_y	L_z	Δx^+	Δy_w^+	$N_{y^+\leqslant 10}$	Δy_{CL}^+	Δz^+	Δt^+	t_{OBS}^+	Δt_s^+
150	1.50	$361 \times 149 \times 433$	$4\pi\delta$	2δ	$\frac{4}{3}\pi\delta$	7.9	0.22	19	4.7	2.1	0.0164	868	0.0164

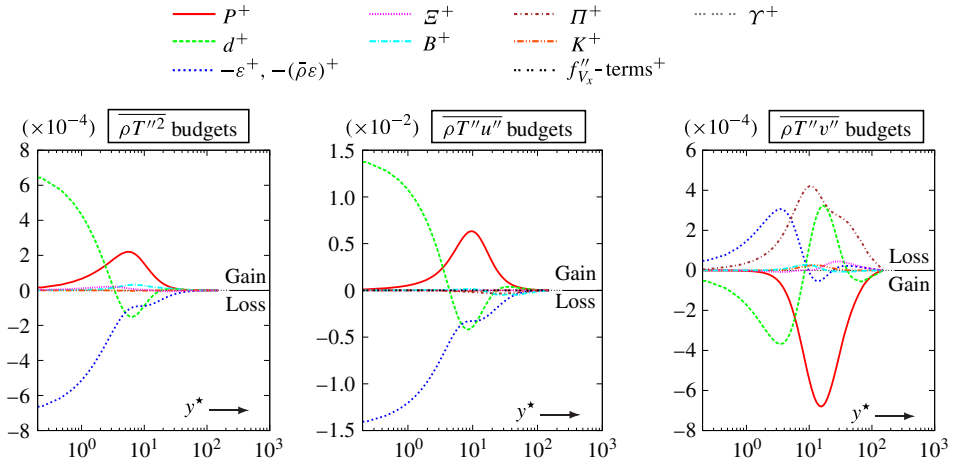

FIGURE 14. (Colour online) Budgets, in wall units (§ 3.2), of the c_v-form of the transport equations (4.7*a*) for the temperature variance $\overline{\rho T''^2}$ ($d_{(\rho T''^2;c_v)}$, $P_{(\rho T''^2;c_v)}$, $-\rho\varepsilon_{(\rho T''^2;c_v)}$, $K_{(\rho T''^2;c_v)}$, $\Xi_{(\rho T''^2;c_v)}$, $B_{(\rho T''^2;c_v)}$) and (4.7*b*) for the temperature fluxes $\overline{\rho T''u_i''}$ ($d_{(\rho T''u_i'';c_v)}$, $P_{(\rho T''u_i'';c_v)}$, $K_{(\rho T''u_i'';c_v)}$, $\Xi_{(\rho T''u_i'';c_v)}$, $B_{(\rho T''u_i'';c_v)}$, $-\bar{\rho}\varepsilon_{(\rho T''u_i'';c_v)}$, $\Pi_{(\rho T''u_i'')}$, $\overline{\rho T''f''_{V_x}}$), obtained from DNS computations ($Re_{\tau^\star} \approxeq 150$, $\bar{M}_{CL} \approxeq 1.50$; table 1), plotted against $y^\star$ (3.1*c*).

$$\underbrace{\frac{\partial \overline{\rho T''u_i''}}{\partial t} + \frac{\partial \overline{\rho T''u_i''}\tilde{u}_\ell}{\partial x_\ell}}_{C_{(\rho T''u_i'')}} = \underbrace{-\frac{\partial \overline{\rho T''u_i''u_\ell''}}{\partial x_\ell} + \frac{\partial \overline{T'\tau_{i\ell}'}}{\partial x_\ell} - \frac{\partial}{\partial x_\ell}\left(\frac{1}{c_p}\overline{u_i'q_\ell'}\right)}_{d_{(\rho T''u_i'';c_p)}}$$
$$\underbrace{-\overline{\rho u_\ell''T''}\frac{\partial \tilde{u}_i}{\partial x_\ell} - \overline{\rho u_i''u_\ell''}\frac{\partial \tilde{T}}{\partial x_\ell} + \frac{1}{c_p}\left(\overline{u_i'\tau_{m\ell}'}\bar{S}_{m\ell} + \overline{u_i'S_{m\ell}'}\bar{\tau}_{m\ell}\right)}_{P_{(\rho T''u_i'';c_p)}}$$
$$\underbrace{-\left(-\frac{1}{c_p}\overline{q_\ell'\frac{\partial u_i'}{\partial x_\ell}} + \overline{\tau_{i\ell}'\frac{\partial T'}{\partial x_\ell}}\right)}_{\bar{\rho}\varepsilon_{(\rho T''u_i'';c_p)}}$$
$$\underbrace{-\left(-\frac{2}{c_p}\overline{q_\ell'\frac{\partial T'}{\partial x_\ell}}\right)}_{\bar{\rho}\varepsilon_{(\rho T''^2;c_p)}} + \underbrace{\frac{2}{c_p}\overline{T''}\left(\overline{\frac{\mathrm{D}p}{\mathrm{D}t}} + \overline{\tau_{m\ell}S_{m\ell}} - \frac{\partial \bar{q}_\ell}{\partial x_\ell}\right)}_{K_{(\rho T''^2;c_p)}}$$
$$+ \underbrace{\frac{2}{c_p}\overline{T'\tau_{m\ell}'S_{m\ell}'}}_{\Xi_{(\rho T''^2;c_p)}} + \underbrace{\frac{2}{c_p}\overline{T'\left(\frac{\mathrm{D}p}{\mathrm{D}t}\right)'}}_{\Upsilon_{(\rho T''^2;c_p)}} \tag{4.9a}$$

$Re_{\tau^\star}$	$\bar{M}_{CL}$	$N_x \times N_y \times N_z$	L_x	L_y	L_z	Δx^+	Δy^+_w	$N_{y^+\leqslant 10}$	Δy^+_{CL}	Δz^+	Δt^+	t^+_{OBS}	Δt^+_s
150	1.50	$361 \times 149 \times 433$	$4\pi\delta$	2δ	$\frac{4}{3}\pi\delta$	7.9	0.22	19	4.7	2.1	0.0164	868	0.0164

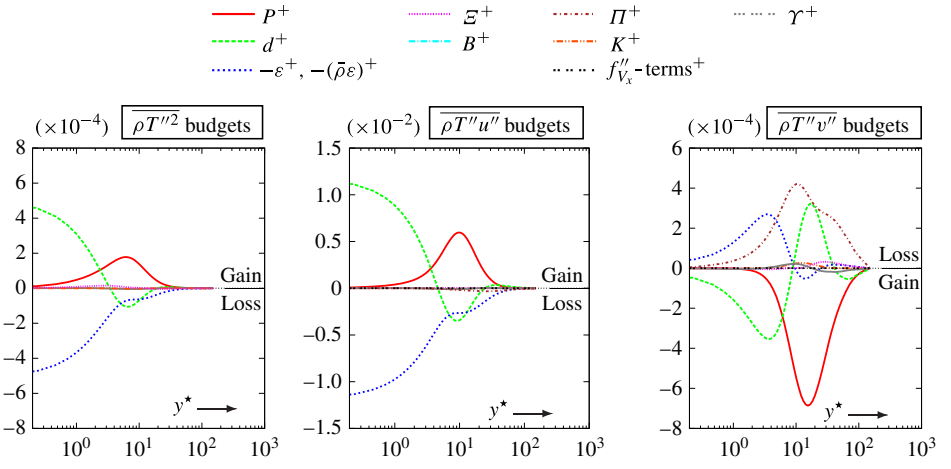

FIGURE 15. (Colour online) Budgets, in wall units (§ 3.2), of the c_p form of the transport equations (4.10*a*) for the temperature variance $\overline{\rho T''^2}$ ($d_{(\rho T''^2;c_p)}$, $P_{(\rho T''^2;c_p)}$, $-\rho\varepsilon_{(\rho T''^2;c_p)}$, $K_{(\rho T''^2;c_p)}$, $\Xi_{(\rho T''^2;c_p)}$, $\Upsilon_{(\rho T''^2;c_p)}$) and (4.10*b*) for the temperature fluxes $\overline{\rho T''u''_i}$ ($d_{(\rho T''u''_i;c_p)}$, $P_{(\rho T''u''_i;c_p)}$, $K_{(\rho T''u''_i;c_p)}$, $\Xi_{(\rho T''u''_i;c_p)}$, $\Upsilon_{(\rho T''u''_i;c_p)}$, $-\bar{\rho}\varepsilon_{(\rho T''u''_i;c_p)}$, $\Pi_{(\rho T''u''_i)}$, $\overline{\rho T''f''_{V_x}}$), obtained from DNS computations ($Re_{\tau^\star} \approxeq 150$, $\bar{M}_{CL} \approxeq 1.50$; table 1), plotted against $y^\star$ (3.1*c*).

$$+\underbrace{\frac{1}{c_p}\overline{u''_i}\left(\overline{\frac{\mathrm{D}p}{\mathrm{D}t}}+\overline{\tau_{m\ell}S_{m\ell}}-\frac{\partial\bar{q}_\ell}{\partial x_\ell}\right)+\overline{T''}\left(-\frac{\partial\bar{p}}{\partial x_i}+\frac{\partial\bar{\tau}_{i\ell}}{\partial x_\ell}\right)}_{K_{(\rho T''u''_i;c_p)}}$$

$$+\underbrace{\frac{1}{c_p}\overline{u'_i\tau'_{m\ell}S'_{m\ell}}}_{\Xi_{(\rho T''u''_i;c_p)}}\underbrace{-\overline{T'\frac{\partial p'}{\partial x_i}}}_{\Pi_{(\rho T''u''_i)}}+\overline{\rho T''f''_{V_i}}+\underbrace{\frac{1}{c_p}\overline{u'_i\left(\overline{\frac{\mathrm{D}p}{\mathrm{D}t}}\right)'}}_{\Upsilon_{(\rho T''u''_i;c_p)}} \tag{4.9b}$$

where

$$\overline{\frac{\mathrm{D}(\cdot)}{\mathrm{D}t}} := \overline{\frac{\partial(\cdot)}{\partial t}+u_j\frac{\partial(\cdot)}{\partial x_j}}=\frac{\partial\overline{(\cdot)}}{\partial t}+\bar{u}_j\frac{\partial\overline{(\cdot)}}{\partial x_j}+\overline{u'_j\frac{\partial(\cdot)'}{\partial x_j}} \tag{4.10a}$$

$$\left[\frac{\mathrm{D}(\cdot)}{\mathrm{D}t}\right]' := \frac{\mathrm{D}(\cdot)}{\mathrm{D}t}-\overline{\frac{\mathrm{D}(\cdot)}{\mathrm{D}t}}=\frac{\partial(\cdot)'}{\partial t}+\bar{u}_j\frac{\partial(\cdot)'}{\partial x_j}+u'_j\frac{\partial\overline{(\cdot)}}{\partial x_j}+u'_j\frac{\partial(\cdot)'}{\partial x_j}-\overline{u'_j\frac{\partial(\cdot)'}{\partial x_j}}. \tag{4.10b}$$

The general shape and relative importance of the dominant mechanisms in the budgets of the transport equations for $\overline{\rho T''^2}$ (4.7*a*), (4.9*a*) and for $\overline{\rho T''u''_i}$ (4.7*b*), (4.9*b*) are quite similar between the c_v form (figure 14) and the c_p form (figure 15), because some of the terms are identical, e.g. the diffusion mechanisms $-\partial_{x_\ell}\overline{\rho T''u''_\ell}$ (4.7*a*), (4.9*a*) and $\partial_{x_\ell}(-\overline{\rho T''u''_i u''_\ell}+\overline{T'\tau'_{i\ell}})$ (4.7*b*), (4.9*b*), the pressure scrambling term $\Pi_{(\rho T''u''_i)}$ (4.7*b*), (4.9*b*), and the production terms $-2\overline{\rho u''_\ell T''}\partial_{x_\ell}\tilde{T}$ (4.7*a*), (4.9*a*) and $-\overline{\rho u''_\ell T''}\partial_{x_\ell}\tilde{u}_i-\overline{\rho u''_i u''_\ell}\partial_{x_\ell}\tilde{T}$ (4.7*b*), (4.9*b*), while many others have a constant ratio

$\gamma = c_v^{-1}c_p = 1.4$ in the present DNS computations. Therefore, the main differences between the two forms (4.7), (4.9) are in the compressible terms $B_{(\cdot)}$ (4.7) and $\Upsilon_{(\cdot)}$ (4.9). Note that the flow symmetries (4.1) $\Longrightarrow \breve{\Theta} = 0$, so that only $B_{(\cdot)}$ remains in (4.8). All compressible terms in (4.7), (4.9), namely $K_{(\cdot)}$, $B_{(\cdot)}$ or $\Upsilon_{(\cdot)}$, are generally weak (figures 14 and 15). The term $\Upsilon_{(\rho T''^2;c_p)} \overset{(4.9a)}{=} 2c_p^{-1}\overline{T'(D_t p)'}$ in (4.9*a*) is negligibly small (figure 15) and much smaller than the weak term $B_{(\rho T''^2;c_v)}$ (figure 14) in (4.7*a*). In both forms (figures 14 and 15), the main mechanisms in the budgets of $\overline{\rho T''^2}$ are similar one with another and with the budgets of $\overline{\rho s''^2}$ (figure 13). Note that $\varepsilon^{-1}_{(\rho T''^2;c_p)}\varepsilon_{(\rho T''^2;c_v)} \overset{(4.7a),(4.7b)}{=} c_v^{-1}c_p = \gamma$ exactly, and that the same applies to the very weak triple correlations $\Xi^{-1}_{(\rho T''^2;c_p)}\Xi_{(\rho T''^2;c_v)} \overset{(4.7a),(4.7b)}{=} \gamma$ (figures 14 and 15). Diffusion $d_{(\rho T''u'';\cdot)}$, destruction $-\bar{\rho}\varepsilon_{(\rho T''u'';\cdot)}$ and production $P_{(\rho T''u'';\cdot)}$ are the main mechanisms governing the $\overline{\rho T''u''}$-budgets (figures 14 and 15), while $\Upsilon_{(\rho T''u'';c_p)}$ (figure 15) is negligibly small and $B_{(\rho T''u'';c_v)}$ (figure 14) is very weak but larger than $\Upsilon_{(\rho T''u'';c_p)}$. Finally, like for s'' (figure 13), the pressure scrambling term $\Pi_{(\rho T''v'';\cdot)} \geqslant 0$ for all $y^\star$, which is common to both forms (4.7*b*), (4.9*b*), is a major loss mechanism in the budgets of $\overline{\rho T''v''} \leqslant 0$ (figure 10).

The terms related with compressibility, apart from the direct compressibility effects $K_{(\cdot)}$, are $B_{(\cdot)}$ in (4.7), recalling that (4.1) $\Longrightarrow \breve{\Theta} = 0$ in (4.8), and $\Upsilon_{(\cdot)}$ in (4.9), and are generally weak. In particular, the very small contribution of $\Upsilon_{(\cdot)}$ in the budgets of (4.9) (figure 14), implies that the corresponding term can probably be neglected, or modelled as a single term without applying further decomposition as in (4.10).

4.4. *Pressure variance and transport*

It is generally accepted that pressure fluctuations p' behave differently than the fluctuations of density ρ' or temperature T', because of their strong dependence on the dynamic field (velocity fluctuations u_i'). In incompressible flow p' are simply a consequence of the velocity field through the Poisson equation for p' (Chou 1945), while studies of the compressible analog of this equation (Gerolymos *et al.* 2013) suggest that, in wall-bounded compressible flows, the extra compressible terms do not alter substantially this subordination to the dynamic field (Foysi *et al.* 2004). Related to this conceptual view of pressure fluctuations is the non-locality of p' (Kim 1989; Chang *et al.* 1999). In this context, Sarkar (1992) split the fluctuating pressure into an incompressible and a compressible part. This (Sarkar 1992, (5), p. 2676) is equivalent to applying a Helmholtz decomposition (Hamba 1999) splitting the fluctuating velocity field, into a solenoidal and a compressible part, and defined solenoidal pressure fluctuations obtained by the solution of a Poisson equation driven by the solenoidal velocity field (Hamba 1999, (16), p. 1625) as a part of the actual thermodynamic pressure fluctuations. Yoshizawa *et al.* (2013) applied a similar distinction between the actual thermodynamic pressure fluctuations and those subordinated to the fluctuating velocity field, to ensure smooth limiting behaviour (incompressible flow limit) of their model as $[\bar{\rho}^{-1}\rho']_{rms} \to 0$ (Gerolymos *et al.* 2013, Appendix A, pp. 45–51). For these reasons, all models for the pressure terms in Reynolds-stress transport closures, even in compressible flow with shock waves (Gerolymos *et al.* 2012*b*), are based on tensorial representations constructed from the strain-rate, vorticity-rate and anisotropy tensors (Gerolymos, Lo & Vallet 2012*a*), eventually augmented by gradients of turbulent quantities (Gerolymos *et al.* 2012*b*).

These observations notwithstanding, it is possible, formally, to derive, using the fluctuating part of (2.4*c*), $(D_t p)' \overset{(2.4c)}{=} -\gamma(p\Theta)' + (\gamma - 1)(\tau_{m\ell}S_{m\ell} - \partial_{x_\ell}q_\ell)'$, transport

equations for the variance $\overline{p'^2}$

$$\underbrace{\frac{\partial\overline{p'^2}}{\partial t}+\tilde{u}_\ell\frac{\partial\overline{p'^2}}{\partial x_\ell}}_{C_{(p'^2)}}=\underbrace{-\frac{\partial\overline{p'^2u''_\ell}}{\partial x_\ell}-\frac{\partial}{\partial x_\ell}\left(2(\gamma-1)\overline{p'q'_\ell}\right)}_{d_{(p'^2)}}$$
$$\underbrace{-2\overline{p'u'_\ell}\frac{\partial\bar{p}}{\partial x_\ell}-2\gamma\overline{p'^2}\breve{\Theta}+2(\gamma-1)\left(\overline{p'\tau'_{m\ell}}\bar{S}_{m\ell}+\overline{p'S'_{m\ell}}\bar{\tau}_{m\ell}\right)}_{P_{(p'^2)}}$$
$$\underbrace{-\left(-2(\gamma-1)q'_\ell\overline{\frac{\partial p'}{\partial x_\ell}}\right)}_{\varepsilon_{(p'^2)}}\underbrace{+2(\gamma-1)\overline{p'\tau'_{m\ell}S'_{m\ell}}}_{\Xi_{(p'^2)}}$$
$$\underbrace{-\overline{\left((2\gamma-1)p'^2+2\gamma\bar{p}p'\right)\Theta''}}_{B_{(p'^2)}}\qquad(4.11a)$$

and, combining with the fluctuating part of the momentum equation (2.1*b*), for the transport by the fluctuating velocity field $\overline{p'u'_i}$

$$\underbrace{\frac{\partial\overline{p'u'_i}}{\partial t}+\tilde{u}_\ell\frac{\partial\overline{p'u'_i}}{\partial x_\ell}}_{C_{(p'u'_i)}}$$
$$=\underbrace{-\frac{\partial}{\partial x_\ell}\left(\overline{p'u'_iu''_\ell}\right)-\frac{\partial}{\partial x_\ell}\left((\gamma-1)\overline{u'_iq'_\ell}\right)+\frac{\partial}{\partial x_\ell}\overline{\left(\frac{p'}{\rho}\tau'_{i\ell}\right)}}_{d_{(p'u'_i)}}$$
$$\underbrace{-\overline{p'u'_\ell}\frac{\partial\bar{u}_i}{\partial x_\ell}-\gamma\overline{p'u'_i}\breve{\Theta}-\overline{u'_iu'_\ell}\frac{\partial\bar{p}}{\partial x_\ell}+\overline{\left(\frac{p'}{\rho}\right)}\left(\frac{\partial\bar{\tau}_{i\ell}}{\partial x_\ell}-\frac{\partial\bar{p}}{\partial x_i}\right)}_{P_{(p'u'_i)}}\cdots$$
$$\cdots\underbrace{+(\gamma-1)(\overline{u'_iS'_{m\ell}}\bar{\tau}_{m\ell}+\overline{u'_i\tau'_{m\ell}}\bar{S}_{m\ell})-\overline{p'\tau'_{i\ell}}\frac{\partial}{\partial x_\ell}\overline{\left(\frac{1}{\rho}\right)}}$$
$$\underbrace{-\left(-(\gamma-1)q'_\ell\overline{\frac{\partial u'_i}{\partial x_\ell}}+\overline{\frac{\tau'_{i\ell}}{\rho}\frac{\partial p'}{\partial x_\ell}}\right)}_{\varepsilon_{(p'u'_i)}}\underbrace{+(\gamma-1)\overline{u'_i\tau'_{m\ell}S'_{m\ell}}-\overline{p'\tau'_{i\ell}\frac{\partial}{\partial x_\ell}\left(\frac{1}{\rho}\right)'}}_{\Xi_{(p'u'_i)}}\underbrace{-\overline{\frac{p'}{\rho}\frac{\partial p'}{\partial x_i}}}_{\Pi_{(p'u'_i)}}$$
$$\underbrace{-\overline{\left(\gamma\bar{p}+(\gamma-1)p'\right)u'_i\Theta''}}_{B_{(p'u'_i)}}+\overline{p'f'_{V_i}}.\qquad(4.11b)$$

The $y^\star$ distributions (figure 16) of the budgets of (4.11) are fundamentally different from those of the other thermodynamic variables, ρ' (figure 12), s'' (figure 13) and T'' (figures 14 and 15). The obvious importance of the dilatational terms $B_{(\cdot)}$, containing Θ'' (2.8*b*) in (4.11), which are invariably comparable in magnitude with

$Re_{\tau^\star}$	$\bar{M}_{CL}$	$N_x \times N_y \times N_z$	L_x	L_y	L_z	Δx^+	Δy_w^+	$N_{y^+\leqslant 10}$	Δy_{CL}^+	Δz^+	Δt^+	t_{OBS}^+	Δt_s^+
150	1.50	$361 \times 149 \times 433$	$4\pi\delta$	2δ	$\frac{4}{3}\pi\delta$	7.9	0.22	19	4.7	2.1	0.0164	868	0.0164

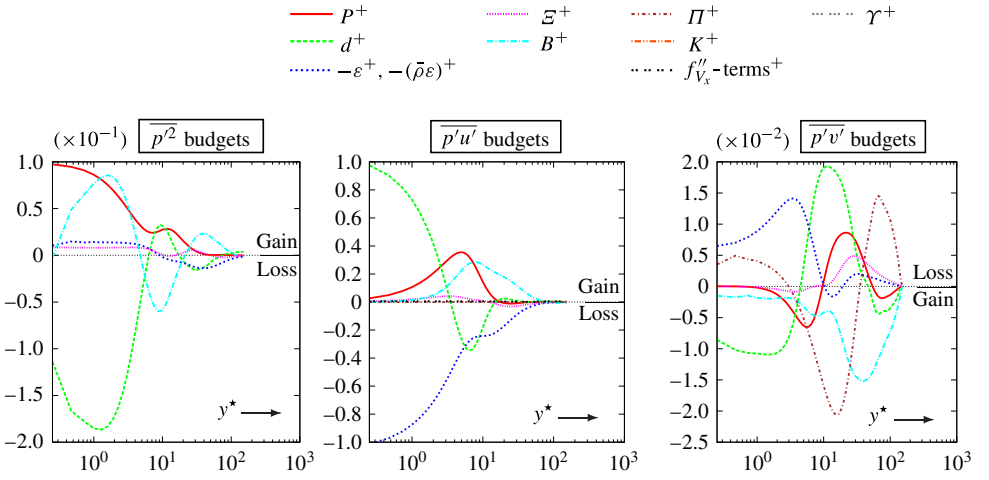

FIGURE 16. (Colour online) Budgets, in wall units (§ 3.2), of the transport equations (4.11*a*) for the pressure variance $\overline{p'^2}$ ($d_{(p'^2)}$, $P_{(p'^2)}$, $-\varepsilon_{(p'^2)}$, $\Xi_{(p'^2)}$, $B_{(p'^2)}$) and (4.11*b*) for the pressure transport $\overline{p'u_i'}$ ($d_{(p'u_i')}$, $P_{(p'u_i')}$, $-\varepsilon_{(p'u_i')}$, $\Xi_{(p'u_i')}$, $\Pi_{(p'u_i')}$, $B_{(p'u_i')}$, $\overline{p'f_{V_x}'}$), obtained from DNS computations ($Re_{\tau^\star} \approxeq 150$, $\bar{M}_{CL} \approxeq 1.50$; table 1), plotted against $y^\star$ (3.1*c*).

the corresponding production terms $P_{(\cdot)}$ (figure 16), contrasts with the weak level of these mechanisms in the budgets of $\{s'', T''\}$ (figures 13–15).

The production of pressure fluctuations $P_{(p'^2)} \geqslant 0$ (gain) increases from centreline to the wall (figure 16), where, contrary to $\{P_{(\rho'^2)}, P_{(\rho s''^2)}, P_{(\rho T''^2)}\}$ (figures 12–15), it reaches its maximum value $[P_{(p'^2)}]_w$, 3.3 times higher than the local maximum at $y^\star \approxeq 12$ (figure 16). This explains the relatively constant shape of $\overline{p'^2}$ in the region $0 \leqslant y^\star \lessapprox 80$ where $[\overline{p'^2}]^{1/2}$ varies by only 20 % (figure 10) in contrast to the r.m.s. of the other thermodynamic fluctuations $\{[\overline{\rho'^2}]^{1/2}, [\overline{\rho s''^2}]^{1/2}, [\overline{\rho T''^2}]^{1/2}\}$ which exhibit much larger variations. In the near-wall region ($y^\star \lessapprox 3$; figure 16), production $P_{(p'^2)}$, diffusion $d_{(p'^2)}$ and the dilatational terms $B_{(p'^2)}$ are the main mechanisms in the $\overline{p'^2}$ budgets, while destruction $-\varepsilon_{(p'^2)} \geqslant 0$ for all $y^\star \lessapprox 10$ and the triple correlation term $\Xi_{(p'^2)} \geqslant 0$ for all $y^\star \lessapprox 10$ both contribute as a weak gain in the near-wall $\overline{p'^2}$ budgets (figure 16). Further away from the wall ($y^\star \gtrapprox 20$; figure 16), all of these mechanisms ($P_{(p'^2)}$, $d_{(p'^2)}$, $B_{(p'^2)}$, $\Xi_{(p'^2)}$) are of equal importance with destruction $-\varepsilon_{(p'^2)} \leqslant 0$ for all $y^\star \lessapprox 20$ (loss). Note also the wavelike shape of $B_{(p'^2)}$ across the channel, generally opposing diffusion (figure 16).

The main mechanisms contributing to the budgets of the streamwise transport $\overline{p'u'} \geqslant 0$ (figure 10) are production $P_{(p'u')} \geqslant 0$ for all $y^\star$ (gain), diffusion $d_{(p'u')}$, destruction $-\varepsilon_{(p'u')} \leqslant 0$ for all $y^\star$ (loss) and the dilatational term $B_{(p'u')} \geqslant 0$ for all $y^\star$ (figure 16), with a weak but discernible contribution of the triple correlations term $\Xi_{(p'u')}$. As for all of the other streamwise fluxes $\{\overline{\rho'u'} \overset{(2.6c)}{=} -\bar{\rho}\overline{u''}, \overline{\rho s''u''}, \overline{\rho T''u''}\}$ (figures 12–15), the body-acceleration term $\overline{p'f_{V_x}'}$ (4.11*b*) is negligible (figure 16). The dilatational term $B_{(p'u')} \geqslant 0$ for all $y^\star$ is practically the unique gain mechanism in

the major part of the channel ($y^\star \gtrapprox 13$; figure 16), where it is principally balanced by destruction $-\varepsilon_{(p'u')} \leqslant 0$ for all $y^\star$ (loss). In the near-wall buffer-layer ($2 \lessapprox y^\star \lessapprox 7$; figure 16), $B_{(p'u')}$ decreases rapidly and is replaced by the production term $P_{(p'u')} \geqslant 0$ as the main gain mechanism, balanced by diffusion $d_{(p'u')}$ and destruction $-\varepsilon_{(p'u')}$. Finally, in the very-near-wall region ($y^\star \lessapprox 2$), diffusion $d_{(p'u')} \geqslant 0$ for all $y^\star \leqslant 2$, which changes sign at $y^\star \approxeq 3.5$, becomes (figure 16) the major gain mechanism at the wall, and is principally balanced by destruction $-\varepsilon_{(p'u')} \leqslant 0$ for all $y^\star$ (loss).

Finally, the budgets of the wall-normal transport $\overline{p'v'} \leqslant 0$ (figure 10) are unlike all of the others, in that all of the mechanisms in (4.11*b*) ($P_{(p'v')}$, $d_{(p'v')}$, $B_{(p'v')}$, $\Pi_{(p'v')}$ and $-\varepsilon_{(p'v')}$) are of equal importance in the major part of the flow (figure 16). The only similarity of the $\overline{p'v'}$ budgets (figure 16) with the other wall-normal fluxes ($\overline{\rho'v'} \overset{(2.6c)}{=} -\bar{\rho}\overline{v''}$, $\overline{\rho s''v''}$, $\overline{\rho T''v''}$; figures 12–15) is the importance of the pressure-gradient term $\Pi_{(p'v')}$, compared with its negligible influence on the streamwise transport budgets ($\overline{\rho'u'} \overset{(2.6c)}{=} -\bar{\rho}\overline{u''}$, $\overline{\rho s''u''}$, $\overline{\rho T''u''}$, $\overline{p'u'_i}$; figures 12–16). On the other hand the particular form of the $\overline{p'v'}$ budgets (figure 16), where most of the terms change sign across the channel, highlights the specific non-local behaviour of p' (Chang *et al.* 1999) and explains the extreme difficulty of single-point closure modelling of pressure diffusion $d^{(p)}_{ij} := -\partial_{x_j}\overline{p'u'_i} - \partial_{x_i}\overline{p'u'_j}$ in Reynolds-stress transport closures (Sauret & Vallet 2007; Vallet 2007; Gerolymos *et al.* 2012*b*). Note, nonetheless, that the dilatational term $B_{(p'v')} \leqslant 0$ for all $y^\star$ (gain), always contributes (figure 16) in generating $\overline{p'v'}$, and so does $B_{(p'u')} \geqslant 0$ for all $y^\star$ (gain) in the $\overline{p'u'}$ budgets (figure 16).

5. Conclusions

Mixed semilocal HCB scaling, $y^\star$ and $Re_{\tau^\star}$ (3.1*c*), introduced by Huang *et al.* (1995), represents reasonably well Re effects in compressible turbulent plane channel flow, not only for the Reynolds stresses, but also for statistics involving thermodynamic variations. Regarding Mach-number effects, it is suggested in the present work, based on analysis of DNS results, that the centreline Mach number, $\bar{M}_{CL}$ (3.1*d*), is the appropriate parameter. In particular, the coefficients of variation of thermodynamic fluctuations ($[\bar{\rho}^{-1}\rho']_{rms}$, $[\bar{T}^{-1}T']_{rms}$ and $[\bar{p}^{-1}p']_{rms}$) scale reasonably well with $\bar{M}^2_{CL}$. Note that, because of the intense viscous heating which causes the ratio of centreline-to-wall temperature, $\bar{T}^{-1}_w\bar{T}_{CL}$, to increase with Mach number, the relation between $\bar{M}_{CL}$ (3.1*d*) and the bulk Mach number M_{B_w} (3.1*a*) is nonlinear, the later increasing faster than the former. The DNS results analysed in the present work cover the range $Re_{\tau^\star} \in [64, 341]$ and $\bar{M}_{CL} \in [0.34, 2.48]$.

Outside of the viscous sublayer ($y^\star \gtrapprox 3$), the ratio of the correlation coefficients of wall-normal transport of thermodynamic fluctuations ($c_{\rho'v'}$, $c_{T'v'}$, $c_{p'v'}$, $c_{s'v'}$) on the shear correlation coefficient $c_{u'v'}$ is a unique function of $y^\star$, practically independent of ($Re_{\tau^\star}$, $\bar{M}_{CL}$), implying a $Re_{\tau^\star}$-dependence of the centreline limiting values of these ratios. The same observation applies to the correlation coefficients between thermodynamic variables ($c_{\rho'T'}$, $c_{p'\rho'}$, $c_{p'T'}$, $c_{s'\rho'}$, $c_{s'p'}$, $c_{s'T'}$), but with a larger scatter between different values of ($Re_{\tau^\star}$, $\bar{M}_{CL}$). The correlation coefficient between entropy and pressure fluctuation, $c_{s'p'} \approxeq 0$ for all $y^\star \gtrapprox 5$, with very little scatter ($|c_{s'p'}| < 0.1$ for all $y^\star \gtrapprox 5$), implying statistical independence of s' and p' everywhere in the channel except in the viscous sublayer, presumably because of the localised influence of the isothermal-wall boundary condition. On the other hand, the correlation coefficients of wall-normal transport of thermodynamic fluctuations ($c_{\rho'v'}$, $c_{T'v'}$, $c_{p'v'}$, $c_{s'v'}$) appear to vary as functions of the outer-scaled wall distance $\delta^{-1}(y - y_w)$ for all $y - y_w \gtrapprox \delta/10$,

with very little scatter for different values of $(Re_{\tau^\star}, \bar{M}_{CL})$. The coefficients of variation of the thermodynamic state variables (p, ρ, T) are always (for all $(Re_{\tau^\star}, \bar{M}_{CL})$ for all $y^\star$) of the same order of magnitude, i.e. $O([\bar{\rho}^{-1}\rho']_{rms}) = O([\bar{T}^{-1}T']_{rms}) = O([\bar{p}^{-1}p']_{rms})$, even at the low-$\bar{M}_{CL}$ limit, in agreement with sustained compressible HIT results.

The evolution equations for the thermodynamic variables (ρ, s, T, p) obtained from the Navier–Stokes equations using thermodynamic derivatives imply exact transport equations for their variances ($\overline{\rho'^2}$, $\overline{\rho s''^2}$, $\overline{\rho T''^2}$ and $\overline{p'^2}$) and fluxes ($\overline{\rho' u_i'}$, $\overline{\rho s'' u_i''}$, $\overline{\rho T'' u_i''}$ and $\overline{p' u_i'}$). The point is made that the Favre-averaging operator does not commute with differentiation, e.g. $\tilde{S}_{ij} \neq (\partial_{x_j}\tilde{u}_i + \partial_{x_i}\tilde{u}_j)/2$ and $S''_{ij} \neq (\partial_{x_j}u''_i + \partial_{x_i}u''_j)/2$, and to avoid widespread notational misuse we introduce specific notation $\breve{S}_{ij} := (\partial_{x_j}\tilde{u}_i + \partial_{x_i}\tilde{u}_j)/2$ and $S''_{ij} := (\partial_{x_j}u''_i + \partial_{x_i}u''_j)/2$. The budgets of the transport equations for the thermodynamic variables were studied using DNS data at $(Re_{\tau^\star}, \bar{M}_{CL}) \cong (150, 1.5)$. There is a strong similarity between the budgets of entropy correlation ($\overline{\rho s''^2}$ and $\overline{\rho s'' u_i''}$) and the budgets of the corresponding correlation of temperature ($\overline{\rho T''^2}$ and $\overline{\rho T'' u_i''}$), associated with the fact that the dilatational terms in the c_v-form or $(D_t p)'$ terms in the c_p-form of the temperature-correlations budgets are very weak and often negligible. Pressure stands apart from the other thermodynamic variables, and in particular the complexity of the budgets of the wall-normal transport $\overline{p'v'}$ is probably the signature of the non-locality of p' and of its subordination to the velocity field. The coefficient of variation of density $[\bar{\rho}^{-1}\rho']_{rms}$ is undoubtedly the best measure of the effects of compressibility on turbulence. Therefore, modelling of density variance (and of the mass fluxes $\overline{\rho' u_i'}$ which govern its production by mean density stratification) is the necessary step in that direction. The main difficulty is probably the dilatational term $B_{(\rho'^2)} = -\overline{\left(\rho^2 - \bar{\rho}^2\right)\Theta''}$ (4.3), which does not contain viscous terms, and further studies on its dynamics and spectra are required.

It is hoped that the present investigation adds to our understanding of compressible turbulent plane channel flow. Nonetheless, to fully understand the influence of $(Re_{\tau^\star}, \bar{M}_{CL})$ on turbulent statistics and budgets, further DNS data, with systematic variation of both these parameters is required and is the subject of ongoing work.

REFERENCES

DEL ÁLAMO, J. C., JIMÉNEZ, J., ZANDONADE, P. & MOSER, R. D. 2004 Scaling of the energy spectra of turbulent channels. *J. Fluid Mech.* **500**, 135–144.

BERNARDINI, M. & PIROZZOLI, S. 2011 Wall pressure fluctuations beneath supersonic turbulent boundary-layers. *Phys. Fluids* **23**, 085102.

BOWERSOX, R. D. W. 2009 Extension of equilibrium turbulent heat flux models to high-speed shear flows. *J. Fluid Mech.* **633**, 61–70.

BRADSHAW, P. 1977 Compressible turbulent shear layers. *Annu. Rev. Fluid Mech.* **9**, 33–54.

BRIDGMAN, P. W. 1961 *The Thermodynamics of Electrical Phenomena in Metals and a Condensed Collection of Thermodynamic Formulas*. Dover.

CANUTO, V. M. 1997 Compressible turbulence. *Astrophys. J.* **482**, 827–851.

CHANG, P. A. III, PIOMELLI, U. & BLAKE, W. K. 1999 Relations between wall-pressure and velocity-field sources. *Phys. Fluids* **11** (11), 3434–3448.

CHERNYSHENKO, S. I. & BAIG, M. F. 2005 The mechanism of streak formation in near-wall turbulence. *J. Fluid Mech.* **544**, 99–131.

CHOU, P. Y. 1945 On velocity correlations and the solutions of the equations of turbulent fluctuations. *Q. Appl. Maths* **3**, 38–54.

CHU, B. T. & KOVÁSZNAY, L. S. G. 1958 Nonlinear interactions in a viscous heat-conducting compressible gas. *J. Fluid Mech.* **3**, 494–514.

COLEMAN, G. N., KIM, J. & MOSER, R. D. 1995 A numerical study of turbulent supersonic isothermal-wall channel flow. *J. Fluid Mech.* **305**, 159–183.

DONZIS, D. A. & JAGANNATHAN, S. 2013 Fluctuation of thermodynamic variables in stationary compressible turbulence. *J. Fluid Mech.* **733**, 221–244.

DUAN, L., BEEKMAN, I. & MARTÍN, M. P. 2010 Direct numerical simulation of hypersonic turbulent boundary-layers – part 2 – effect of wall temperature. *J. Fluid Mech.* **655**, 419–445.

DUAN, L., BEEKMAN, I. & MARTÍN, M. P. 2011 Direct numerical simulation of hypersonic turbulent boundary-layers – part 3 – effect of Mach-number. *J. Fluid Mech.* **672**, 245–267.

DUAN, L. & MARTÍN, M. P. 2011 Direct numerical simulation of hypersonic turbulent boundary-layers – part 4 – effect of high enthalpy. *J. Fluid Mech.* **684**, 25–59.

ECKERT, E. R. G. & DRAKE, R. M. 1972 *Analysis of Heat and Mass Transfer*. McGraw-Hill.

ERLEBACHER, G. & SARKAR, S. 1993 Statistical analysis of the rate of strain tensor in compressible homogeneous turbulence. *Phys. Fluids* A **5** (12), 3240–3254.

FAVRE, A. 1965 Equations des gaz turbulents compressibles – I – formes générales. *J. Méc.* **4**, 361–390.

FOYSI, H., SARKAR, S. & FRIEDRICH, R. 2004 Compressibility effects and turbulence scalings in supersonic channel flow. *J. Fluid Mech.* **509**, 207–216.

FRIEDRICH, R. 2007 Compressible turbulent flows: aspects of prediction and analysis. *Z. Angew. Math. Mech.* **87** (3), 189–211.

FRIEDRICH, R., FOYSI, H. & SESTERHENN, J. 2006 Turbulent momentum and passive scalar transport in supersonic channel flow. *J. Braz. Soc. Mech. Sci. Engng* **28** (2), 174–185.

GATSKI, T. B. & BONNET, J.-P. 2009 *Compressibility, Turbulence and High Speed Flow*. Elsevier.

GEROLYMOS, G. A. 1990 Implicit multiple-grid solution of the compressible Navier–Stokes equations using k–ε turbulence closure. *AIAA J.* **28** (10), 1707–1717.

GEROLYMOS, G. A., LO, C. & VALLET, I. 2012*a* Tensorial representations of Reynolds-stress pressure–strain redistribution. *Trans. ASME J. Appl. Mech.* **79** (4), 044506; (1–10).

GEROLYMOS, G. A., LO, C., VALLET, I. & YOUNIS, B. A. 2012*b* Term-by-term analysis of near-wall second moment closures. *AIAA J.* **50** (12), 2848–2864.

GEROLYMOS, G. A., SÉNÉCHAL, D. & VALLET, I. 2009*a* Analysis of dual-time-stepping with explicit subiterations. *AIAA Paper* 2009-1608, 47. *Aerospace Sciences Meeting, 5–8 January 2009, Orlando*.

GEROLYMOS, G. A., SÉNÉCHAL, D. & VALLET, I. 2009*b* Very-high-order WENO schemes. *J. Comput. Phys.* **228**, 8481–8524.

GEROLYMOS, G. A., SÉNÉCHAL, D. & VALLET, I. 2010 Performance of very-high-order upwind schemes for DNS of compressible wall-turbulence. *Intl J. Numer. Meth. Fluids* **63**, 769–810.

GEROLYMOS, G. A., SÉNÉCHAL, D. & VALLET, I. 2013 Wall effects on pressure fluctuations in turbulent channel flow. *J. Fluid Mech.* **720**, 15–65.

GEROLYMOS, G. A. & VALLET, I. 1996 Implicit computation of the 3-D compressible Navier–Stokes equations using k–ε turbulence closure. *AIAA J.* **34** (7), 1321–1330.

GHOSH, S., FOYSI, H. & FRIEDRICH, R. 2010 Compressible turbulent channel and pipe flow: similarities and differences. *J. Fluid Mech.* **648**, 155–181.

GHOSH, S., FRIEDRICH, R., PFITZNER, M., STEMMER, C., CUENOT, B. & EL HAFI, M. 2011 Effects of radiative heat transfer on the structure of turbulent supersonic channel flow. *J. Fluid Mech.* **677**, 417–444.

GUARINI, S. E., MOSER, R. D., SHARIFF, K. & WRAY, A. 2000 Direct numerical simulation of a supersonic turbulent boundary-layer at Mach 2.5. *J. Fluid Mech.* **414**, 1–33.

HAMBA, F. 1999 Effects of pressure fluctuations on turbulence growth in compressible homogeneous shear flow. *Phys. Fluids* **11** (6), 1623–1635.

HAMBA, F. & BLAISDELL, G. A. 1997 Towards modelling inhomogeneous compressible turbulence using a 2-scale statistical theory. *Phys. Fluids* **9** (9), 2749–2768.

HANSEN, C. F. 1958 Approximations for the thermodynamic and transport properties of high-temperature air. *Tech. Note* 4150. NACA, Ames Aeronautical Laboratory, Moffett Field, [CA, USA].

HU, Z. W., MORFEY, C. L. & SANDHAM, N. D. 2006 Wall pressure and shear stress spectra from direct simulations of channel flow. *AIAA J.* **44** (7), 1541–1549.

HUANG, P. G., COLEMAN, G. N. & BRADSHAW, P. 1995 Compressible turbulent channel flows: DNS results and modelling. *J. Fluid Mech.* **305**, 185–218.

HULTMARK, M., BAILEY, S. C. C. & SMITS, A. J. 2010 Scaling of near-wall turbulence in pipe flow. *J. Fluid Mech.* **649**, 103–113.

JEONG, J., HUSSAIN, F., SCHOPPA, W. & KIM, J. 1997 Coherent structures near the wall in a turbulent channel flow. *J. Fluid Mech.* **332**, 185–214.

KESTIN, J. 1979 *A Course in Thermodynamics,* vol. 1, 1st edn. Hemisphere. McGraw-Hill.

KIM, J. 1989 On the structure of pressure fluctuations in simulated turbulent channel-flow. *J. Fluid Mech.* **205**, 421–451.

KIM, J. 2012 Progress in pipe and channel flow turbulence, 1961–2011. *J. Turbul.* **13**, 000045.

KIM, J., MOIN, P. & MOSER, R. 1987 Turbulence statistics in fully developed channel flow at low-Reynolds-number. *J. Fluid Mech.* **177**, 133–166.

KOVÁSZNAY, L. S. G. 1953 Turbulence in supersonic flow. *J. Aero. Sci.* **20**, 657–674; 682.

KREUZINGER, J., FRIEDRICH, R. & GATSKI, T. B. 2006 Compressibility effects in the solenoidal dissipation-rate equation: *a priori* assessment and modelling. *Intl J. Heat Fluid Flow* **27**, 696–706.

LAGHA, M., KIM, J., ELDREDGE, J. D. & ZHONG, X. 2011*a* Near-wall dynamics of compressible boundary layers. *Phys. Fluids* **23**, 065109.

LAGHA, M., KIM, J., ELDREDGE, J. D. & ZHONG, X. 2011*b* A numerical study of compressible turbulent boundary-layers. *Phys. Fluids* **23**, 015106.

LECHNER, R., SESTERHENN, J. & FRIEDRICH, R. 2001 Turbulent supersonic channel flow. *J. Turbul.* **2**, 001.1-25.

LIEPMANN, H. W. & ROSHKO, A. 1957 *Elements of Gasdynamics*. John Wiley and Sons.

MAEDER, T., ADAMS, N. A. & KLEISER, L. 2001 Direct simulation of turbulent supersonic boundary-layers by an extended temporal approach. *J. Fluid Mech.* **429**, 187–216.

MAHLE, I., FOYSI, H., SARKAR, S. & FRIEDRICH, R. 2007 On the turbulence structure of inert and reacting compressible mixing layers. *J. Fluid Mech.* **593**, 171–180.

MARTÍN, M. P. 2007 Direct numerical simulation of hypersonic turbulent boundary-layers – part 1 – initialization and comparison with experiments. *J. Fluid Mech.* **570**, 347–364.

MONTY, J. P., HUTCHINS, N., NG, H. C. H., MARUSIC, I. & CHONG, M. S. 2009 A comparison of turbulent pipe, channel and boundary layer flows. *J. Fluid Mech.* **632**, 431–442.

MORINISHI, Y., TAMANO, S. & NAKABAYASHI, K. 2003 A DNS algorithm using b-spline collocation method for compressible turbulent channel flow. *Comput. Fluids* **32**, 751–776.

MORINISHI, Y., TAMANO, S. & NAKABAYASHI, K. 2004 Direct numerical simulation of compressible turbulent channel flow between adiabatic and isothermal walls. *J. Fluid Mech.* **502**, 273–308.

MORKOVIN, M. V. 1962 Effects of compressibility on turbulent flows. In *Mechanics of Turbulence (Proceedings of the International Colloquium, 28 August–2 September 1961, Marseille, France)* (ed. A. Favre), Colloques Internationaux du CNRS, vol. 108, pp. 367–380. Editions du CNRS.

MOSER, R. D., KIM, J. & MANSOUR, N. N. 1999 Direct numerical simulation of turbulent channel flow up to $Re_\tau = 590$. *Phys. Fluids* **11** (4), 943–945.

PANDA, J. & SEASHOLTZ, R. G. 2002 Experimental investigation of density fluctuations in high-speed jets and correlation with generated noise. *J. Fluid Mech.* **450**, 97–130.

PANTANO, C. & SARKAR, S. 2002 A study of compressibility effects in the high-speed turbulent shear layer using direct simulation. *J. Fluid Mech.* **451**, 329–371.

PIROZZOLI, S. & BERNARDINI, M. 2013 Probing high-Reynolds-number effects in numerical boundary-layers. *Phys. Fluids* **25**, 021704.

PIROZZOLI, S., GRASSO, F. & GATSKI, T. B. 2004 Direct numerical simulation and analysis of a spatially evolving supersonic turbulent-boundary-layer at $M = 2.25$. *Phys. Fluids* **16** (3), 530–545.

POPE, S. B. 2000 *Turbulent Flows*. Cambridge University Press.

LE RIBAULT, C. & FRIEDRICH, R. 1997 Investigation of transport equations for turbulent heat fluxes in compressible flows. *Intl J. Heat Mass Transfer* **40** (11), 2721–2738.

RISTORCELLI, J. R. 1997 A pseudosound constitutive relationship for the dilatational covariances in compressible turbulence. *J. Fluid Mech.* **347**, 37–70.

RUBINSTEIN, R. & ERLEBACHER, G. 1997 Transport coefficients in weakly compressible turbulence. *Phys. Fluids* **9**, 3037–3057.

SARKAR, S. 1992 The pressure-dilatation correlation in compressible flows. *Phys. Fluids* A **4** (12), 2674–2682.

SARKAR, S. 1995 The stabilizing effect of compressibility in turbulent shear flow. *J. Fluid Mech.* **282**, 163–186.

SARKAR, S., ERLEBACHER, G., HUSSAINI, M. Y. & KREISS, H. O. 1991 The analysis and modelling of dilatational terms in compressible turbulence. *J. Fluid Mech.* **227**, 473–493.

SAURET, E. & VALLET, I. 2007 Near-wall turbulent pressure diffusion modelling and influence in 3-D secondary flows. *Trans. ASME J. Fluids Engng* **129** (5), 634–642.

SCHLATTER, P. & ÖRLÜ, R. 2010 Assessment of direct numerical simulation data of turbulent boundary-layers. *J. Fluid Mech.* **659**, 116–126.

SCHLICHTING, H. 1979 *Boundary-Layer Theory*, 3rd edn McGraw-Hill.

SÉNÉCHAL, D. 2009 DNS des ecoulements turbulents compressibles: fluctuations de pression, de masse volumique et de température. *Doctorat*, Université Pierre-et-Marie-Curie, Paris, France.

SESTERHENN, J. 2001 A characteristic-type formulation of the Navier–Stokes equations for high-order upwind schemes. *Comput. Fluids* **30**, 37–67.

SHAHAB, M. F., LEHNASCH, G., GATSKI, T. B. & COMTE, P. 2011 Statistical characteristics of an isothermal, supersonic developing boundary layer flow from DNS data. *Flow Turbul. Combust.* **86**, 369–397.

SMITS, A. J., MCKEON, B. J. & MARUSIC, I. 2011 High-Reynolds number wall turbulence. *Annu. Rev. Fluid Mech.* **43**, 353–375.

SPINA, E. F., SMITS, A. J. & ROBINSON, S. K. 1994 The physics of supersonic turbulent boundary-layers. *Annu. Rev. Fluid Mech.* **26**, 287–319.

TAMANO, S. & MORINISHI, Y. 2006 Effect of different thermal wall boundary-conditions on compressible turbulent channel flow at $M = 1.5$. *J. Fluid Mech.* **548**, 361–373.

TAULBEE, D. & VANOSDOL, J. 1991 Modeling turbulent compressible flows: the mass fluctuating velocity and squared density. *AIAA Paper* 1991-0524 (doi:10.2514/6.1991-524).

TEITEL, M. & ANTONIA, R. A. 1993 Heat transfer in fully developed turbulent channel flow: comparison between experiment and direct numerical simulations. *Intl J. Heat Mass Transfer* **36**, 1701–1706.

TSUJI, Y., FRANSSON, J. H. M., ALFREDSSON, P. H. & JOHANSSON, A. V. 2007 Pressure statistics and their scalings in high-Reynolds-number turbulent boundary-layers. *J. Fluid Mech.* **585**, 1–40.

TSUJI, Y., IMAYAMA, S., SCHLATTER, P., ALFREDSSON, P. H., JOHANSSON, A. V., HUTCHINS, N. & MONTY, J. 2012 Pressure fluctuation in high-Reynolds-number turbulent boundary-layer: results from experiments and DNS. *J. Turbul.* **13**, 000050.

VALLET, I. 2007 Reynolds-stress modelling of 3-D secondary flows with emphasis on turbulent diffusion closure. *Trans. ASME J. Appl. Mech.* **74** (6), 1142–1156.

WEI, L. & POLLARD, A. 2011*a* DNS of compressible turbulent channel flows using the discontinuous Galerkin method. *Comput. Fluids* **47**, 85–100.

WEI, L. & POLLARD, A. 2011*b* Interactions among pressure, density, vorticity and their gradients in compressible turbulent channel flow. *J. Fluid Mech.* **673**, 1–18.

WHITE, M. F. 1974 *Viscous Fluid Flow*. McGraw-Hill.

XU, S. & MARTÍN, M. P. 2004 Assessment of inflow boundary conditions for compressible turbulent boundary-layers. *Phys. Fluids* **16** (7), 2623–2639.

YOSHIZAWA, A. 1992 Statistical analysis of compressible turbulent shear flows with special emphasis on turbulence modeling. *Phys. Rev.* A **46**, 3292–3306.

YOSHIZAWA, A., MATSUO, Y. & MIZOBUCHI, Y. 2013 A construction of the Reynolds-averaged turbulence transport equations in a variable-density flow, based on the concept of mass-weighted fluctuations. *Phys. Fluids* **25**, 075105.